

**Quantitative Investigations of Rubber Blend Compatibility and  
Transport Phenomena in Rubbers influenced  
by the Chemical Structure of the Low Molecular Components**

Von der Naturwissenschaftlichen Fakultät der  
Gottfried Wilhelm Leibniz Universität Hannover

zur Erlangung des Grades

Doktorin der Naturwissenschaften  
Dr. rer. nat.

genehmigte Dissertation

von

Dipl. Chem. Ing. Cristina Rosca

geboren am 26.04.1976 in Avrig, Rumänien

Hannover 2007

Referent: Prof. Dr. R. H. Schuster  
Korreferentin: Prof. Dr. C. Vogt  
Tag der Promotion: 08.10.2007

## Abstract

### Quantitative Investigations of Rubber Blend Compatibility and Transport Phenomena in Rubbers influenced by the Chemical Structure of the Low Molecular Components

Cristina Rosca, Dissertation, University of Hannover, 2007

Modern rubber products are multicomponent systems. In order to optimise the properties of this system, it is important to characterize each component of the recipe to obtain further knowledge about the effect of additives in rubber. The amount and the type of each component influence the final properties of the compound.

In this work the phase morphology of NR-based blends in relation to the polarity of the second blend constituents (NBR, SBR with varying vinyl content, epoxidized NR and SBR) was investigated. The polymers were thermodynamically characterized by their solubility parameter. The phase morphology was determined by employing dynamic-mechanical spectroscopy and transmission-electron-microscopy (TEM). It was shown that the domain size of the minor constituent increases linearly with interfacial tension. The degree of compatibility was classified by the solubility parameter difference and in addition using the  $T_g$  shift and the half width of the damping maxima. The phase inversion region is determined from the stepwise increase in the loss modulus.

Model processing aids with well-defined molecular structure (alcohols, acids and esters derived from  $C_{12}$ - and  $C_{18}$ -hydrocarbons) were investigated in SBR for the plasticizing efficiency at low temperatures, the solubility and the viscoelastic properties of the rubber mixes. The influence of the molecular weight and the functional group on solubility in rubber was investigated by means of swelling. It was discussed the influence of additives on plateau modulus  $G_N^0$  and the reptation time  $\tau_{rep}$  by viscoelastic analysis.

The diffusion process of a homologous series of phthalates (DMP, DEP, DBP, DOP and DDP) in different nitrile rubbers (NBR), hydrogenated nitrile rubber (HNBR) and styrene butadiene rubbers (SBR) was investigated by using two methods based on FT-IR Spectroscopy, namely the macroscopical "time-lag" method and the microscopical "concentration-distance" analysis. Within the homologous series of the phthalates the diffusion coefficient demonstrates significant structure-property relationships concerning (i) the chain length of the alkyl groups of the phthalates, (ii) the content of nitrile groups in the matrix, (iii) the unsaturation of the rubber and (iv) the crosslinking density of the matrix.

An automatic permeation apparatus was built in order to measure the permeation rate and the diffusion coefficient in rubber mixes. The influence of the constitution and the type of polymer, the crosslinking density of the rubber matrix, the dispersion and distribution of the filler as well as the effect of the morphology of the rubber blends on permeation and diffusion processes was discussed.

Keywords: Compatibility, solubility, phase morphology, plasticizing efficiency, diffusion, permeation

## Abstract

### **Quantitative Untersuchungen zur Verträglichkeit von Kautschukverschnitten und Einfluß der Chemischen Struktur niedermolekularer Komponenten auf Transportphänomene in Kautschuken**

**Cristina Rosca, Dissertation, Universität Hannover, 2007**

Kautschukmischungen sind komplexe Vielstoffsysteme. Um eine effiziente Eigenschaftsoptimierung vorzunehmen, sind eine möglichst komplette Charakterisierung der einzelnen Komponenten einer Kautschukmischung und eine weitgehende Kenntnis von Auswirkung auf die Additive in Kautschuk die nötige Voraussetzung. Die Menge und Art jede Einzelkomponenten tragen zum gesamten Eigenschaftsbild bei.

In dieser Dissertation wurde die Phasenmorphologie von NR Verschnitten in Abhängigkeit von der Polarität der Verschnittkomponenten untersucht. Als Verschnittkomponenten wurden hierbei NBR, SBR-Typen mit unterschiedlichem Vinylgehalt, sowie epoxidiertes NR und epoxidiertes SBR eingesetzt. Sämtliche Kautschuke wurden thermodynamisch anhand des Löslichkeitsparameters charakterisiert. Die Phasenmorphologie wurde mit Hilfe von dynamisch-mechanischer Spektroskopie und Transmissions-Elektronen-Mikroskopie (TEM) untersucht. Der Grad der Verträglichkeit wurde zusätzlich zur Differenz der Löslichkeitsparameter über die  $T_g$ -Verschiebung und die Verbreiterung des Dämpfungssignals beschrieben.

Modell-Verarbeitungshilfsmittel mit definierter molekularer Struktur (Alkohole, Säuren und Ester von  $C_{12}$ - und  $C_{18}$ -Kohlenwasserstoffen) wurden in SBR auf ihre Weichmacherwirksamkeit, Löslichkeit und viskoelastische Effekte untersucht. Die Löslichkeit der Stoffe wurde bei tiefen Temperaturen thermoanalytisch untersucht. Der Einfluss der Molmasse als auch der funktionellen Gruppe des Verarbeitungshilfsmittel auf die Löslichkeit wurde mittels Quellungsmessungen durchgeführt. Durch Untersuchung des viskoelastischen Verhaltens wurde der Einfluss der Modell-Verarbeitungshilfsmittel auf den Plateaumodul  $G_N$  und die charakteristische Relaxationszeit diskutiert.

Der Diffusionsprozess einer homologen Reihe von Phthalaten (DMP, DEP, DBP, DOP und DDP) wurde in verschiedenen Nitrilkautschuken (NBR), in hydriertem Nitrilkautschuk (HNBR) und Styrol-Butadienkautschuken (SBR) mit Hilfe von zwei FT-IR-spektroskopischen Methoden untersucht, nämlich mit der makroskopischen "Durchbruch" - Methode und der mikroskopischen "Konzentrations-Weg" Analyse. Durch Untersuchungen der Transportprozesse von Phthalaten wurden die Einflüsse (i) der Länge der Alkylreste (ii) des Gehaltes an Nitrilgruppen in der Kautschukmatrix und (iii) dem Gehalt an Doppelbindungen, sowie (iv) der Vernetzungsdichte der Matrix auf die Diffusionsgeschwindigkeit bestimmt.

Ein Schwerpunkt war dabei der Aufbau einer automatisierten Permeationsapparatur zur Bestimmung der Permeationsrate wie auch des Diffusionskoeffizienten. Im Besonderen ist der Einfluss von Polymertyp und dessen Mikrostruktur, der Vernetzung, der Füllstoffe und deren Dispersion und Distribution, sowie die Auswirkungen der Morphologie im Fall von Polymerverschnitten zu untersuchen.

Schlüsselwörter: Verträglichkeit, Löslichkeit, Phasenmorphologie, Weichmacherwirkung, Diffusion, Permeation

This work was done in Deutschen Institut für Kautschuktechnologie e. V. (DIK) under the supervision of Prof. Dr. R. H. Schuster and Prof. Dr. C. Vogt from May 2002 until April 2006.

I would kindly want to thank to Prof. Dr. R. H. Schuster for the worthwhile discussions, ideas, criticism and the advices received during this time, which helped me to finish this work.

I truly appreciate and thank to Prof. Dr. C. Vogt from Institute for Inorganic Chemistry for the acceptance as supervisor of this work.

My thanks go also to Prof. Dr. Eng. G. Poll from Institute for Machine Parts, Construction Design and Tribology for taking on the supervising of this work.

I would like to express my thanks to Dr. U. Giese for the useful discussion concerning my work and for the support showed over those years.

Mrs. G. Philipp and Mrs. A. Höft, I thank you for the assistance and the help you gave to me during the time spent in DIK. My appreciation goes to Mrs. Hanne, who always encouraged me and supported as being my mother.

I really admire the work done together with my colleagues from elastomer-chemistry and elastomer-physics laboratories: Mr. G. Körner, Mrs. B. Schwiedland, Mr. F. Boller, Mr. B. Matschke, Mr. J. Hamann, Mr. A. Heier and Mr. P. Erren. Also I want to give my appreciation to N. Tricas for the collaboration during my work in DIK.

I would like to address my gratitude to Deutsche Kautschukgesellschaft, Rhein Chemie Rheinau GmbH for the financial support of this Ph.D. thesis.

My special thanks goes to my family that always supported me and nevertheless to my friend, Gerd, for the understanding that he showed to me in the last months and for the motivation that he gave to me in order to complete this work.

For my beloved parents

The following works are part of this thesis and were presented at different conferences:

Posters:

„Impact of Vinyl Groups on the Morphology of NR-SSBR by Dynamic-Mechanical Analysis“

C. Rosca, J. Ziegler, J. Meier, G. N. Bandur, R. H. Schuster

5. Kautschuk-Herbst-Kolloquium, 30.10.-01.11.2002, Hannover, Germany

„Diffusion of accelerators in rubber compounds“,

C. Rosca, U. Giese, T. Früh

South Brazilian Rubber Conference, 28.09.-01.10.2003, Porto Alegre, Brazil

„Diffusion of additives in rubbers“

C. Rosca, U. Giese, R. H. Schuster

International Rubber Conference 2004, 30.06.-03.07.2004, Moscow, Russland

„Diffusion of Dithiophosphates in Rubber Compounds“

C. Rosca, U. Giese, R. H. Schuster, I. Manovicu, T. Früh

Junior EUROMAT, 06.09.-10.09.2004, Lausanne, Switzerland

„Permeability of elastomers“

C. Rosca, U. Giese, R. H. Schuster, I. Manovicu

6. Kautschuk-Herbst-Kolloquium, 10.11.-13.11.2004, Hannover, Germany

„Influence of additives on processing properties of elastomers“

C. Rosca, J. Meier, R. H. Schuster, L. Steger

6. Kautschuk-Herbst-Kolloquium, 10.11.-13.11.2004, Hannover, Germany

„Evaluation of permeation behaviour of fluids through polymer membranes“

C. Rosca, U. Giese, R. H. Schuster, I. Manovicu

X. International Macromolecular Colloquium, 10.04.-13.04.2005, Gramado, Brazil

### Oral presentations:

„Diffusion und Verteilung von Dithiophosphaten“

C. Rosca, U. Giese, R. H. Schuster,

DKG-Tagung Rheinland Westfalen, 24.03.-25.03.2004, Bad Neuenahr-Ahrweiler, Germany

„Study of phase morphology in blends of natural rubber“

C. Rosca, T. Rocha, R. H. Schuster

Simposio Latinoamericano de Polimeros 2004, 12.07.-16.07 2004, Valencia, Spanien

„Additives Influence on Elastomers Properties“

C. Rosca, R. H. Schuster

10th International Seminar on Elastomers, 05.04.-08.04 2005, Rio de Janeiro, Brazil

„Permeationsdichtigkeit von Elastomeren“

C. Rosca, U. Giese, R. H. Schuster

DKG Forschungsprojektepräsentation, 20.04.2005, Fulda, Germany

### Publications:

„Influence of polymer polarity on phase morphology of NR-blends“

T. Rocha, C. Rosca, J. Ziegler, R. H. Schuster

Kautschuk Gummi Kunststoffe, **1/2**, (2005) 22.

„Study of Plasticizing Efficiency and Viscoelastic Effects of Processing aid in S-SBR“

C. Rosca, R. H. Schuster

Kautschuk Gummi Kunststoffe, **12**, (2005) 662.

„Investigation of Diffusion of Phthalates in Nitrile Rubber“

C. Rosca, U. Giese, R. H. Schuster

Kautschuk Gummi Kunststoffe, **3** (2006) 86.



**Table of contents**

<b>1</b>	<b>Introduction.....</b>	<b>5</b>
<b>2</b>	<b>Aim of the work.....</b>	<b>7</b>
<b>3</b>	<b>Theoretical background.....</b>	<b>9</b>
<b>3.1</b>	<b>Compatibility of rubbers.....</b>	<b>9</b>
3.1.1	Theory of miscibility.....	9
3.1.2	The solubility parameter concept.....	13
3.1.3	Analysis of blend morphology.....	16
3.1.4	Evaluation of the interphase in rubber blends.....	20
<b>3.2</b>	<b>Interaction of rubber with additives.....</b>	<b>22</b>
3.2.1	The free volume theory.....	23
3.2.2	Influence of the additive on the glass transition temperature.....	24
3.2.3	Influence of the additive on the viscoelastic properties.....	25
<b>3.3</b>	<b>Transport processes in rubber.....</b>	<b>28</b>
<b>3.3.1</b>	<b>Permeation and diffusion processes.....</b>	<b>28</b>
3.3.1.1	Solutions to the Fick's differential equation.....	31
3.3.1.2	The theories of diffusion.....	33
3.3.1.3	Concentration-distance analysis.....	35
3.3.1.4	Factors affecting the transport processes.....	36
<b>3.3.2</b>	<b>Determination of the diffusion coefficient and permeation rate.....</b>	<b>42</b>
3.3.2.1	IR-spectroscopy.....	43
3.3.2.2	Concentration-distance analysis.....	43
3.3.2.3	Swelling investigations.....	44
3.3.2.4	Permeation experiments.....	44

---

<b>4</b>	<b>Results and discussion</b> .....	45
<b>4.1</b>	<b>Polymer compatibility</b> .....	46
4.1.1	Estimated interfacial tension.....	47
4.1.2	Phase morphology.....	48
4.1.3	Interphase.....	61
<b>4.2</b>	<b>Rubber-additive interaction</b> .....	64
4.2.1	Impact on glass transition.....	67
4.2.2	Solubility of model processing aids.....	71
4.2.3	Relationship between swelling and plasticizing efficiency.....	74
4.2.4	Viscoelastic properties.....	75
<b>4.3</b>	<b>Diffusion and Permeation of the low molecular components</b> .....	77
4.3.1	Determination of diffusion coefficient by means of ATR-FT-IR-Spectroscopy	77
4.3.2	Determination of the diffusion coefficient with concentration-distance analysis	88
4.3.3	Determination of the diffusion coefficient by swelling.....	91
4.3.4	Determination of the diffusion coefficient with the two-chamber method.....	103
<b>4.4</b>	<b>Relationship of oil exposition and properties</b> .....	111
4.4.1	General requirements to be met by elastomer material for rotary shaft seals	114
4.4.2	Chemical resistance of the rotary shaft seals with respect to different oils....	115
4.4.3	Chemical investigation of material damages after dynamic stress.....	119
4.4.4	Investigation of additives used in lubricants and their influences.....	123
<b>5</b>	<b>Conclusions</b> .....	125
<b>6</b>	<b>Experimental part</b> .....	129
<b>7</b>	<b>Annexes</b> .....	134
<b>8</b>	<b>Literature</b> .....	136

**Abbreviations**

ACN	Nitrile content
$a_{\text{IPH}}$	Thickness of the interphase
ATR	Attenuated Total Reflectance
ASTM	American Society for Testing and Materials
BR	Poly (butadiene), (Butadiene Rubber)
D	Diffusion coefficient
DIK	Deutsches Institut für Kautschuktechnologie e. V.
DMA	Dynamical mechanical analysis
DSC	Differential scanning calorimetry
$E_D$	Activation energy
ENR	Epoxidized natural rubber
EpSBR	Epoxidized styrene butadiene rubber
FT-IR	Fourier-Transform-Infrared spectroscopy
$G'$	Dynamic storage modulus
$G''$	Dynamic loss modulus
GC	Gas chromatography
f	Frictional force
$F_i$	Molar attraction constant
J	Diffusion flux
$J_0$	Mass flow density
Q	Swelling degree
M	Molar mass
$N_A$	Avogadro number
NBR	Poly (acryl-nitrile-co-butadiene)
NR	Poly (1,4-cis-isopren), (Natural Rubber)
P	Permeation rate
phr	Parts per hundred parts rubber
$\langle R_g \rangle$	Average radius of gyration
$\tan \delta$	Loss factor
TGA	Thermo-gravimetical analysis
S	Sorption coefficient
SBR	Poly (styrene-co-butadiene), (Styrene Butadiene Rubber)
T	Temperature
TEM	Transmission electron microscopy
$T_g$	Glass transition temperature

---

$V_f$	Free volume in the system
$V$	Volume of a sample
$V_0$	Volume occupied by the polymer molecule
$\Delta E_{\text{vap}}$	Energy of vaporisation
$\Delta h_M$	Heat of mixing
$\Delta H_m$	Mixing enthalpy
$\Delta M/\Delta t$	Mass flow
$\Delta S_m$	Mixing entropy
$\Delta G_m$	Free mixing enthalpy
$\alpha$	Thermal expansion coefficient
$\beta$	Distribution coefficient
$\gamma$	Interfacial tension
$\delta$	Solubility parameter (HILDEBRAND-Parameter)
$\varepsilon$	Deformation
$\eta$	Viscosity
$\rho$	Density
$\sigma$	Tension
$\tau$	Time lag
$\phi$	Volume fraction
$\phi_{\text{IPH}}$	Volume fraction of the interphase
$\chi$	Flory-Huggins interaction parameter
$\chi_s$	Entropic contribution to $\chi$
$\chi_H$	Enthalpic contribution to $\chi$
$\varpi$	Mass fraction
$\zeta$	Frictional coefficient

## 1. Introduction

Polymer science and technology has undergone a quite impressive expansion over the last decades, primarily through the diversity in chemical constitution and macrostructure of the raw polymers [1, 2]. The variety of monomers, their ability to form copolymers and several polymerisation techniques lead to tailored or modified polymers covering a large range of physico-chemical as well as mechanical properties.

In addition to the chemical approach the concept of physically (mechanically) blending two or more existing polymers opened numerous possibilities for producing new materials with interesting properties and commercial utilization [3]. As a matter of fact only by blending two or more rubbers to a multiphase polymer system, the sophisticated demands for high performance and long service life can be satisfied in the field of entropy - elastic material (crosslinked rubbers). The implementation of this material concept requires different knowledge about the thermodynamic phase behaviour, rheology and processing, co-crosslinking as well as reinforcement by nano-scaled fillers.

Compatible blends involve thermodynamic miscibility and are characterized by the presence of one phase and a single glass transition temperature while incompatible blends are phase separated, presenting the glass transition temperatures characteristic to each phase of the blend [4, 5]. Consequently, the first group of blends demonstrates new physical and mechanical properties, which are not common to the original blend constituents. Two representative examples for single phase blends are poly (2,6-dimethyl-1,4-phenylene oxide) PPO / (polystyrene) PS [6] and poly (acryl-nitrile-co-butadiene) NBR / poly (vinyl chloride) PVC [7]. The latter group of blends shows mainly the properties of the original blend constituents. Prominent examples are the combinations of the high abrasion resistance and good grip properties of modern tire treads achieved by blending BR (low  $T_g$ ) with SBR (high  $T_g$ ) or the combination of good ageing resistance from EPDM [8] with the oil resistance of the polar NBR [9]. However, the overall performance of rubber blends depends on its phase morphology, the interfacial properties between the blend phases and, nevertheless, on the individual component properties.

The majority of the investigations on blend morphology highlight the influence of the polymer constitution and the processing parameters [2]. The morphology was investigated by direct microscopical approaches (TEM, SEM and AFM) or by exploiting specific physical properties of the blend constituents such as the thermal expansion coefficient, the heat capacity, the dielectric permittivity and the mechanical moduli [4]. Theoretical approaches to understand miscibility and phase behaviour of polymer blends were successfully developed [10]. However, the experimental exploitation of theoretical prediction to rubber blends was initiated only two

decades ago [11]. More specific aspects related to interfacial tension, interfacial thickness and phase behaviour as a consequence of the polymer constitution were rarely investigated for rubber blends. Despite the reduced number of studies in this field it was shown that theoretical predictions are quite well verified for blends of non-polar rubber [12].

In order to process such blends properly and with low energetic expenses, the viscosities of the blend constituents have to be adjusted by using processing aids [13 -15]. In general, such ingredients increase the free volume of the mixtures and facilitate cooperative chain movements as long as the additives are clearly soluble in the polymer phases [16]. Due to the fact that such additives are complex mixtures of low molecular weight compounds their impact on the compatibility of blends, the rheology and the crosslinking behaviour etc. are not well understood at the moment. In addition, the transport mechanism of low molecular components in rubber blends represents an important issue either for knowing the time to reach an equilibrium distribution in the discrete polymer phase or for establishing rules achieving homogeneous systems. This is important especially as far materials with special properties are concerned. However, data on diffusion and permeation of such substances in different rubber matrices are lacking. It is important to know how fast the distribution process in a given polymer or a blend system takes place. The distribution of the additives in multiphase elastomers is controlled by the compatibility between the components [16 - 19]. The successful choice of an additive has to be made with regard to the mixing, vulcanisation and processing steps in order to improve the mixing parameters, e.g. reducing mixing energy and time, increasing filler dispersion and lowering batch viscosity. On the other hand, it was observed that low molecular weight additives could improve the filler dispersion and distribution, reduce energy consumption in mixing and extrusion, and increase scorch safety. Above that, changes in damping behaviour can lead to improved wet traction without negative influence on rolling resistance [20]. Several investigations on additives were focused on studying the plasticizing effect, such as the reduction in viscosity and increase of low temperature flexibility of rubber parts with beneficial application in automotive industry [21 - 23].

On the other hand permeation of ingredients from lubricants, engine oils, cooling media in air condition systems through rubber membranes, sealing, tubes etc becomes increasingly more interest. For example, materials with a high resistance against fuel and oil are nowadays extensively researched in automotive industry because the regulations concerning the emissions of these components became more and more stringently enforced, particularly in developed countries such as USA, Germany and UK.

## 2. Aim of the work

As described in the previous section, blends of polymers are often used to meet special targets. Hereby, the final properties of a product are influenced by the compatibility between the components and by the distribution of the additives in the rubber phases.

With respect to this, a first goal of this work is to study the compatibility and phase morphology in blends of polydiene rubbers (non epoxidized and epoxidized rubber blends) by exploiting the interfacial tension as a thermodynamic ruler for the degree of compatibility. With the help of transmission electron microscopy (TEM) and dynamic-mechanical spectroscopy, it is intended to show the effect of polymer polarity on average domain size and the phase inversion region. Moreover, the study of the phase network connectivity gives the possibility of a quantitative estimation of the interphase volume fraction, which is responsible for ultimate properties of the blend under consideration.

However, the rubber performance is determined not only by the right choice of the main compounding materials used in the formulation but also by the low molecular components that are present. The transport process of these components between the polymer phases will give information about the plasticizing efficiency at low temperatures, solubility and viscoelastic properties of the rubber mixes. In order to accomplish this goal, the influence of well defined substances, which could be part of the complex mixtures of processing aids used in rubber technology on the low temperature properties of SBR rubber, will be investigated. Therefore, the effects of the linear  $C_{12}$  - and  $C_{18}$  - alcohols, acids and esters in the range of small concentrations will be studied (up to 6 phr). Information about the solubility of technically used processing aid in SBR rubber will be investigated through turbidity measurements, DSC and optical microscopy.

Further, considering the structure-property relationships, the transport processes of low molecular components, such as a homologous series of phthalates in (i) NBR with varying nitrile content, (ii) styrene butadiene rubber (SBR) with varying the vinyl content and (iii) hydrogenated nitrile rubber (HNBR) will be studied. The determination of the diffusion coefficient for the systems under investigation will be undertaken by means of "time-lag" method based on the ATR-FT-IR spectroscopy and swelling measurements. The following influences on diffusion coefficient will be evaluated:

1. the chain length of the alkyl groups of the low molecular components;
2. the content of nitrile groups in the matrix;
3. the chemical structure of the rubber (unsaturation / saturation);
4. the crosslinking density of the rubber matrix on diffusion coefficients.

The determination of the diffusion coefficient in dependency of temperature, which is comprehensively expressed by the activation energy, will be examined.

An additional goal of this work is the determination of the diffusion coefficient from permeation experiments as well as the permeation rate of low molecular components in rubber and rubber blends. In this respect, the following targets will be emphasized:

1. construction and validation of a measuring apparatus (the direct connection of a gas chromatograph with a permeation unit via an automatic multidirectional valve with specimen loop);
2. investigations of the parameters influencing permeation:
  - a) the acrylonitrile content and the crosslinking density of NBR rubber,
  - b) the filler type and various filler concentrations,
  - c) surface modification;
3. investigations, by means of swelling and the "time lag" method of the parameters influencing the diffusion coefficient:
  - a) the acrylonitrile content and the crosslinking density of NBR rubber,
  - b) the vinyl content and the crosslinking density of SBR rubber,
  - c) the NBR/SBR blend's phase morphology.

The last part of the work will discuss the relationship of oil exposition in rubbers and properties. The investigation will be done on several shaft seals used in industry considering swelling measurements, the modification of the mechanical properties as well as the damages that appeared after dynamical stress.

The research work performed in this thesis is schematically presented in the flow chart shown in *Figure 1*.

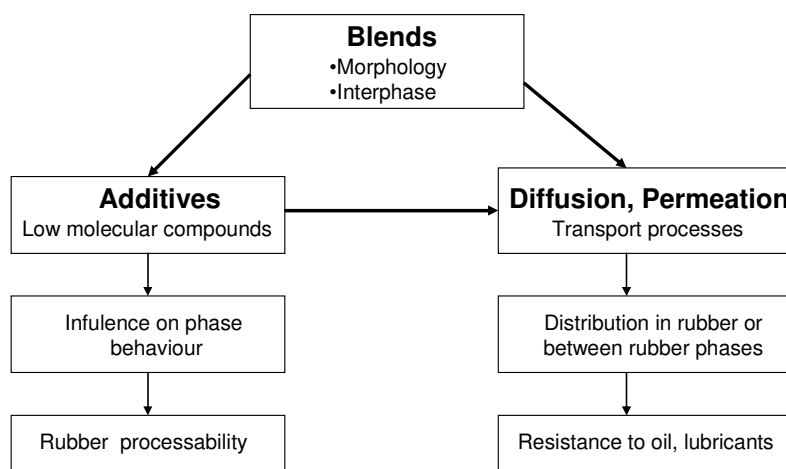


*Figure 1: Schematically representation of the work*



### 3. Theoretical background

Corresponding to the main issues of this work the following section will summarize the theoretical and methodical fundamentals as well as the actual state of knowledge.

#### 3.1 Compatibility of rubbers

##### 3.1.1 Theory of miscibility

Blending two or more polymers was successfully used to obtain compounds with desirable property combinations as an alternative route to the synthesis of new polymers [10, 15, 24]. The spectrum of polymers developed is large and by the choice of these materials, the properties profile of a multi-component system can be predicted. A tire is a representative example of such a complex system. It should be elastic, hard and soft in order to fulfil some contradictory properties like good traction on the street and high abrasion resistance. That means, a compromise should be found with a view of attaining the required demands. The formulations obtained represent a mix of properties characteristic to each component and describes a system, which is not compatible overall the whole range. In other words, after the mixing process the polymers used will be phase separated.

In very general terms, if a polymer blend in question possesses properties analogous to a single-phase material, the blend will be considered as a miscible one. By definition for a single-phase material the chemical composition as well as the bulk physical properties (density, expansion coefficient, mechanical moduli etc) does not change along an imaginary space coordinate. In case of a polymer blend this requires a dispersion of both constituents at a molecular scale. Blends of components having a single glass transition are commonly classified as miscible ones.

However, experience has shown that two-phase (or multiphase) blends exhibiting two (or more) glass transitions occur more abundantly. For these blends, each polymer or contributions of the two constituents form discrete domains with specific physical properties, which can be used at the same time as markers for the number of phases present in a blend system under consideration.

However, the length scale addressed by the glass transition corresponds to a few polymer coil dimension or at least to the size of a few chain segments. Miscibility in a thermodynamic sense is therefore not necessarily satisfied by the glass-transition criterion.

One major question is to define the heterogeneous two-phase system and contrast them from the single phase ones. Therefore, the main question to be addressed about any polymer blend system is whether the constituents are miscible or not. By definition, the term miscibility describes a single phase system over the entire concentration range under isothermal conditions. Therefore, miscibility is governed by the concentration dependency of the free energy of mixing ( $\Delta G_m$ ). One of the necessary conditions to be fulfilled is that  $\Delta G_m$  must be

negative for a system to be thermodynamically stable. In order to distinguish between single- and two-phase regions in a general phase diagram of a polymer blend (Figure 2) the second derivate of the free energy of mixing is required [4]:

$$\Delta G_m < 0 \quad \text{Equ. (1)}$$

$$\partial^2 G_m / \partial^2 \phi^2 > 0 \quad \text{Equ. (2)}$$

Single phase behaviour can be observed only if the two criteria are fulfilled. This is true for the two concentration regions in the phase diagram were one of the blend constituents is present in high concentrations. The region for which  $\partial^2 G_m / \partial^2 \phi^2 < 0$  is termed the miscibility gap. Two boundaries of the miscibility gap are formed by unstable compositions.

With increasing (or decreasing), the temperature the concentration range of the miscibility gaps may change. At a critical temperature, the system undergoes a transition into the single-phase region for which Equ.s (1) and (2) are fulfilled for any blend composition.

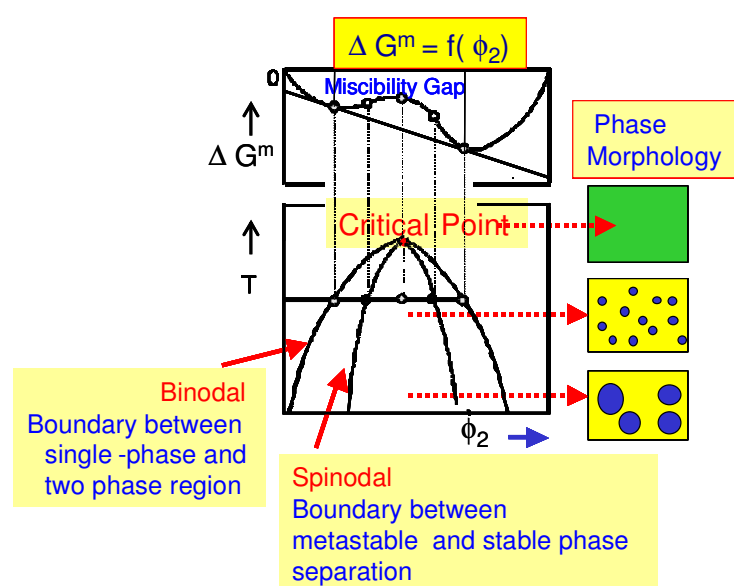


Figure 2: Phase diagram of a polymer blend: the variation of the free mixing energy  $\Delta G^m$  as a function of composition (in the upper part), the miscibility intervals as a function of composition and temperature (in the lower part). Scheme of corresponding phase morphology at the right side

The formation of the miscibility gap is a function of the composition as well as the temperature and represents the region where the systems are miscible (one phase system). Beyond the boundaries of this region, the phase separation occurs in the system. These boundaries are determined by the minimum of the free mixing energy as a function of composition.

The condition expressed in Equ. (1) is generally met if the entropy of mixing ( $\Delta S_m$ ) is larger than the enthalpy of mixing ( $\Delta H_m$ ) or if  $\Delta S_m$  is small but the mixing enthalpy is negative. This requires strong intermolecular interactions established by polar polymers. For positive values of  $\Delta H_m$  and small positive values of  $\Delta S_m$ , the phase separation is an inevitable consequence. This is the case for most of the blends of non-polar rubbers. However, miscibility can occur when the contribution of the mixing enthalpy ( $\Delta H_m$ ) is smaller than the contribution of the entropy of mixing.

The challenge in deriving theoretically an analytical expression for  $\Delta G_m$  is the modelization of  $\Delta H_m$ . In order to calculate  $\Delta S_m$ , Flory and Huggins [26 - 28] used a rigid lattice model. The combinatorial entropy of mixing was calculated for polymer-solvent system from the number of arrangements of  $N_2$  polymer chains and  $N_1$  solvent molecules in the lattice by using the Boltzmann equation. Taking into account that a polymer segment has at least two adjacent sites occupied by other polymer segments, the entropy of mixing  $\Delta S_m$  is given by the equation:

$$\Delta S_m = -k(N_1 \ln \phi_1 + N_2 \ln \phi_2) \quad \text{Equ. (3)}$$

where  $N_i$  is the number of the molecules and  $\phi_i$  is the volume fraction of the constituents.

The enthalpic contribution was considered by introducing interaction parameter between polymer segments and solvent. This parameter, which can only be experimentally determined [29], plays a decisive role, when blend systems are evaluated.

By extending the Flory-Huggins theory to polymer mixtures, Scott [30] and Tompa [31] calculated the free mixing energy on a volume basis, introducing an interacting segment volume. The free mixing energy of a total volume is determined by the Equ. (4) [30]:

$$\Delta G_m = \frac{RTV}{V_r} \left[ \sum \frac{\phi_i}{x_i} \ln \phi_i + \chi_{12} \phi_1 \phi_2 \right] \quad \text{Equ. (4)}$$

where  $x_i$  is the degree of polymerisation.

It can be seen that the entropy contribution decreases with the degree of polymerization according to a hyperbolic function. Miscibility can be achieved for high molecular weight non-polar polymers only if  $\chi$  is very small or at least zero.

Commercial rubbers are generally high molecular weight polymers with low and medium polarity. When they are mixed together they form blends that are typically not miscible in the thermodynamic sense and demonstrate very large miscibility at ambient as well as at the processing temperatures.

Among the thermodynamically miscible rubber blends the system NR/1,2 BR has to be mentioned. Due to the similar polarisability of cis 1,4-isoprene units and 1,2-butadiene units as well as similar thermal expansion coefficients of both polymers the  $\chi$  parameter of this system tends to zero [11]. In case of increasing dissimilarity of the chain segments the  $\chi$  parameter

increases above a critical value and phase separation cannot be avoided even at intensive mechanically mixing.

The  $\chi$ -parameter is an important tool for quantifying the degree of compatibility of polymers. One very useful application is the estimation of the interfacial tension in phase-separated blends. In any heterogeneous blend system, an interdiffusion process driven by the enthalpic and entropic contributions builds up a finite interphase. The interdiffusion process takes place until the critical  $\chi$ -parameter is reached.

The interfacial tension, which arises mainly from the difference in polarities of the two polymer phases, was theoretically shown to be proportional to the square root of the polymer-polymer interaction parameter  $\chi$  [32].

$$\gamma = \rho_0 RT \sqrt{\frac{\chi \langle R_g^2 \rangle}{N}} \quad \text{Equ. (5)}$$

where  $\rho_0$  is the average segment density,  $\langle R_g^2 \rangle$  is the squared average radius of gyration,  $N$  is the number of the statistical chain segment and  $\chi$  is the polymer-polymer interaction parameter. In any heterogeneous blend system a finite interphase will be occurs due to the enthalpic and entropic contributions. The equilibrium thickness of the interphase  $a_{IPH}$  is shown to be inversely proportional to the interaction parameter  $\chi$  or to the solubility parameter difference [12]:

$$a_{IPH} \approx \frac{1}{\sqrt{\chi}} \quad \text{Equ. (6)}$$

Basically, improving the compatibility between the blend constituents increases the thickness of the interphase [33].

As far as blends of non-polar polymers are concerned it was shown that the  $\chi$ -parameter decreases with increasing the occurrence of temperature [34]. In some cases, an upper critical solution temperature (UCST) was observed [35]. As shown for  $\chi$ -parameter, the interfacial tension of non-polar blends systems decreases nearly linearly with temperature. This temperature dependency certainly affects the phase morphology of rubber blends processed or stored at different temperatures. Above of the influence of the interfacial tension the phase morphology of a blend is controlled by the viscosity of the matrix, the viscosity ratio of the components and the share rate employed during mixing. Especially, the viscosity is responsible for the formation of the average domain size ( $\bar{d}$ ) of the dispersed phase during mixing. Thus, the interfacial tension controls the morphology development. For dispersed phase morphology the resulting domain sizes can be described as follows [36]:

$$\bar{d} = c(\gamma/\eta_m)^* f(\eta_m/\eta_d)^* dV_x/d_y \quad \text{Equ. (7)}$$

where  $\gamma$  is the interfacial tension,  $\eta_m$  is the viscosity of the matrix,  $\eta_d$  is the viscosity of the dispersal phase and  $dV_x/dy$  is the shear rate.

During the mixing of rubber blends, the dispersed domains are deformed during passage through the high shear regions and will be broken up to small particles. However, these particles collide and often coalesce to form large dispersed domains [37] and a transient phase boundary in the system is reached. As a matter of fact, the break-up is closely related to the stress level exerted on the particle by the flowing matrix and the number of the particles produced upon break-up is depending on not only on the external forces but also on the relative viscosity of the components of the system [38]. As the external stress in the blend is vanished, the transient phase boundary becomes its stability again.

### 3.1.2 The solubility parameter concept

The difficulties in determining the  $\chi$ -parameter can be avoided by using the approach introduced first by Hildebrand. The solubility parameter  $\delta$  was demonstrated to be a useful quantity for the characterisation of the strength of interaction of low molecular weight substances [39]. The extension to polymer-polymer systems was popularised by Bohn [10]. The solubility parameter is defined as the square root of the energy of vaporisation per unit volume of material (cohesive energy density). It is given by the following equation [39]:

$$\delta = \left( \frac{\Delta E^V}{V} \right)^{\frac{1}{2}} \quad \text{Equ. (8)}$$

The attractiveness of this concept was its ability to characterize a mixture by using the component properties only. Consequently, the interaction parameter  $\chi$  for a blend can be calculated by the Equ. (9) [39]:

$$\chi = (\delta_2 - \delta_3)^2 V / RT \quad \text{Equ. (9)}$$

Further, a relationship between the solubility parameter and the enthalpic contribution can be made through the following equation:

$$\Delta H_m = V(\delta_2 - \delta_3)^2 \phi_2 \phi_3 \quad \text{Equ. (10)}$$

The difference of the solubility parameters is a measure of the interaction that takes place between the segments of the polymers. The miscibility in the system is reached when  $\chi \approx 0$ , that means the difference of the solubility parameters tends to zero. Thermodynamic similarity of the blend constituents is a prerequisite for a miscible blend.

#### *Determination of the solubility parameter*

The solubility parameter of a polymer cannot be directly determined because the polymers cannot be vaporized without thermal decomposition. Indirect methods as swelling [40, 41],

inverse-gas chromatography [42], intrinsic viscosity [43], osmotic pressure [44] as well as correlation methods as refractive index [45], group contribution methods [46] or theoretical calculation using the increment method [47], were used to calculate the solubility parameter. The solubility parameter is represented as the same as that of a solvent in which a polymer is mixed in different proportion and takes place without heat effect and volume change.

#### *Increment method*

The estimation of the solubility parameter by increment method can be calculated from the structural formula of the substance and its density taking into consideration the molar attraction constants (F) which are given in tables after Small [43] and Hoy [47]. The molar attraction constants are additive and are related to the solubility parameter through the following equation:

$$\sum_i F_i = \delta \frac{M}{\rho} \quad \text{Equ. (11)}$$

where  $\rho$  represents the density, M is the molecular weight.

#### *Equilibrium swelling*

The method consists in determining the swelling degree of the slightly crosslinked polymers in different solvents with known solubility parameters. The solvents have to exhibit chemically similar structures, such as, homologues. The degree of swelling in the state of equilibrium swelling is plotted versus the solubility parameters of the solvents used. The point of maximum swelling can be taken as the solubility parameter of the polymer. The swelling degree, Q, is defined by equation [40]:

$$Q = \frac{V_P + V_{\text{Solvent}}}{V_P} \quad \text{Equ. (12)}$$

where  $V_P$  is the polymer volume before swelling and the  $V_{\text{Solvent}}$  is the volume of the solvent taken during swelling. Typical results for different solvents are shown in Figure 3.

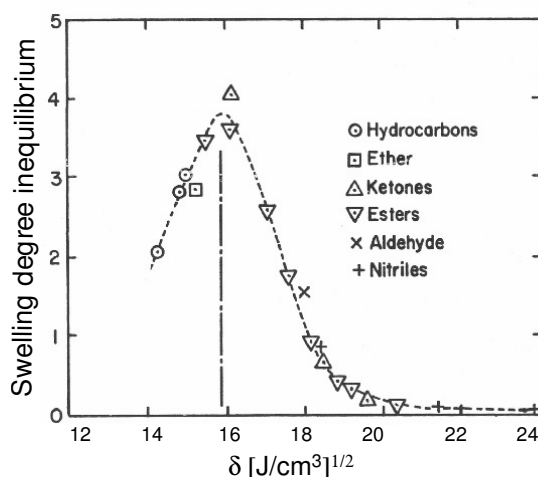


Figure 3: Swelling degree of NR in solvents with different solubility parameters [48]

*Intrinsic viscosity*

Another method used for the determination of solubility parameter is the intrinsic viscosity of the polymer in different solvents, with the condition that the polymer under investigation is soluble in them. An example using this method for polyisobutene (A) and polystyrene (B) is presented in Figure 4 where the intrinsic viscosity is plotted over the solubility parameters of various solvents.

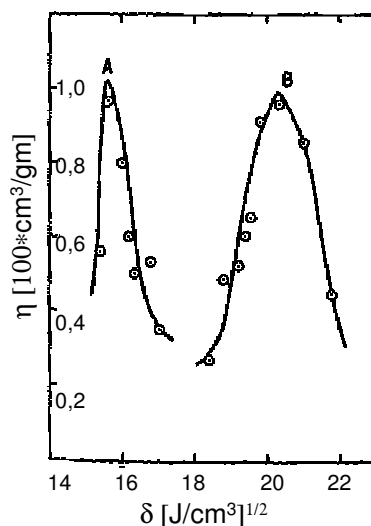


Figure 4: Determination of the solubility parameter using the intrinsic viscosity [41]

The intrinsic viscosity is related to the chain expansion coefficient and the polymer molecular weight [29]. The chain expansion factor is related to the polymer-solvent interaction parameter in the Flory–Huggins theory. If the chain conformation is most extended in the best solvent the hydrodynamic volume tends to a maximum value and the intrinsic viscosity will be highest.

*Inverse gas chromatography*

This method was used by many researchers for determination of the solubility parameter at infinite dilution [49 - 54]. An advantage of this method is that it allows measurement of the thermodynamic values since the columns are prepared properly. The polymer represents the stationary phase in the gas chromatography column. The solubility parameter is related to the specific retention volume of the solvent in the column. The molar volume ( $V_i$ ) which can be determined from the density equation given in literature as well as the enthalpy of vaporization ( $\Delta H_i$ ) that can be calculated at the experimental temperature, must be known at the temperature of the column [51].

Through this method, the solubility parameter can be obtained at infinite solution over a temperature range. This is important for the prediction of phase equilibrium at higher temperature [55].

### 3.1.3 Analysis of blend morphology

It is appropriate to describe the methods used for the characterisation of the blend morphology considering that for both elastomer-elastomer and elastomer-plastic different methods vary in their effectiveness, depending on the combination are involved. A first group of these methods are direct methods like transmission electron microscopy (TEM), scanning electron microscopy (SEM) and of increasing importance these days atomic force microscopy (AFM). They offer a direct view of phase structure and domain size distribution. The second group are the indirect methods which emphasis a physical properties such as the mechanical modulus, the caloric capacity, the dielectric constant  $\epsilon'$  and the dielectric loss factor  $\epsilon''$ . In this group of methods, the dynamic mechanical analysis (DMA) as well as the calorimetric methods is predominant. Another group of methods used for the investigation of the blend morphology is represented by the spectroscopic techniques that examine microstructural aspects of polymers and the chain involved in the interaction. This includes the infrared spectroscopy (IR), nuclear magnetic resonance spectroscopy (NMR), ultraviolet spectroscopy. An elegant mode of studying a blend was done also by using scattering methods such as light scattering method, pulse-induced critical scattering (PICS), neutron scattering method and X-ray scattering. By these measurements the irradiation usually results in scattering of part of the incident intensity, so that the energy and propagation vectors of the scattered waves may differ from those of the incident radiation. However, the angle dependence of the elastic scattering provides morphological information. X-ray and neutron scattering all result from heterogeneities in the structure of the irradiated material.

#### *Direct methods*

The presence of two phases in a blend was used as a preliminary indication of the degree of miscibility in a polymer-polymer system. The most widely method used for polymer-polymer studies was TEM. By investigated the PVC/NBR system with 40% acrylonitrile by means of TEM a heterogeneous system was found although only one glass transition was observed [56]. Electron microscopy was also used in studies of gum- and black filled elastomer blends [57, 58]. Elastomer-plastic blends are somewhat easier to identify in electron microscopy than elastomer-elastomer system as stains like osmium tetroxide can be used for contrast. Different researches were done on rubber reinforced with polystyrene using this method [59, 60]. In a recent work, by investigating the phase morphology of i-polypropylene (iPP)/acrylate rubber (ACM) and polyamide (PA)/ACM systems by means of AFM it was shown that blends of iPP with polar rubbers should be improved by the use of an "in-situ" generation of compatibilizers, whereas for PA based blends phase compatibilization does not play an important role but it could be used as an option for further property optimization [61].



*Indirect methods*

The calorimetric methods are used to determine the glass transition of polymers and their respective blends. The most common instrument is the differential scanning calorimetry (DSC) which measures the amount of heat required to increase the sample temperature by a value  $\Delta T$  over that required to heat a reference material by the same  $\Delta T$ . Extended studies using this method were done also by investigating the phase stability in heterogeneous compositions of NBR [62], or studying polyurethane block polymers [63].

Another method used extensively by various authors was dilatometry when a correlation of glass transition with chemical structure of the polymer was done [64]. The two-phase behaviour of a blend of syndiotactic poly(methyl methacrylate) ( $T_g=120^\circ\text{C}$ ) and isotactic poly(methyl methacrylate) ( $T_g=45^\circ\text{C}$ ) was determined by considering the two discontinuities in the derivate curve  $dV/dT$  corresponding to the  $T_g$ 's of the respective phases [65].

Mechanical methods for determination of the transition behaviour of polymer and polymer blends were cited more frequently than the other techniques. The dynamic-mechanical spectroscopy performed on crosslinked rubber blends exploits the different mechanical moduli of the discrete rubber phases. It was considered an indirect measure at least for the number of polymer phases in the blend and to some extends for the supramolecular periods a detailed picture of the supramolecular structure of a blend, if one assumes that a sufficient optical contrast is provided by the chemical nature of the polymers. Assuming that the polymer domains exceed a critical size the corresponding phase demonstrates a typical glass transition, which is characterized by a maximum value of the mechanical energy dissipation. This glass transition process is recorded as a maximum of  $G''$  (damping maximum). Thus, if the temperature dependency of  $G''$  is considered, it can be evaluated whether or not the blend contains one or more phases. However, if the temperature difference between the glass transitions of the blend constituents is small, the assignment becomes uncertain.

There are in principle four distinct cases which can appear when blend morphology is examined from  $G'(T)$  or  $G''(T)$ -curves. Figure 5 describes schematically the variation of the modulus with temperature from the investigations of multi-phase systems by means of DMA taking into consideration the dependency on the solubility of the polymers.

The diagrams illustrated in Figure 5 indicate four characteristic situations:

- a) non-miscible system [7];
- b) miscible system [66];
- c) partial soluble system [4];
- d) meta stable system [67].

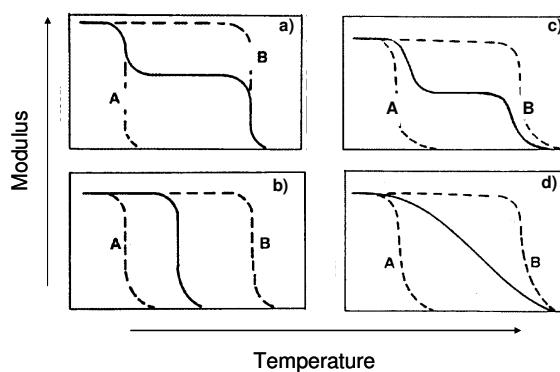


Figure 5: Schematic representation of the phase transition in multi-phase systems [68]

If by mixing of two components, two  $T_g$ 's that coincide with those of the pure components appear, the system is not miscible (Figure 5 a). The presence of a single  $T_g$  in a rubber blend is characteristic for the totally miscible system (Figure 5 b). Two discrete transition levels that can occur between the range defined by the  $T_g$ 's of the pure components is characteristic to the partial soluble system (Figure 5 c) and if only one glass transition occurs but the transition stretches over a very broad range between the  $T_g$  of the pure components, the system is meta stable system but consists of more phases with different compositions (Figure 5 d).

The electrical properties of polymers are analogous to mechanical properties in that the dielectric constant  $\epsilon'$  is similar to compliance, the dielectric loss factor  $\epsilon''$  is similar to the mechanical loss and the dielectric strength is analogous to tensile strength. Dielectric relaxation measurements provide data for characterisation of blends. A wide range of frequencies can be used. This makes possible the determination of the dielectric constants as a function of temperature over many frequencies or as a function of frequency at given temperatures. Using this method studies of blends of cis-BR with NR and SBR [69], blends of PVC/ poly (ethyl vinyl acetate) EVA were done [70].

### *Spectroscopic methods*

In application of these methods to polymer systems those methods will show that systems with high miscibility will produce spectra showing strong deviation from an average of the spectra of the two components. The degree of deviation of miscibility cannot be predicted but these methods provide information on the specific interaction between polymers and can indicate possible ways of improving miscibility.

$^1\text{H}$  NMR spectroscopy on polymers confined to studying the spin-spin and spin-lattice relaxation process as a function of temperature and composition [71]. The spin-lattice relaxation time is called  $T_1$  while the spin-spin relaxation time is named  $T_2$ . The advantage of this method consists on that the signal is independent on the shape and interconnectivity of the phases in a two phase system. The heterogeneity of filled elastomers [72] or molecular motion in block

copolymers [73] was researched using this method. In another work was shown that broad line NMR is a sensitive tool for detection of small amount of soft phase imbedded in a hard matrix. This is due to the fact that the resonance of protons in the soft phase is relatively sharp compared with the resonance band of the matrix protons [74].

Infrared spectroscopy was often used in analysis of polymer mixtures such as polyurethane in polyester or polyethers [75] or sulphur cured SBR/BR blends [76]. Infrared and ultraviolet spectroscopy on blends of PS/PPO provided valuable information led to the following conclusions: PPO is loosely packed in the glassy state and the addition of PS reduces the free volume. The chains of both components are interpenetrating significantly, which means a high miscibility of the system. The reason is a strong interaction between the phenylene group of the PPO with the phenyl group of the PS [77].

### *Scattering methods*

Irradiation of matter results in scattering of part of the incident intensity so that the energy and the propagation vectors of the scattered waves may differ from those of the incident radiation. The morphological information are provided by the angle dependence of the elastic scattering while the energy dependence of the scattering is related to dynamic process in the scattering medium. Light scattering, neutron scattering and X-ray result from heterogeneities in the structure of the irradiated material.

In a multiphase polymer system, the angle dependence of the scattering reflects the size and the spatial distribution of the phases and can be used for investigation of the phase morphology [78]. In a homogeneous system, responsible for the scattering are thermal fluctuations in density and composition, the extrapolated zero-angle intensity represents a measure of the polymer-polymer interaction parameter [79].

While light scattering is sensitive to concentration and density fluctuation, X-ray to density fluctuation, the neutron scattering measures the differential neutron scattering cross section of small concentrations of protonated polymer dispersed in a matrix of deuterated polymer. Because of this the conformation of the polymer can be determined with high precision. Important studies were done in the area of small-angle neutron scattering (SANS) where the structures investigated were similar to those in small-angle X-ray studies (SAXS). In a PVC / poly( $\epsilon$ -caprolactone) PCL blend with a PVC concentration range varying from 0 to ~ 60%, X-ray studies provided information about the repeat period of poly( $\epsilon$ -caprolactone) PCL lamellar structures, the thickness of the PCL crystalline layer and the thickness of the amorphous layer which contain both PVC and PCL [80].

In a blend consisting of two polymer components, each with different physical characteristics like mechanical moduli, glass transition temperatures, expansion coefficient, and the presence of the phases is described by the occurrence of these characteristics.

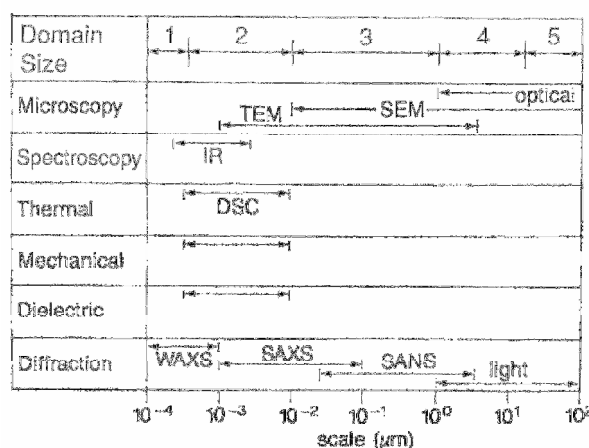


Figure 6: Experimental techniques used to study the blend morphology [4]

The numbers of phases present in the blend, the homogeneity of the polymer blends as well as the partial solubility of the components can be studied with the help of the methods above described and are briefly presented in Figure 6. They characterize the compatibility of polymer blends from micro to macro scales.

#### 3.1.4 Evaluation of the interphase in rubber blends

The number of the polymer phases present in a rubber blend can be investigated by dynamic mechanical method by recording the damping peaks ( $G''$ ) along the temperature axis. Careful analysis of the peaks with one or more shoulders indicates the presence of discrete phases. In such cases the signal of the minor component can be de-convoluted from  $G'$  or  $G''$  trace.

In a multiphase structure, the interphase is situated at the rubber-rubber contact surface and its formation is determined by the phase boundary and depends on the interaction between polymer segments. It is known that the interfacial tension between two polymers is correlated to the free energy that is required for the formation of the interphase between two polymers. Some studies shown that a linear relationship between the interfacial tension and the difference of the solubility parameters of the components exists [54, 81].

Based on the quantitative analysis of the loss modulus  $G''$  in the glass transition region of the blend, the structure of the interpenetrating phase networks was described [82]. The volume fraction of the interphase in rubber blends is an important issue and delivers information about the miscibility of the components of the blend.

Microscopic methods such as TEM [58], SEM [83], and of increasing importance these days AFM offer a direct view of the sharpness of the polymer blend interphase [84].

In recent work the prediction of the interphase in polymer blends was done, considering the quantitative analysis of the loss modulus  $G''$  in the glass transition region of the blend. It was assumed that with decreasing temperature one phase undergoes a glass transition while the other remains fluid, then the elastic modulus of the blend is dominated by that of harder glassy

phase. The results of the investigation done on EPDM/BR and NR/SBR blends demonstrated that the storage and loss modulus of rubber blends exhibit a critical behaviour with respect to the blend ratio that can be related to the formation of a phase network [85].

A quantitative estimation of the interphase in rubber blends was done by employing dynamic mechanical investigations as shown schematically in Figure 7. The experimental loss modulus - temperature curve is reconstructed by the contributions of the pure polymer phases (A and B) by using a parameter-modified spline fit function of the single polymers (A, B) [82]. The spline parameters considered are the amplitude, the broadness and the temperature shift of the damping maximum in the blend. A fit of the experimental curve of the blend A/B can be achieved by varying the parameters of the A-phase and B-phase splines for the best-fit temperature range until the first damping maximum is reached and above the temperatures where the second damping maximum occurs. The deviation of the fit obtained from the experimental curve in the region between the two damping maxima indicates excess, which cannot be predicted from the contributions of the blend constituents. Only assuming an interaction between the blend constituents that leads to an interphase allows this third contribution to the blend loss modulus to be explained.

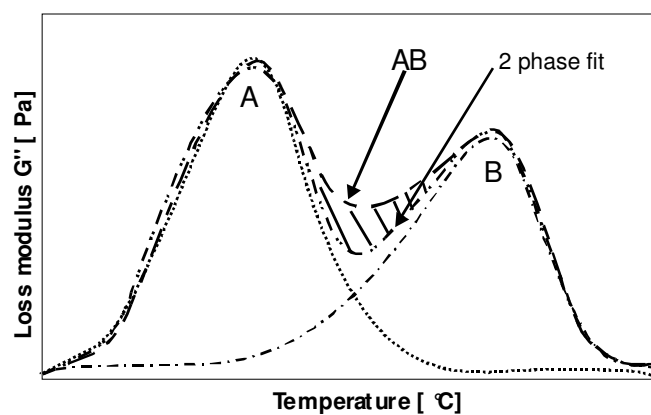


Figure 7: Fitting procedure for an unfilled blend AB. The shaded area between the experimental data (AB) and two-phase fit is considered as interphase signal

Thus, the excess represents the signal of the interphase with a discrete contribution to the glass transition and the corresponding damping behaviour not shown for the single polymers A and B. The method has its limitations as much as the damping maxima at the glass transition of the blend constituents can be deconvoluted.

With this method, the volume fraction of the interphase  $\phi_{IPH}$  can be evaluated. It was assumed that the amount of the interphase is proportional to the contact probability of the two phases that is given by the product of the volume fractions of the rubbers  $\phi_A$  and  $\phi_B$ . At low concentrations and high viscosity of one phase, the component represents the dispersed phase with separated

domains located in the continuous phase. Increasing the concentration and decreasing the viscosity the neighbouring domains tend to flow together. Above a critical concentration a co-continuous phase structure occurs and may be seen as an interpenetrating network of the different phases.

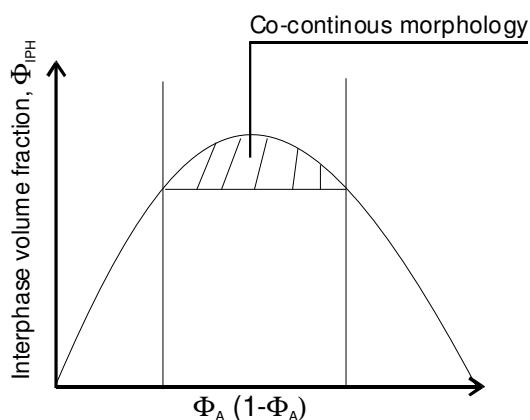


Figure 8: Interphase signal vs. volume fraction of the rubber

The volume fraction of the interphase depends on the degree of compatibility, the temperature and the blend composition. It was shown that the interphase of crosslinked blends is higher than of uncrosslinked ones. If the blends are compatible the dimension of the interphase is up to 15-20 nm and if a poor compatibility between the blends components occurs the dimensions of the interfacial layer is reduced to 1-1.5 nm.

### 3.2 Interaction of rubber with additives

The rubber processing can be improved by the addition of small quantities of low molecular weight substances, named additives. As far these components are soluble in the rubber, respectively in rubber mixtures the free volume in the system can be increased as much that physical and rheological properties are changed [86 - 90].

Thus, the addition of additives determines the decreasing of the glass transition temperature, reduces the viscosity of the rubber, and leads to the changes of the frequency dependency of dynamic mechanical properties of rubber melts as well as their corresponding crosslinked material. These effects are caused by changes in the intermolecular interaction between the polymer chains while chain segments undergo energetically beneficial interactions with the additives molecules.

The decrease of the glass transition is directly correlated with the amount of the soluble low molecular weight additive present in the mix and an estimation of the  $T_g$  evolution can be predicted from the equation [91]:

$$1/T_g = w_1(1/T_g)_1 + w_2(1/T_g)_2 \quad \text{Equ. (13)}$$

where  $w$ 's are the mass fractions of component 1 and 2.

Taking into consideration the chemical structure, polarity and molar mass of the additives, the equilibrium distribution of the additive concentration between the phases of a rubber blend can be evaluated by means of the solubility parameter concept. It was shown that the addition of oligomers with defined chain length and chemical constitution to a rubber phase changes the solubility parameter of entire phase [92, 93]. Consequently, the partition of the additives in both phases of blends of non-polar rubbers leads to a predictable reduction of the  $\delta$ -parameter difference. In such cases the additives exerts a phase compatibility effect.

### 3.2.1 The free volume theory

The segment movements in a melted polymer can take place if in the system exists sufficient free volume [94 - 96]. The free volume is supplementary to the hardcore volume of the polymer the space where the polymers can do rotation and translation movements. A decrease in the temperature lowers these movements and simultaneous through the free spaces or "holes" the free volume in the system decreases. The free volume can reach a critical value when the temperature decreases and leads to its contraction. At this temperature, there is not sufficient free space to allow large motion of the segments. These considerations represent the background of the free volume theory.

The temperature where the critical value of the free volume is reached is the glass temperature. At this temperature, the total volume of the sample  $V_g$  is considered to be given by the volume occupied by the polymer molecules in the glassy state  $V_0$  at 0 K, the free volume  $V_f$  and the increased volume, which changed with the temperature (Figure 9).

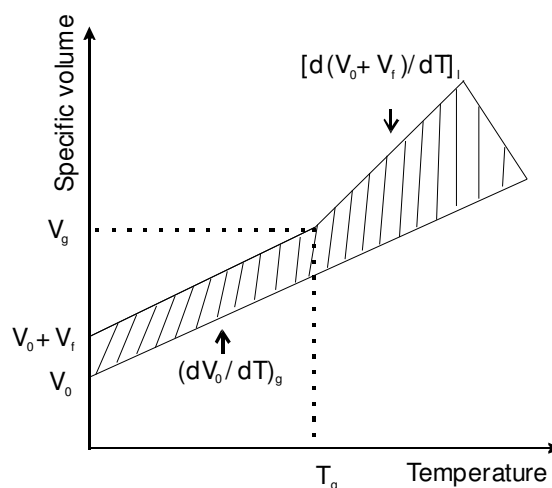


Figure 9: Schematic representation of the free volume at 0 K

Above the  $T_g$ , the distance between the segments increases due to the formation of new holes in the system. In the melted state, the total volume of the polymer  $V_l$  is delivered by the polymer

volume  $V_g$  at the glass transition and the increased volume through the expansion of the glass and the free volume.

$$V_g = V_0 + V_f + \left( \frac{dV}{dT} \right)_g T \quad \text{Equ. (14)}$$

$$V_l = V_g + \left( \frac{d(V_0 + V_f)}{dT} \right)_1 (T - T_g) \quad \text{Equ. (15)}$$

Simha and Boyer [97] used the relationship between the glass transition temperature and the difference in expansion coefficients above and below the glass transition

$$\alpha_l = (1/V_g) (dV/dT)_l \quad \text{Equ. (16)}$$

$$\alpha_g = (1/V_g) (dV/dT)_g \quad \text{Equ. (17)}$$

for the calculation of the free volume fraction in the total volume:

$$f_g = (\alpha_l - \alpha_g) T_g = V_f / V_g = 0.113 \quad \text{Equ. (18)}$$

It was suggested that the free volume fraction is the same for all polymers, i.e. 11.3 per cent of the total volume in the glassy state.

### 3.2.2 Influence of the additive on the glass transition temperature

A polymer sample can be made more flexible by lowering its glass transition. This can be achieved by incorporating low molecular components in the material. A linear decrease of  $T_g$  versus temperature is observed and the slope obtained deliver information about the plasticizing efficiency ( $\Delta T_g / \Delta c$ ). The plasticizing efficiency is defined as the decrease in  $T_g$  provoked by the concentration unit (in mole). As it was described in reference [98] in more detail, this parameter is valid for single-phase systems only and should be considered at very small concentrations of an additive.

DSC-thermograms give valuable information about the variation of the glass transition with concentration of the additive. Two cases of phase behaviour can be noticed:

1. Miscible systems which show only one glass transition at any concentration;
2. Partially soluble system that demonstrates a linear decrease of the  $T_g$  up to a critical solubility limit. When this limit is reached the glass transition does not depend any more on concentration. Above this limit, the glass transition remains constant.

Figure 10 gives examples of the two groups of phase behaviour. In Figure 10a a continuous decrease of the glass transition can be seen, if the concentration of the hydrocarbon increases and means that the decaline is soluble in EPDM.



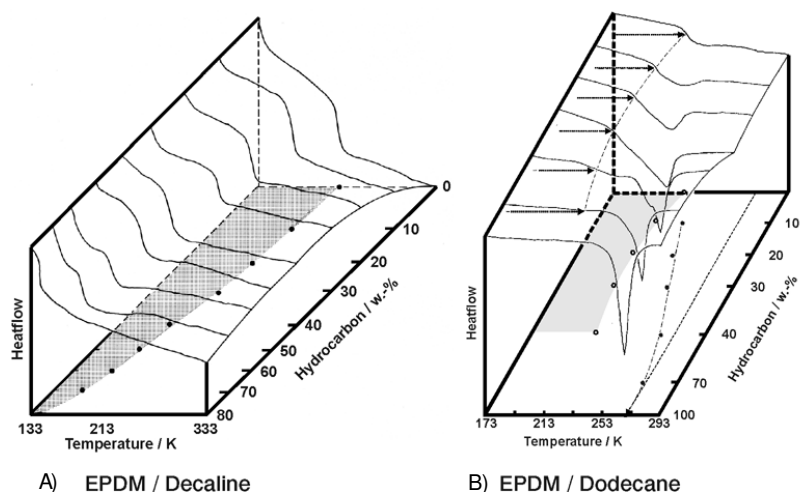


Figure 10:  $T_g$ -concentration-phase diagrams [99]

Opposite to this case, dodecane decreases the glass transition of EPDM until a critical solution concentration is reached and the signal of melting enthalpy becomes obvious and increases in intensity (Figure 10b). Above this critical concentration, the glass transition remains almost constant.

### 3.2.3 Influence of the additive on the viscoelastic properties

The viscoelastic materials are materials that respond to external forces in a manner between an elastic solid and a viscous liquid.

A material is considered ideal elastic if it returns completely to its original dimensions by the stress removal. Hooke's law describes this phenomenon by Equ. (19), showing that the strain is proportional to the stress:

$$\sigma = G \varepsilon \quad \text{Equ. (19)}$$

where  $\sigma$  is tension,  $\varepsilon$  is deformation and  $G$  is tensile modulus (Young's modulus) if a stress-strain experiment is considered.

An ideal fluid has no elastic character and it is described by the Newton equation:

$$\sigma_s = \eta \frac{d\gamma}{dt} = \eta \dot{\gamma} \quad \text{Equ. (20)}$$

where  $\eta$  is the viscosity and  $d\gamma/dt$  the applied shear rate.

The linear viscoelastic properties can be predicted by means of different models like: Maxwell, Voigt, Maxwell-Wiechert and Voigt-Kelvin which are based on a set of characteristic relaxation times when the chain length and the chemical constitution of a polymer are taken into consideration [100, 101].

Maxwell's model (Figure 11 a) consists of a single spring attached in series to a damping cylinder (dashpot) while the Kelvin-Voigt model (Figure 11 b) is based of a parallel arrangement of spring and dashpot.

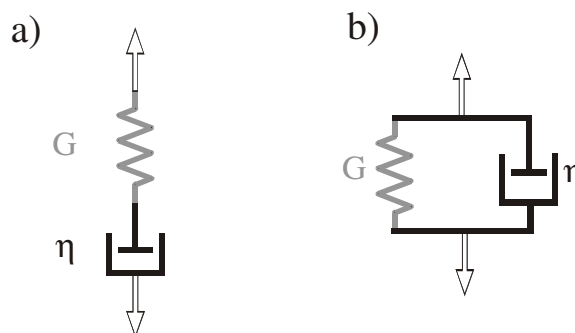


Figure 11: Mechanical models: a) Maxwell and b) Kelvin-Voigt [101, 102].

The Maxwell model offers the possibility to study the viscoelastic behaviour as a function of frequency and is described by the combination of an elastic response characterized by the elastic modulus  $G$  and a viscous response characterised by the viscosity  $\eta$ . The two units are connected in series and the deformations of the elastic and viscous components are additive and expressed by Equ. (21) [103]:

$$\gamma_{tot}^* = \gamma_{el}^* + \gamma_{vis}^* \quad \text{Equ. (21)}$$

Considering the equation which describes the tension:

$$\sigma_{el}^* = G \dot{\gamma}_{el}^* , \quad \sigma_{vis}^* = \eta \dot{\gamma}_{vis}^* \quad \text{Equ. (22)}$$

can be written for a viscoelastic material the Equ. (23):

$$\dot{\gamma}_{tot}^* = \frac{\sigma_v^*}{\eta} + \frac{\dot{\sigma}_{el}^*}{G} \quad \text{Equ. (23)}$$

The frequency sweep of dynamic mechanical moduli delivers valuable information about the viscoelastic properties. If the frequency dependency of  $G'$  and  $G''$  is considered four characteristic zones on the frequency scale become evident (Figure 12): the terminal zone, the plateau zone, the transition zone and the glassy zone.

In the entire terminal flow zone  $G''(\omega)$  has a higher value than  $G'(\omega)$ . All uncrosslinked and mono-disperse polymers demonstrate at very low frequencies similarities which scale in a characteristic way with the molecular weight. The polymer behaviour in the terminal zone is theoretically well described by models, which assume entangled chains.

The tube model was proposed by de Gennes [104] and later reformulated by Doi and Edwards [105]. According to this model the polymer chain goes through an imaginary tube. The time necessary to snake out from the imaginary tube is named relaxation time ( $\tau_M$ ) and was calculated according to following equation:

$$\tau_M = \frac{\eta}{G} \quad \text{Equ. (24)}$$

Considering the frequency dependency of modulus was theoretically predicted for mono-disperse polymers [105]:

$$G_{(w)} = G_N^0 \frac{8}{\pi^2} \sum_{p=1,3,5}^{\infty} \frac{1}{p^2} \frac{-p^2 t}{\tau_M} \quad \text{Equ. (25)}$$

For very small deformation frequencies,  $\omega \rightarrow 0$ , and  $p = 1$  the storage modulus become proportional with  $\omega^2$  whereas the loss modulus is increasing with the frequency  $\omega$  by the power of 1.

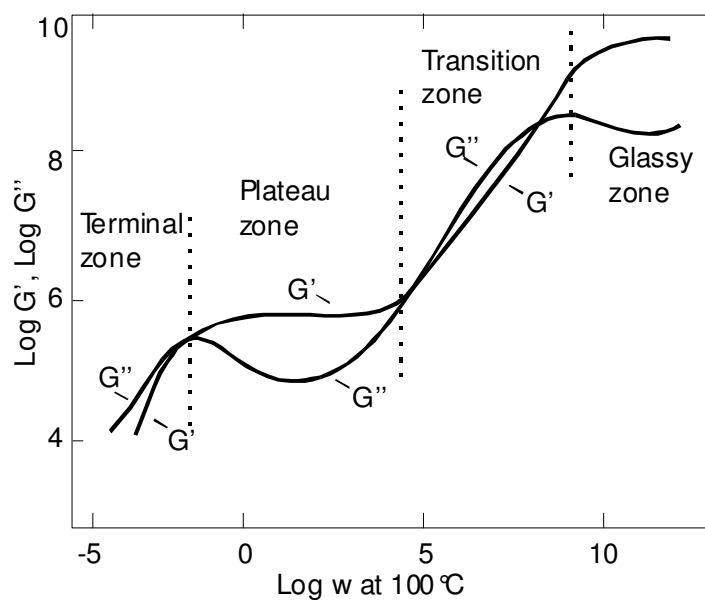


Figure 12: An idealized stress relaxation master curve [101, 106]

In both functions the plateau modulus  $G_N^0$  specifies the molecular weight independent modulus of the entanglement network in a time scale (or frequency) where entanglements are not slipping. The plateau modulus is expressed as follows:

$$G_N^0 = \frac{4\rho RT}{5M_e} \quad \text{Equ. (26)}$$

where the  $\rho$  is the density of the polymer,  $M_e$  is the entanglement molar mass (between neighbouring entanglements),  $R$  is constant of the gases and  $T$  is the temperature.

The boundary between the terminal zone and the plateau region is clear cut if mono-disperse polymers are considered and is called crossover point. At frequencies above this point the maximum of  $G''(\omega)$  and the  $G'(\omega)$  changes little with frequency, but  $G''(\omega)$  passes through a minimum. This behaviour is explained by the model that entangled chains form a temporary network. With increasing chain length, the probability to form entanglements increases. Therefore, the width of the plateau zone is enlarged. With regard to technical polymers with broad molecular weight distribution, a less flat plateau zone is observed [107]. The height of the plateau is specified in terms of the molecular weight-independent plateau modulus  $G_N^0$  and it

was found that  $G_N^0$  decreases with the amount and the size of chain side groups [108]. In the transition zone both viscoelastic functions  $G'$  and  $G''$  strongly increases with the frequency, but  $G'$  is normally higher than  $G''$ . At very high frequencies, no configuration of the polymer chains can occur within the period of oscillation but most of the energy is dissipated. This issues becomes more importance since it is known that this process play a decisive role for tire traction. In the glassy zone, no configurational rearrangements of chain backbones occur within a period of oscillation. The stress response for a given small strain is very high.

### 3.3 Transport processes in rubber

#### 3.3.1 Permeation and diffusion processes

Permeation is understood to be the passage of a gaseous or fluid substance through a nonporous solid. Permeation is defined as the process in which the components are transported in rubber than the process leads finally to a state of equilibrium in which concentration becomes equal in each volume element of the system under isothermal conditions. Further, the components diffuse to a region of lower concentration where the components can again evaporate.

The permeation is governed by two independent physical processes: the solubility of the low molecular component and its diffusion in rubber. The purpose of the permeation studies of low molecular component is to obtain information about the transport mechanism of those substances involved in a given system.

However, during the last decades information of this subject was obtained, both experimental and theoretical [109 - 115], and it became apparent that the determination of the diffusion coefficient in polymers showed sometimes inaccurate values which could not be explained. As a mater of fact, many studies should be further done in order to obtain more accurate results, high performing permeation equipment should be developed in order to acquire results with higher precision [116,117]. Another reason for development precise permeation measurements techniques is due to the new restrictive regulations concerning the amount of evaporative emissions allowed for automobiles [118,119]. From one country to another, the composition of the fuels used for automobiles varies and is in a continuous evolving process. The repercussions of permeation are notable, because the addition of some components in fuel may affect the permeability of various polymers [120], which leads to an increase of the fuel emissions.

When the material situation for minimizing fuel permeation and the intended application of corresponding components occurs, a complex spectrum of properties must be taken into consideration concerning the material requirements such as high media-resistance (minimal swelling), low diffusion coefficients for the permeates, high temperature stability and adequate

physical-mechanical properties, e.g. low compression set, high strength and good elasticity. As measurements were proven, low chain mobility characterized by a high polymer glass transition temperature, by the nature and high content of fillers and by a high crosslinking density has a favourable effect on impermeability [121 - 123].

Nevertheless, during the engine development was done a parallel development of the fuels used to power them [124]. The fuels are mixtures of different components such as sulphur and aromatic species. Lacks of the firsts minimizes the lubricity of the fuel and reduces the lifetime of the parts, which are exposed to the fuel. If the aromatics components are in low amount, the tendency of the fuel to swell the elastomer (like O-ring) is obviously reduced [125,126]. A blend of synthetic and aromatic fuels is the choice in order to obtain the desired swelling character.

The permeation rate depends on the chemical structure and the morphology of the polymers, on the temperature and the size of the diffusing molecules. Observations of the physical-chemical aspects of permeation media through a polymer matrix allow the description of this process by three distinctive stages [127 - 129] (Figure 13):

1. Adsorption of the permeate in the polymer matrix on the side with the higher medium concentration;
2. Diffusion process through which the substance is transported through the polymer matrix in the direction of lower concentration;
3. Desorption of permeates from the surface of the polymer matrix on the lower-concentration side.

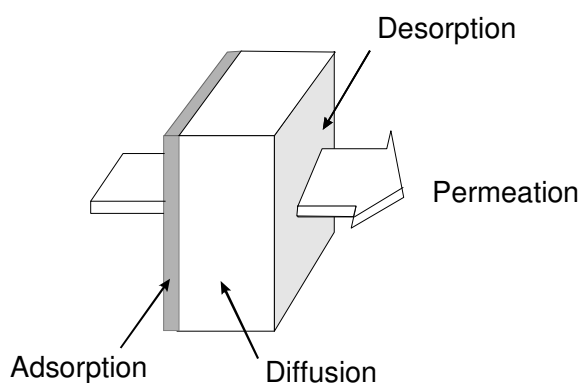


Figure 13: Schematically description of the permeation process

The 1<sup>st</sup> stage makes evident the necessity of low swelling for low permeation. This condition is met if the chemical compatibility between permeates and polymer matrix is low. This means that the difference in the solubility parameters of the components involved is sufficiently high and the Flory-Huggin's interaction parameter  $\chi$  has a relatively high value [39, 130, 131]. After swelling a state of equilibrium is reached, a stationary state with an orientated substance transport

through the polymer matrix that is attained in the 2<sup>nd</sup> stage of the permeation process. In the second stage, the transport process involves diffusion.

Diffusion is a molecular process in which the molecules float because of random thermal motion from a region with higher concentration to one of lower concentration. The transport of a liquid into a rubber is a similar process. When a piece of rubber is immersed in a liquid, the surface layer immediately absorbs the liquid in early stages and with increasing time, the liquid penetrates further and further into the bulk of the material until equilibrium is reached in which the liquid is uniform everywhere throughout the rubber. The movement of the liquid obeys the law of diffusion. The speed of movement is characterized by the diffusion coefficient of the liquid in rubber.

The presence of liquids in rubber can have a significant influence on physical properties such as tensile strength, tear strength, and fatigue resistance and abrasion resistance if the concentration of the liquid is high. It is possible that compounds, which encounter a liquid that has a high solubility in the rubber matrix, would suffer a high loss in strength properties. For the design life of some components, this aspect can be negligible because the time taken for a liquid to penetrate to a significant depth may be very long [132].

As a rule, diffusion in polymers is understood to refer to the transfer processes of molecules in polymers such as low-molar substances [133, 134]. The theory of free volume and free chain mobility generally explains the diffusion mechanism in polymers at a temperature above the glass transition temperature [133 - 136] and is described by the Fick's law of diffusion. The diffusion coefficient  $D$  is a substance specific variable that can be regarded as constant at low concentrations, whereas a concentration dependency prevails at high concentrations. The 1<sup>st</sup> Fick's diffusion law says that the flow of the particles  $J$  is proportional with the concentration gradient [137]. For the case when in a diffusion process a direction of current is given:

$$\frac{\partial C(x, y, z)}{\partial x} \neq 0 \quad \frac{\partial C(x, y, z)}{\partial y} = 0 \quad \text{and} \quad \frac{\partial C(x, y, z)}{\partial z} = 0 \quad \text{Equ. (27)}$$

the diffusion results in one dimension:

$$J = -D \frac{\partial C}{\partial x} \quad \text{Equ. (28)}$$

The 2<sup>nd</sup> Fick's diffusion law for the diffusion process, which was obtained from the mass balance of a uniaxial diffusing molecule in a unit volume, is given by the relation:

$$\frac{\partial C}{\partial t} = \frac{\partial}{\partial x} \left( D \frac{\partial C}{\partial x} \right) \quad \text{Equ. (29)}$$

The Equ. (29) describes the concentration of the diffusing species in each place and time in polymer matrix. In order to solve this equation a limiting condition set is required corresponding to the shape and dimension of the specimen as well as an initial condition which gives information about the concentration distribution at a defined time (i.e.  $t=0$ ).

In the 3<sup>rd</sup> stage of permeation, the permeates follow up the desorption process which is dependent mainly on the steam pressure of the components involved and rise, in the ideal situation, to a concentration gradient that comes very close to zero. Thus, always exists a maximum driving force for the diffusion of the diffusate or permeate [133]. The mass flow density  $J_0$  and the mass flow  $\Delta m/\Delta t$  of the permeation process can be described mathematically by following equation [129]:

$$J_0 = \frac{1}{A} * \frac{\Delta m}{\Delta t} = \frac{c_0 * D}{d} \quad \text{Equ. (30)}$$

$$\frac{\Delta m}{\Delta t} = \frac{c_0 * D * A}{d} \quad \text{Equ. (31)}$$

When the sorption coefficient  $S$  is taken into account, the permeation coefficient  $P$  can be determined by means of Henry's law of solubility [129, 138]:

$$\frac{\Delta m}{\Delta t} = \frac{S * D * p * A}{d} = P * \frac{p * A}{d} \quad \text{Equ. (32)}$$

$$P = S * D \quad \text{Equ. (33)}$$

$$P = \frac{\Delta m}{\Delta t} * \frac{d}{p * A} \quad \text{Equ. (34)}$$

where  $D$  is the diffusion coefficient,  $m$  is the mass of permeate,  $t$  is the time of permeation,  $d$  is the thickness of the membrane,  $A$  is the permeation area and  $p$  is the pressure.

The three processes, adsorption, diffusion and desorption, can influence the permeation process to a certain extend. Nevertheless, the diffusion process brings a distinct contribution to the permeation process due to its complexity. The Fick's law of diffusion provides the mathematical description of this process and it will be discussed in detail in the following chapter.

### 3.3.1.1 Solutions to the Fick's differential equation

#### *Steady state*

If the case of the diffusion process through a plane sheet of thickness  $l$  whose surfaces are maintained at constant concentrations  $C_1$  and  $C_2$  is considered, the steady state is reached after a time when the concentration remains constant at all points of the sheet. The diffusion equation in one dimension will have the form [134]:

$$\frac{\partial^2 C}{\partial x^2} = 0 \quad \text{Equ. (35)}$$

where the diffusion coefficient  $D$  is constant. By integrating with respect to  $x$  it will be given a constant concentration gradient:

$$\frac{\partial C}{\partial x} = \text{constant} \quad \text{Equ. (36)}$$

By further integration and introducing the conditions at  $x=0$ ,  $x=l$  for the steady state it can be written:

$$C = \frac{C_2 - C_1}{l} x + C_1 \quad \text{Equ. (37)}$$

Equ. (36) as well as Equ. (37) display the linear changing of the concentration from  $C_1$  to  $C_2$  in the sheet. The flow is the same overall the sheet and is given by the Equ. (38):

$$J = -D \frac{\partial C}{\partial x} = D \frac{C_1 - C_2}{l} \quad \text{Equ. (38)}$$

### *Non-steady state*

Crank and Parker used a kinetic study of the sorption and desorption of vapours and gases for determining the diffusion coefficient [136]. The mass of the polymer increases due to the migration of the liquid in polymer as a result of the interaction between the polymer and the liquid. If the following limiting condition are taken into consideration:

$C=C_1$	$x=0$	$t \geq 0$
$C=C_2$	$x=l$	$t \geq 0$
$C=f(x)$	$0 < x < l$	$t=0$

from the variation of the concentration  $C$  the relation between the total amount of the diffusing substance,  $M_t$ , which enters into the sheet during the time  $t$  and the corresponding amount by infinite time,  $M_\infty$  can be described. Table 1 shows the results for a plate sheet, a cylinder and a sphere.

By representing the normalized amount of the solvent diffused into the sample  $M_t/M_\infty$  as a function of the  $t^{1/2}$ , the diffusion coefficient can be calculated from the beginning of the slope when the thickness of the sample is known. A plot of  $M_t/M_\infty$  versus  $(t/l)^{1/2}$  is initially linear and from the slope  $D$  can be calculated with an error of 0.001%:

$$D = \frac{0.049}{(t/l^2)^{1/2}} \quad \text{Equ. (39)}$$

According to Crank, the solution of the 2<sup>nd</sup> Fick's diffusion law for the total amount of the diffusing substance  $Q_t$  that passed through a plane sheet in time  $t$  when the system is out of steady state ( $t \rightarrow \infty$ ) can be calculated by the Equ. (40):

$$Q_t = \frac{DC_1}{l} \left( t - \frac{l^2}{6D} \right) \quad \text{Equ. (40)}$$



Table 1. Examples of the solutions to the differential equation for non-steady state [134]

Form of the test material	The total amount of the diffusing substance, $M_t$ , which enters into the sheet during the time $t$ and $M_\infty$ is the corresponding amount by infinite time	The approaches for short times, Condition: $(Dt)/l^2 < 1$
Plane sheet (thickness $d=2l$ )	$\frac{M_t}{M_\infty} = 1 - \sum_{m=0}^{m=\infty} \frac{8}{\pi^2 (2m+1)^2} \exp\left\{-\frac{D(2m+1)^2 \pi^2 t}{4l^2}\right\}$	$\frac{M_t}{M_\infty} = \frac{2}{l} \left[ \frac{Dt}{\pi} \right]^{1/2}$
Cylinder (diameter $\phi=2l$ )	$\frac{M_t}{M_\infty} = 1 - \sum_{m=1}^{m=\infty} \frac{4}{\alpha_m^2 l^2} \exp\{-\alpha_m^2 Dt\}$ $\alpha_m$ is the solution from $J_0(s\alpha_m) = 0$ , $J_0$ -Bessel function	$\frac{M_t}{M_\infty} = \frac{4}{l} \left[ \frac{Dt}{\pi} \right]^{1/2}$
Sphere (diameter $\phi=2l$ )	$\frac{M_t}{M_\infty} = 1 - \sum_{m=0}^{m=\infty} \frac{6}{\pi^2 m^2} \exp\left\{-n^2 \pi^2 \frac{Dt}{l^2}\right\}$	$\frac{M_t}{M_\infty} = \frac{6}{l} \left[ \frac{Dt}{\pi} \right]^{1/2}$

For the Equ. (40) it is necessary to make the assumptions that by the diffusion through a film, the equilibrium will be reached at entering face and no diffusant is detected at the exit face. From the representation of  $Q_t$  in dependency of time, the intercept on the  $t$ -axis permit the determination of the “time lag“,  $\tau$ , which can be calculated by the following equation:

$$D = \frac{l^2}{6\tau} \quad \text{Equ. (41)}$$

The diffusion coefficient can be calculated if the thickness of the membrane and the time lag are known. It was found that high values of the time lag lead to a decrease of the diffusion coefficient [111].

### 3.3.1.2 The theories of diffusion

The “hole” theory of diffusion was first popularised by Barrer [139] and studied further by many authors [140]. The theory illustrates the diffusion model based on the formation of the “holes” in the matrix. The penetrant molecule can migrate only when there is a free space to receive it. These holes can be created through the Brownian movements of the polymer chain segments. The diffusion process happens by means of “change of place” phenomena and is described by the “jumping” mechanism. If the molecule acquires sufficient thermal energy and moves in the direction where the neighbouring place is vacant, the molecule can “jump” from its own position to a new equilibrium position. In the free space another molecule can “jump” and in this way such kind of movements gives the chance to the diffusion motion. A molecule can make

different jumps in time. The diffusion coefficient is calculated considering the frequency  $\phi$  and the jump distance  $\delta$  :

$$D = \frac{1}{6} \phi \delta^2 \quad \text{Equ. (42)}$$

In different research works, authors tried to find out the theoretical expressions for the frequency and the jump distance taking into consideration the nature of the diffusants and the polymers. For the description of these two parameters, two different approaches were emphasised: the activation energy and nevertheless the free volume theory.

Glasstone, Laidler and Eyring [140] proposed the theory of the state transition in which they considered that the activation energy is necessary to form a hole of proper dimensions, and derived the following equation for the calculation of the diffusion coefficient:

$$D = e \lambda^2 \frac{kT}{h} \exp\left[\frac{\Delta S^*}{R}\right] \exp\left[-\frac{E_D}{RT}\right] \quad \text{Equ. (43)}$$

where  $h$  is the Plank's constant,  $k$  is Boltzmann's constant,  $\lambda$  is the mean free path of the diffusing molecule in the solid,  $\Delta S^*$  is the entropy and  $E_D$  is the activation energy of the diffusion process.

Another theory that derived the diffusion coefficient based on energy consideration is Barrer's zone theory [141]. This theory describes that the diffusing molecule moves to successive positions of equilibrium if a sufficient amount of activation energy was acquired by the diffusant and its surrounding. The activation energy is delivered in the system through many degrees of freedom. The diffusion coefficient is calculated by equation:

$$D = \frac{\nu}{2} \delta^2 \sum_{f=1}^{f_{\max}} \rho_f \left\{ \left( \frac{E}{RT} \right)^{f-1} \left[ \frac{1}{(f-1)!} \right]^{-1} \right\} \exp\left(-\frac{E}{RT}\right) \quad \text{Equ. (44)}$$

where  $\nu$  is the thermal vibration frequency of the penetrant molecule,  $\delta$  is the jump distance,  $f'$  is the number of degrees of freedom,  $E$  is the total energy of 1 mole of the activated zones under consideration and  $\rho_f$  is the probability that  $f'$  will cooperate in a diffusion step. The complete expression in the square brackets is the probability that the energy  $E$  is distributed over degrees of freedom.

In the works of Meares [142] and Fujita [143] the free volume theory provides valuable understanding about the segmental motion of the polymer. Useful information about the diffusion phenomena in polymer systems considering the concept of free volume is comprised in studies of Buche [144], Frisch [145], DiBenedetto and Paul [146], Kumins and Kwei [147]. These works investigated the diffusion of gases and organic vapours. It was shown that the

mobility of the polymer segment and the diffusant molecule in a polymer mixture are determined by the amount of free volume present in the system.

The method developed by Shah [148] is based on a Monte Carlo simulation of polymer microstructure and permits the estimation of the free volume fraction taking into account the size of the diffusant. Mauritz und Storey [149] extended the theory of Cohen and Turnbull [150] and approaches a molecular aspect where it was taken into consideration both the molecular size and shape of diffused species and the interaction with the polymer. The diffusion coefficient was calculated by means of Equ. (45):

$$D = \left(\frac{\delta}{6}\right) \sqrt{\frac{RT}{M}} \exp\left(\frac{1}{2} - \frac{V^*}{V_f}\right) \quad \text{Equ. (45)}$$

where  $M$  is the molecular weight of the diffusing substance,  $V^*$  is the effective volume of the diffusing substance and  $V_f$  is the free volume per polymer unit.

### 3.3.1.3 Concentration-distance analysis

This approach considers the mass transport of the diffusant from a reservoir domain with a concentration  $C_1$  (reservoir) through a linear border into another domain with the concentration 0. If the mass transport is considered as a function of time the concentration in the reservoir is decreasing more near the border and less with growing distance from the border. Vice versa, the domain that receives the diffusant demonstrates the highest concentration at the border and continuously decreasing concentration with growing distance from the border. Consequently, for a given time during the process typical concentration-distance profiles are obtained. On this analysis the processes take place at the border of two joint plates of material - one with and the other without diffusant leads to the expression of the diffusion coefficient  $D$  as follows [147]:

$$D_{c=c_1} = -\frac{1}{2t} \frac{dx}{dc} \int_0^{c_1} x dC \quad \text{Equ. (46)}$$

where  $x$  - position of the initial interface border between the two components.

The concentration-distance curve is plotted for a known time and the diffusion coefficient is evaluated from the concentration profiles using Equ. (46). The diffusion coefficient  $D_{C=C_1}$  is determined for each increment,  $C_1$  is the concentration at the increment  $x$ , the  $dx/dc$  is the inverse of the concentration  $dc/dx$  and the integral term is the area under the concentration - distance curve.

### 3.3.1.4 Factors affecting the transport processes

The diffusion coefficient and the permeation rate respectively are significantly influenced by several factors as: the nature of the polymer, concentration, shape and size of the penetrating molecules [151], temperature [152], filler [153], nature of penetrate [154]. In earlier investigations, Amerongen showed that synthetic rubbers like butyl and nitrile rubber have permeability values of hydrogen from one third to one eighth of natural rubber (NR) [155].

Besides its reinforcement ability, filler was founded to have a great influence on diffusion and permeation in polymers. Addition of filler in rubber compound represents a more cost effective method to reduce the permeability. In a later work, Amerongen investigated the effect of carbon black (50phr) and mineral filler (20 vol%) on gas permeability on NR and demonstrated that the addition of the filler reduced permeability of the base polymer [156]. Another study concerning the transport process through fluoroelastomers indicated that the permeability and diffusivity of ether through the polymer matrix were lowered by the addition of filler [153]. These findings lead to the question: does the interphase created by the contact rubber-filler have any influence on diffusion coefficient? For this study, a model was proposed and discussed later in the work.

The surface modification of a rubber plate by plasma treatment or coating with a given product offers a new field of application and could give very interesting properties to the material. Significant changes of the adhesion towards rubber matrix and the surface properties were described in literature [157,158]. The influence of these surface modifications can also affect the diffusion and permeation behaviours [159].

A closer understanding of those influences on the transport processes is necessary because the diffusion experiments can provide valuable information about thermodynamic aspects of polymer blends.

#### 3.3.1.4.1 Influence of the shape and the size of the diffusant

If a particle has a spherical shape, the Stokes-Einstein equation [160, 161] was used for the calculation of diffusion coefficients by means of Equ. (47):

$$D = \frac{kT}{6\pi r \eta} \quad \text{Equ. (47)}$$

where  $k$  is Boltzmann's constant,  $T$  the absolute temperature,  $r$  is the radius of the sphere,  $\eta$  is the viscosity of the solvent.

Another approach employed for the determination of diffusion coefficient was proposed by Sutherland, who modified the Equ. (48) introducing a sliding friction coefficient  $\beta$  [162]:

$$D = \frac{kT}{(6\pi\eta r)(1 + 2\eta/\beta r)(1 + 3\eta/\beta r)} \quad \text{Equ. (48)}$$

In conclusion it was noticed that the higher  $r$  or  $\beta$  the slower the diffusion process takes place.

Eyring and Ewell [163] showed that the activation energy for viscous flow is related to the work required to form a hole in the liquid and they proposed an equation in which the activation energy  $E_{vis}$  is correlated to the heat of vaporization  $\Delta E_{vap}$  :

$$E_{vis} = \frac{\Delta E_{vap}}{n} \quad \text{Equ. (49)}$$

In order to determine the factor  $n$  that gives an indication of the size of the hole, the viscosities ( $\log \eta$ ) were plotted versus the temperature ( $1/T$ ). The results showed that for non-polar molecules that have spherical or approximately spherical symmetry  $n$  is nearer 3 and for polar molecules or long chain hydrocarbons not having spherical symmetry  $n$  is about 4 and  $n$  increases with temperature [164].

The investigation on long chain hydrocarbons made by Kauzmann and Eyring [165] pointed out the influence of the increasing chain length on the relationship between the activation energy and heat of vaporization. They admitted that the longer the chain the higher tendency of the chain to become coiled. Because of this behaviour the heat of vaporization is no longer a measure of the energy required for the formation of a hole. In consequence it was assumed that the hydrocarbon chain moved as a single unit and the energy required to form a hole would be one quarter of the extrapolated heat of vaporization  $\Delta E'_{vap}$ .

In a later work, Kirkwood showed the correlation of the diffusion coefficient with the size of molecule by using the Equ. (50) [166]:

$$D = \frac{kT}{N_A \rho} \left[ 1 + \frac{\rho}{6\pi\eta N_A} \sum_{i=0}^{N_A} \sum_{j=0}^{N_A} (1 - \delta_{ij}) \langle R_{ij}^{-1} \rangle \right] \quad \text{Equ. (50)}$$

where  $N_A$  is Avogadro's number,  $\rho$  the density of the solution and  $R_{ij}$  is the distance between the polymer segments.

Since the Einstein equation [167] gives the fundamental relationship between the diffusion process and the frictional force ( $f$ ) of the diffusing molecule,  $f$  can be expressed in the form:

$$f = n\zeta \left( 1 + \frac{\zeta}{6\pi\eta} \sum_{i,j=1, i \neq j}^n \left\langle \frac{1}{R_{i,j}} \right\rangle \right)^{-1} \quad \text{(Equ. 51)}$$

where  $n$  is unit monomer number and  $\zeta$  is the frictional coefficient of each individual monomer unit.

#### 3.3.1.4.2 Influence of the molecular weight of the diffusant

By increasing the molecular weight of the diffusant, the diffusion coefficient approaches a limit value. The dependence of the diffusion coefficient on the molecular mass of the diffusing species in a given polymer matrix is described by a power law [168].

$$D = KM^{-\alpha} \quad \text{Equ. (52)}$$

when  $K$  and  $\alpha$  are constants.

For the self diffusion coefficient of polymers an exponent  $\alpha$  of 2 was derived from the reptation theory by DeGennes [104]. Bueche determined in his work a value of 3,5 for this constant [169]. Recent works [170, 171] studied the diffusion process of n-alkane, aliphatic esters with high molecular weight where it was found that this exponent has a value of 2. For the diffusion process of substances with an average molecular weight between  $C_6 - C_{16}$  less studies exist concerning the proportionality between the diffusion coefficient and molecular weight.

#### 3.3.1.4.3 Influence of the temperature

The diffusion coefficient is temperature dependent and obeys to a relationship similar to the Arrhenius equation [172]:

$$D = D_0 \exp\left[-\frac{E_D}{RT}\right] \quad \text{Equ. (53)}$$

where  $D$  is the diffusion coefficient,  $D_0$  is the pre-exponential factor,  $E_D$  is the activation energy of diffusion,  $R$  is the gas constant and  $T$  is the temperature in Kelvin. The activation energy,  $E_D$ , is a measure of the energy extended against the cohesive forces of the polymer in forming the holes (free volume) through which diffusion will take place. The experimental results showed that the  $E_D$  is proportional with the diameter of the molecule at square respectively with the diameter of the hole and the cohesive energy density [135]:

$$E_D \approx d^2 \Delta E^V \quad \text{Equ. (54)}$$

Van Amerongen [173] explained that the dependency of the activation energy on temperature could be interpreted by Eyring theory of rate processes [140] by taking into consideration the variation of the enthalpy and entropy with temperature.

#### 3.3.1.4.4 Influence of the nature of the rubber

Taking into consideration the "hole" theory of diffusion, the diffusion process depends on the number and size distribution of holes, which in turn depend on the packing degree of the chains and is related to the free volume. The diffusion process depends also on the ability of hole formation which is closely correlated with the segmental chain mobility. These features can influence to a certain extent the thermal expansion coefficient and the glass transition.

It was found experimentally that the diffusion coefficient of a liquid in different rubbers is related to the glass transition temperature of the rubber. From the investigations of the diffusion coefficient of n-decane in different rubber was observed that the high diffusion coefficient is registered for butadiene rubber (BR) and the small for NBR. By decreasing the glass transition of the rubber more free volume is introduced into the system and as a result the diffusion coefficient decreases [174].

When the effect of nitrile groups on the diffusion of gas in a series of butadiene-acrylonitrile copolymers was studied [133], it was found that the introduction of polar groups in the chains causes a decrease of the diffusion constant. The glass transition temperature of the polymer is directly influenced by the chain flexibility. An increase of the glass transition temperatures of the polymers leads to a decrease of the diffusion coefficient.

#### 3.3.1.4.5 Influence of the crosslinking density

The vulcanization process involves the conversion of raw rubber into a network due the formation of *crosslinks*, chemical bonds or bridges that associate the rubber macromolecules [175]. Through the vulcanisation the rubber elasticity is increased meanwhile its plasticity is reduced.

The crosslink atoms usually employed are sulphur [176] due to its lower cost and its better control during the vulcanisation process in comparison with other vulcanising agents used such as organic peroxides [177], metal oxides.

During vulcanisation with sulphur [178] crosslinks in the form of  $-S_x-$  ( $x=1,2,\dots$ ) between the carbon atoms of the different rubber molecules with different length of the sulphur chains will be formed. The amount of mono-, di- and polysulfidic crosslinks present in the networks is calculated from the crosslink concentrations per unit volume (crosslink density).

Knowledge about the crosslink density and especially  $S_x$ -distribution offers the possibility to optimize the curing conditions, to produce new products with better mechanical and aging properties.

The experimental techniques used for the determination of crosslink density are namely swelling investigations based on the theory of Flory-Rehner [94,131], mechanical tests analyzed by Mooney-Rivlin method [179], magnetic resonance techniques [180, 181], high resolution  $^{13}\text{C}$ -NMR MAS solid-state spectroscopy [182].

#### *Determination of crosslinking density from swelling investigations*

The crosslinking density can be determined by measuring the equilibrium swelling of an elastomer in a solvent. The method includes the chemical crosslinking density, which exist in the raw material besides the entanglements. Considering the crosslinking density definition, the network chain density  $\nu$  can be calculated by following equation:

$$v = \rho_p / M_c \quad \text{Equ. (55)}$$

where the  $\rho_p$  is the density of the polymer and  $M_c$  is the molecular weight between crosslinks. The swelling experiment of the elastomer is done in the solvent at constant temperature. The weight of the sample is recorded in dependence of time until the equilibrium swelling is reached. The swelling degree of the elastomer is inverse proportional with the crosslinking density. That means, the shorter the distance between the crosslink is (smaller  $M_c$ ) the smaller the swelling. For the calculation of the network, chain density the fundamental equation by Flory and Rehner is used:

$$v = \ln (1 - V_r) + V_r + \chi V_r^2 / V_0 (V_r^{1/3} - 0.5 V_r) \quad \text{Equ. (56)}$$

where  $v$  is the chain density in mol/cm<sup>3</sup>,  $V_0$  is the molar volume of the solvent,  $\chi$  is Huggins' interaction parameter,  $V_r$  is volume of the polymer in gel which is calculated by:

$$V_r = 1 / [1 + (\rho_p / \rho_s) Q] \quad \text{Equ. (57)}$$

$$Q = (m_1 - m_2) / m_2 \quad \text{Equ. (58)}$$

where  $\rho_s$  is the density of the solvent,  $Q$  is the swelling degree,  $m_1$  is the mass of the sample at the equilibrium swelling and  $m_2$  is the mass of the sample in original state.

#### *Determination of crosslinking density from mechanical test*

Another method employed for the determination of the network chain density is the mechanical investigation that studies the stress-strain behaviour of a rubber plate. From the elongation measurements results, the calculation of  $v$  using the relationship described by Mooney and Rivlin could be done:

$$F = 2 A_0 \left( C_1 + \frac{C_2}{\lambda} \right) \left( \lambda + \frac{1}{\lambda^2} \right) \quad \text{Equ. (59)}$$

where  $F$  is the force,  $A_0$  is the original cross section area,  $\lambda$  is the extension ratio and  $C_1$  and  $C_2$  are constants.

The values of the constants  $C_1$  and  $C_2$  can be obtained graphically by plotting stress-strain data in the form  $F/[2 A_0 (\lambda - \lambda^2)]$  as a function of  $\lambda^{-1}$ . For the calculation of network chain density, the kinetic theory of rubber elasticity gives the following equation:

$$v = 2C_1 / RT \quad \text{Equ. (60)}$$

The effect of the crosslinking density of the rubber on diffusion was investigated in different studies [183,184]. It was noticed that the diffusion constants decrease with increasing the crosslinking density due to the immobility introduced into the chain molecules. The reversed effect was observed for small amounts of crosslinkings.



### 3.3.1.4.6 Influence of the filler

Fillers like silica and carbon black are used to reinforce unfilled polymers. Reinforcement of elastomers by fillers requires strong physical interactions between polymer chain segments and filler surfaces [185,186]. The addition of fillers enhances strength properties ( $G'$  modulus, abrasion resistance, tear, increase) and modifies viscoelastic behaviour, which can be observed by an increase in the viscosity that can influence the processability of the rubber. Simultaneously, the heat build up,  $\tan \delta$  and resilience decrease [187].

Carbon black is used in high concentration in tire tread mixes in order to confer traction and abrasion resistance [188] while the compound reinforced by silica provides better traction [189]. In some cases, the chemical contact between the polymer and the filler surface is improved by using coupling agents that support the reinforcing effect [190,191]. This makes it possible to obtain filled silica compounds that meet the performance requirements generally achieved by the use of carbon black.

By incorporating particulate fillers and by increasing their concentration in the rubber almost all of the rheological and physical properties are influenced. Both, the loss modulus  $G''$  and the storage modulus  $G'$  are influenced by the filler loading as well as the degree of filler dispersion obtained during the mixing process. The experimental results showed that extended mixing of rubber compounds leads to a higher degree of filler dispersion and consequently to a decrease values of  $G'$  and  $G''$ .

Einstein described the hydrodynamic effect for the first time by studying the flow behaviour of spherical particles in Newton's solutions. He considered the viscosity of the filled and unfilled compounds and the volume fraction of filler [192,193]. Later, Smallwood [194] brought into the concept the modulus  $G$  and Guth und Gold [195,196] extended it through a term that is related to the interaction between the particles. This approach is known as Einstein-Guth-Gold equation and is expressed by the following form:

$$G_f = G_0(1 + 2.5\phi + 14.1\phi^2) \quad \text{Equ. (61)}$$

It was experimentally shown that Equ. (61) was limited for very large particle with spherical shape and filler concentration with  $\phi$  smaller than 2.

Another approach was proposed considering the asymmetry of the filler when the volume fraction  $\phi$  was corrected by an adjustable shape factors  $f$  [197,198]

$$G_f = G_0(1 + 0.67\phi + 1.62 f^2 \phi^2) \quad \text{Equ. (62)}$$

or by an effective filler volume fraction  $\phi_{\text{eff}}$  [199, 200] which substitutes the  $\phi$  leads to

$$G_f = G_0(1 + 2.5\phi + 14.1\phi_{\text{eff}}^2) \quad \text{Equ. (63)}$$

It was suggested [199] that the rubber could be occluded in the filler aggregates and partly shielded from an external deformation. Although a part of the rubber is occluded, a good

interaction between polymer and filler can occur if the effective volume fraction is high enough. That means that at the filler surface the rubber that is fixed in a layer is reduced and then the hydrodynamic effect occurs. This effective volume fraction depends on the testing temperature, the strain deformation and nevertheless on the surface activity of the filler used.

#### *Filler-polymer interaction*

The filler-polymer interactions are strongly influenced by the structure and surface of the filler and its interaction with the polymer. When the filler is dispersed in rubber, the polymer is partially immobilized in the form of occluded rubber, which behaves like the filler rather than like the polymer matrix. In this case, their contribution to the elastic behaviour of the matrix is annulated.

#### *Filler-filler interaction*

Through some detailed studies made by Payne it was shown that the filler-filler interaction affects the strain-dependent contribution to the modulus [201, 202]. This effect considers the decrease of the storage modulus as a function of the double strain amplitude in logarithmic scale in a varying amplitude range from zero until a plateau is reached. The Payne effect is dependent on the type of filler. The effect is stronger for silica than for carbon black due to a faster destruction of the silica network over a certain level of deformation [203].

### 3.3.2 Determination of diffusion coefficient and permeation rate

Both because of the rubber technology involvement and for scientific reasons, there is an increasing interest in efficient measuring methods for characterizing the diffusion behaviour of low molecular additives in different rubber matrices. A problem with most methods is, on one hand, the high expense in terms of time and preparation and the application limitation imposed by the measuring principle. On the other hand, there are, moreover, hardly any methods that allow a direct, locally resolved analytic determination of the diffusant as a function of time. Depending on the system under investigation, different methods have been applied for characterization of transport processes of low molecular substances [204,205] and crosslinking chemicals in polymer matrices that play an important role in diffusion processes through polymers [206 - 208]. ATR-FT-IR spectroscopy (ATR-attenuated total reflectance) was used for the evaluation of additive diffusion in polymer films [209] or the analysis of polymers surface [204]. Using micro-interferometry, it was shown that considerable change in diffusion coefficient with curative concentration occurs. It was also demonstrated that the sulphur diffusion between different polydienes like NR, SBR and BR is quite similar to diffusion in the homopolymer [210]. Another method used for monitoring the amount of diffusing substance across a polymer liquid interface as a function of time is the equilibrium swelling method [211]. Specifically for the determination of cases of equilibrium concentration distribution, conventional methods of analysis are applied, such as extraction and chromatography, or elemental analyses in

conjunction with special test configurations like sandwich structures consisting of a reservoir and a matrix where the low molecular components diffuse [212].

Recently measurements of the simultaneous diffusion, surface enhancement and the evaporation of a plasticizer from a polymer, thin-film matrix by using neutron reflection techniques were presented [213]. It was pointed out that the volume fraction profiles and the rate of evaporation of the plasticizer at the substrate interface are both consistent with the attractions of the surface that governs the bulk attractions between the miscible plasticizer and the polymer. Another work presents a new approach to  $(1)H$  multiple-quantum NMR that gives quantitatively information on chain ordering, dynamics and heterogeneities in polymer networks. This method can be used on simple low-field NMR spectrometers and was employed for investigation of filler effects in technical elastomers and the swelling process of a model network [214].

For the study of diffusion of solvents in rubbers various models were proposed and among them are those based on (a) free volume [215], (b) non-Markovian processes [216], (c) existence of a stress [217]. The Edwards-Cohen model [218] was modified where the chemical potential of diffusion through polymeric systems was assumed to be a function of the concentration and the stress induced by the swelling.

### 3.3.2.1 IR-Spectroscopy

The “time lag” ( $\tau$ ) taken for the diffusant to penetrate into a polymer thin film with a constant thickness  $l$  was measured by FT-IR-Spectroscopy method. With these two values the diffusion coefficient was calculated according to the simplified Equ. (41), Chap. 3.3.1.1

### 3.3.2.2 Concentration-distance analysis

The system used for this study is made up of two separated layers (Table 33, Chap. 7). One layer contains the rubber and the diffusing substance being considered the reservoir. The other layer has of the same chemical constitution. During the whole process, the condition of the conservation of mass had to be satisfied. This required from the experimental design to measure the concentration along the  $x$ -axis from the initial position of the boundary between the two components.

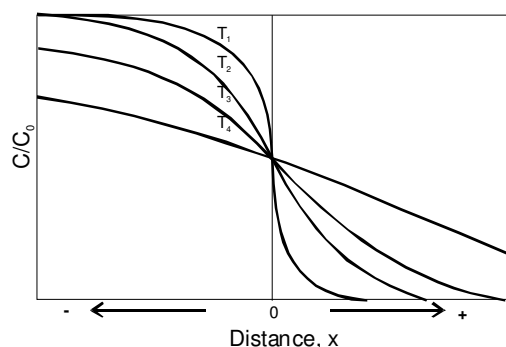


Figure 14: Evaluation of diffusion coefficient from a concentration – distance curve

The changes in concentration (concentration profiles) were recorded at several times as a function of the distance using the borderline as origin. The concentration-distance curve was plotted (Figure 14) for a given time  $t$  of observation and the diffusion coefficient  $D$  was evaluated from the concentration profiles using Equ. (46), Chap. 3.3.1.3.

### 3.3.2.3 Swelling investigations

Equilibrium swelling experiments of crosslinked rubber plates in different test substances were performed at different temperatures. The weight of the sample was measured before and after immersing it in solvent. The weight of the swollen samples at different times was determined after removing the solvent by blotting with filter paper from the surface of the sample. The swelling degree of several solvents in a plane sheet was determined gravimetrically using the formula displayed in Table 1, Chap. 3.3.1.1. For the study of the thickness influence on the transport process, the variation of the swelling degree with the time was investigated photographically.

### 3.3.2.4 Permeation experiments

The permeation equipment developed in this work consists of two separate chambers separated by a polymer membrane of different thickness. The fluid to be permeated is introduced in the upper chamber under normal pressure conditions (open system). The test fluid permeates from the upper chamber into the lower chamber and with the help of the carrying gas the diffusing sample is transported through a small steel duct to the six-way valve. By using a switching program of the valve (for given intervals of time), the gas flow is conducted to a loop of the valve so that at each valve switching a constant gas volume is introduced in the column of the gas chromatograph. The flame ionisation detector (FID) was employed to analyse the sample and the data will be registered in a chromatogram using a computer.

#### 4. Results and discussion

This work should contribute to a deeper understanding of the compatibility of polymers as well as to the solubility and the transport processes of low molecular compounds in polymers. On one hand, the influence of the chemical constitution and the structure of polymers with low glass transition temperature on the phase morphology of blends should be examined. Hereby the focus is on the description of the interfacial tension with the help of the  $\delta$ -parameter concept as well as on the estimation of the interphase volume fraction formed by interdiffusion of unlike polymers. This investigation is made on crosslinked blends by means of the dynamic-mechanical spectroscopy described in Chap. 3.1.3. As it was shown, there the characteristics and dimensions of the interphase can be influenced by the method used for evaluation as well as by the type and degree of crosslinking of the rubber matrix.

On the other hand, the solubility of the chosen low molecular compounds, that represent the structure analogue model compounds for processing components in the rubber industry, should be examined in different rubbers. Hereby one focus is the investigation of transport phenomena of low molecular compounds depending on their chemical structure and in crosslinked polymers. A comparison of different methods for the determination of the diffusion coefficient and the permeation rate should highlight the precision and correctness of the employed methods. On the other side, the transport phenomena will be investigated as a function of the molecular characteristics of the polymer matrix as well as of the low molecular diffusants as an aspect, which was not investigated so far by others. Based on these results the influence of nano-structured fillers is to be examined. Here the contribution of polymer interphase at the filler surface should be studied in some detail. Last but not least it should be clarified how far the supra-molecular phase morphology and whether or not the decisive role of the major phase or co-continuous phase morphology of blends influences the transport phenomenon.

To achieve these targets a number of commercial polymers as well as modified polymers were used (Table 2).

The chosen selection enables a sufficient variation of the structural parameters to show the significant changes of the molecular characteristics such as polarizability of the chain segments, the chain flexibility, the free volume and the glass transition temperature. When using poly (styrene-co-butadiene) grades this was achieved by a systematic variation of the 1,2-butadiene units and by substituting double bonds in the main chain under defined conditions by oxirane rings. The replacement of cis/trans 1,4-butadiene units by 1,2-units reduce the average polarizability of the polymer and decrease consequently the  $\delta$ -parameter. Opposite to this, the epoxidation reaction leads to an increase of the polarizability and higher value of  $\delta$ -parameter. In

the case of poly(acryl-nitrile-co-butadiene) on one hand the concentration of acryl nitrile units and on the other hand the degree of saturation were varied.

The characterisation of the investigated polymers was done by means of DSC and dynamical mechanical investigation. The results are shown in Table 2.

Table 2. Characteristics of rubbers used

Sample	Trade Name	Chemical composition [wt%]					Epoxid. [mol%]	Tg [°C]
		1,4-cis isoprene	1,4-cis/trans butadiene	1,2-butadiene	styrene	acrylo-nitrile		
NR	SMR CV50	99.9	-	-	-	-	-	-62
BR	CB 10	-	96.0	-	-	-	-	-103
SBR1	Buna VSL 5025-0	-	25	50	25	-	-	-18
SBR2	Buna VSL 2525-0	-	50	25	25	-	-	-44
SBR3	Buna VSL 25-0	-	68	8	25	-	-	-63
SBR4	Krylene 1500	-	62	14,5	23,5	-	-	-51
ENR	ENR50	-	-	-	-	-	50	-17
EpSBR		-	20	25	25	-	30	-31
NBR1	Perbunan NT 1845	-	67	15	-	18	-	-45
NBR2	Perbunan NT 2845	-	64	8	-	28	-	-31
NBR3	Perbunan NT 3445	-	59	7	-	34	-	-22
NBR4	Perbunan NT 3945	-	56	5	-	39	-	-12
HNBR1	Zetpol 2010	-	9	-	-	36	-	-24

#### 4.1 Polymer Compatibility

Whenever polymer blends are prepared by mechanical or solution mixing, the first and essential question to be answered is - do the polymers form discrete phases or do they mix intimately on a molecular scale. The first case of phase-separated blends is observed most frequently. As it was discussed in Chap. 3.1.1, phase separation is supported by high molecular weight as well as by unfavourable and weak interactions of unlike chain segments.

Due to the fact that technically used polymers do have high molecular weights ( $>10^5$ g/mol), the entropy of mixing ( $\Delta S_m$ ) delivers only a small negative contribution to the free energy of mixing ( $\Delta G_m$ ). The most important question is therefore the magnitude of the enthalpy of mixing ( $\Delta H_m$ ). In the case of non-polar or slightly polar polymers, this contribution can be estimated by using the solubility parameter concept [39].

The thermodynamic characterization of the interaction potential of polymers by their solubility parameter is important for questioning the phase morphology of blends as well as the solubility of low molecular compounds in these blends. The solubility parameter values used in this work were determined with the help of inverse-gas-chromatography [55] and equilibrium swelling [40].

Using the  $\delta$ -parameter concept the blends consist of at least one polar component were discussed.

#### Estimated interfacial tension

For this part NR blends with different types of SBR were studied. The styrene content in SBR was kept constant while the content of 1,2-butadiene units was varied stepwise. Due to the fact that cis-1,4-butadiene units are more polarizable than 1,2-butadiene units and 1,2-butadiene units demonstrates a similar polarizability as cis-1,4-isoprene units the decreasing content of 1,2-butadiene units in SBR 1 to 3 (Table 2) leads to an increase of the average polarizability of the polymer (Table 3).

*Table 3.  $\delta$ -parameters of rubbers used as determined by IGC*

Polymer	$\delta(\text{J}/\text{cm}^3)^{1/2}$
NR	16,7
BR	17,2
SBR1	17,4
SBR2	17,6
SBR3	17,7

Thermodynamic similarities in the blend constituents expressed in similar solubility parameters lead to negligible or no longer detectible interfacial tension. If the interaction between the components of the system decreases and the  $\delta$ -parameter difference of the two rubbers ( $\Delta\delta$ ) rises, the interfacial tension increases. In this manner, the solubility parameter difference can be used to estimate the interfacial tension in a rubber blend.

As consequence, the solubility parameters of the corresponding polymers increase in the sequence SBR1 > SBR2 > SBR3. If the compatibility towards NR is impaired, some sequences and the interfacial tension expressed by the solubility parameter difference  $|\delta_{\text{NR}} - \delta_{\text{SBR}}|$  are increasing. From Table 2 one can easily predict that the interfacial tension in the system is increasing in the sequence

$$\text{NR/SBR 3} < \text{NR/SBR 2} < \text{NR/SBR 1}$$

Thus, 1,2-butadiene units provide the SBR with a higher thermodynamic similarity with NR. Contrary to the effect of vinyl groups, the introduction of oxirane rings (epoxy groups) in the polymer backbones significantly changes the strength of inter- and intermolecular interaction because it changes the concentration and the distribution of dipoles and induced dipoles along the polymer chains.

A considerable increase in the solubility parameter is obtained by introducing 50 wt.% epoxy groups into NR of about  $18,5 \text{ (J/cm}^3)^{1/2}$  and by substituting cis- and trans-1,4-butadiene units by 30 wt.% epoxy groups into SBR2 respectively a solubility parameter of about  $18,8 \text{ (J/cm}^3)^{1/2}$  is founded (Figure 15).

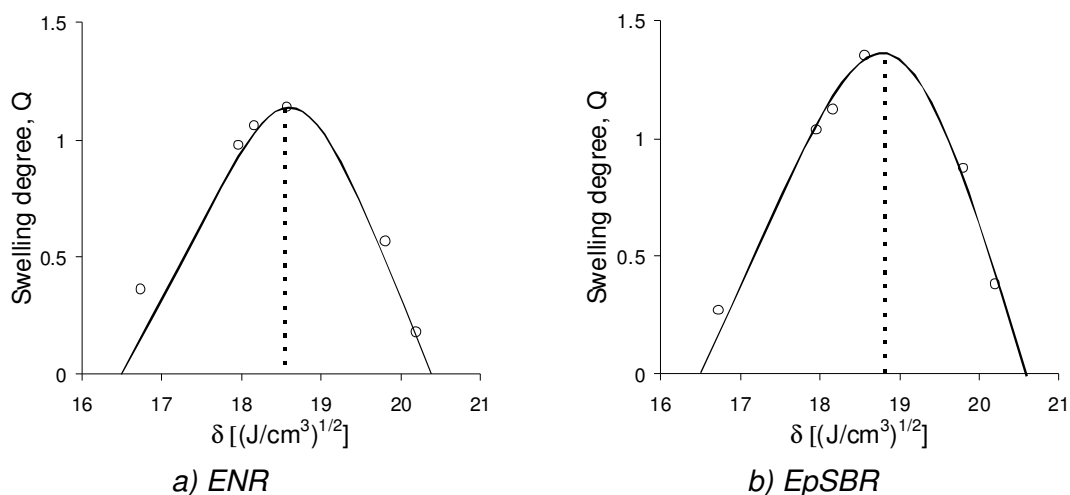


Figure 15: Determination of solubility parameter for epoxidized rubbers by swelling

The estimates obtained from equilibrium swelling measurements indicate a slightly higher  $\delta$ -parameter for EpSBR than for ENR. Based on the data obtained, interfacial tension for the blends with epoxidized rubbers is ENR/EpSBR < ENR/SBR2 < NR/ENR < NR/EpSBR.

#### Phase morphology

Besides the estimates based on the solubility parameter concept, the blends manufactured under the same mixing conditions were investigated simultaneously by using DSC, DMA and TEM.

#### BR/SBR blends

The influence of the microstructure of SBR on the glass transition temperature in BR/SBR blends was investigated by DSC using the pure rubbers as reference (Table 4). First of all, the increasing content of 1,2-butadiene units decrease significantly the chain flexibility and therefore increases the corresponding  $T_g$ . A careful investigation of the thermograms reveals the existence of two phases in the blend. The  $T_g$ -shift of each phase indicates that the blend constituents demonstrate increasing partial solubility when the content of 1,2-butadiene units in the SBR increases. The increase of the vinyl content in SBR-phase provokes a shift of  $T_g$  to lower temperatures with 40 °C because the higher content of 1,2-butadiene reduce the polarity imparted by the styrene rings.



Table 4. DSC investigation of BR/SBR blends

Blend	$T_g$ [°C]							
	100/0		50/50		30/70		0/100	
BR/SBR1	-103	-	-90	-64	-89	-50	-	-21
BR/SBR2	-103	-	-95	-81	-90	-65	-	-44
BR/SBR3	-103	-	-98	-85	-91	-68	-	-63

The DSC results were compared with the results obtained from DMA measurements (Figure 16). The characterization of rubber blends with the help of dynamic-mechanical spectroscopy was focused on the evolution of the loss modulus  $G''$  of the pure components and the blends as a function of temperature. The DMA measurements of the systems under investigation confirmed the results obtained by DSC (Figure 16). The damping peaks ( $G''_{max}$ ) for BR as well as SBR are considerably shifted towards each other.

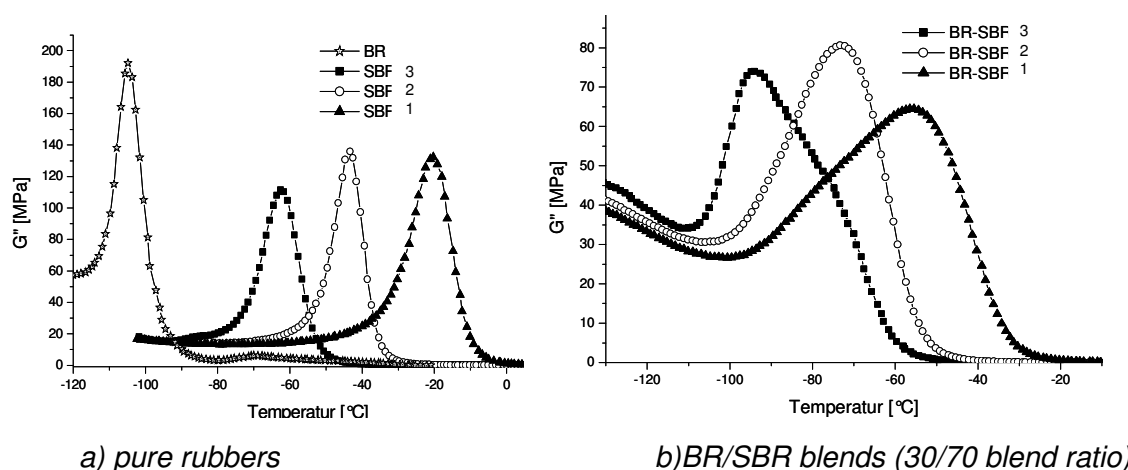


Figure 16: Dynamic mechanical analysis of pure rubbers and rubber blends

It can be seen that the damping peak becomes broader and shows a shoulder, which is characteristic for the SBR-phase or BR-phase. This is a clear indication for phase separation and leads to the statement that the lower the vinyl content the less the compatibility of the BR/SBR blend. However, for BR/SBR2 such a bimodal peak is not observed. Both  $T_g$ 's are shifted almost equally and result in a very broad damping maximum. To obtain a complementary view of the influence of the microstructure on the phase morphology TEM investigations were performed.



Figure 17: TEM micrographs of BR (30/70) blends with: a) SBR1; b) SBR2; c) SBR3

Figure 17 highlights the differences between the three blends. The bright domains represent the SBR-phase that is dispersed in the dark BR-phase. Immediately evident is the difference in shape of the bright domains. They become larger as the amount of vinyl groups in SBR decrease. In the BR/SBR3, further decreases of the amount of the vinyl groups produce a significant phase separation. These results confirm the ones obtained by DMA measurements.

#### NR/SBR blends

In the case of NR/SBR blends, a first characterization was made by dynamic mechanical investigation of the pure rubbers. By comparing the curves  $G''$  vs (T) for the raw polymers NR, SBR1, SBR2 and SBR3 it can be seen that the signals for NR and SBR3 are almost overlapping whereas for SBR2 and SBR1 with a higher content of 1,2-butadiene units the glass transition occur at considerable higher temperatures (Figure 18). The blend NR/SBR3 exhibits one single damping peak caused by the rare incidence of the  $T_g$ 's of the polymers under consideration. Therefore, it cannot be decided by DMA whether the polymers are incompatible.

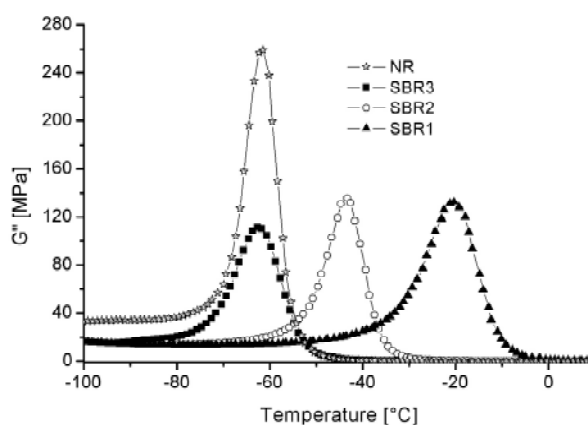


Figure 18: Loss modulus vs. temperature for pure components NR, SBR1, SBR2 and SBR3

Similar results conducted on these rubber blends were obtained by DSC measurements. Table 5 shows the presence of one  $T_g$  for NR/SBR3 while the NR/SBR2 blend presents two distinctive  $T_g$  characteristics for both rubbers.

Table 5. DSC investigation of NR/SBR blends

Blend	$T_g$ [°C]							
	100/0		50/50		30/70		0/100	
NR/SBR2	-63	-	-62	-46	-61	-45	-	-44
NR/SBR3	-63	-	-61		-62		-	-63

As discussed, due to the fact that NR and SBR3 displays the same  $T_g$ , a more detailed dynamic analysis was applied only for the systems NR/SBR2 and NR/SBR1 (Figure 19). As a first observation, it can be seen that the damping maxima for the major blend constituent are systematically shifted from the glass transition temperature of the pure polymer with the lower  $T_g$  towards higher temperatures and for the one with the higher  $T_g$  towards lower temperatures respectively. This temperature shift is an expression of the chain interactions at the phase boundaries of the blend. This behaviour can be explained by assuming an interphase formed by interdiffusion of unlike chains. This interphase will provide a mechanical link able to transmit molecular chain impulses of the more mobile phase (lower  $T_g$ ) to the glassier phase (higher  $T_g$ ). Therefore, the low  $T_g$ -phase reaches the same state of mobility as the pure low  $T_g$ -polymer at higher temperatures. The inverse holds for the high  $T_g$ -phase.

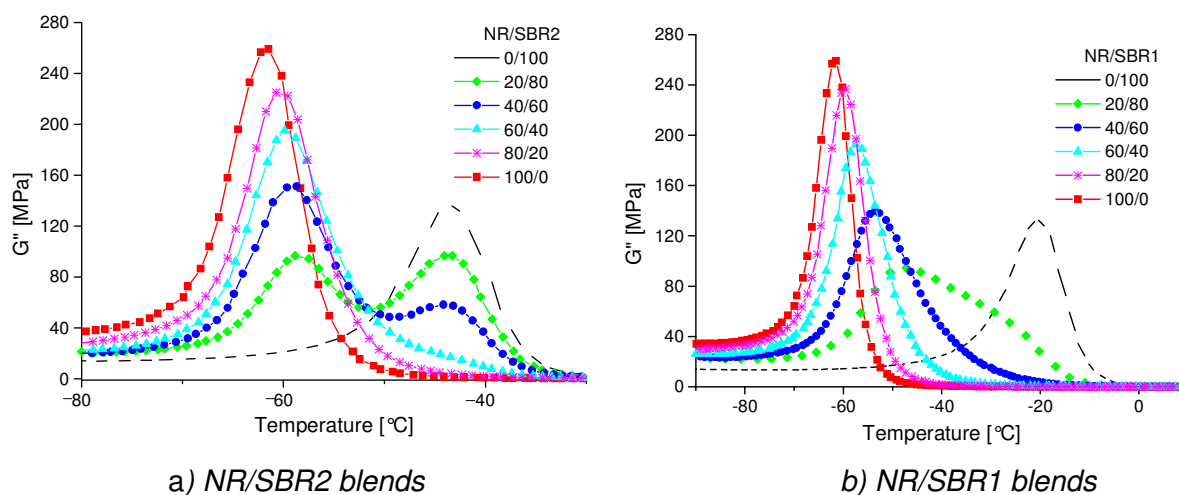


Figure 19: Loss Modulus vs. temperature at different compositions

At a blend ratio of 20/80 NR/SBR1 (Figure 19b), the loss modulus curve covers a large bimodal region with two discrete shoulders related to the NR and SBR1 phase respectively. The strong shift in both damping maxima results in partly overlapping signals. However, this thermodynamic driven behaviour has direct influence on the energy dissipation process in the  $T_g$  region. The broad damping maximum should positively affect the properties of the elastomer contact mechanics such as traction and grip.

Another feature of two-phase systems becomes obvious from the damping curves of both systems. The damping peak of the high  $T_g$  component is not seen until a critical concentration of ca. 20-30 wt.% is reached. Since this concentration is passed the damping signal of the glassy component increases exponentially. This scaling behaviour was observed also for EPDM/SBR [12]. The effect is attributed to the mechanical contribution of the glassy co-continuous phase that is formed above the critical concentration.

A parallel examination of NR/SBR1 at different compositions was performed by DSC (Figure 20). The shift of glass transition to lower value for the NR-phase and to higher values for SBR-phase underlines the interaction between the chains in the interphase that occurs in those blends.

These investigations on blend systems demonstrate that a two-phase behaviour can reveal three significant features:

- (i) the shift of the damping maximum of the low  $T_g$ -phase towards higher temperatures and the shift of the high  $T_g$ -phase towards lower temperatures;
- (ii) the width of the damping curve becomes larger if the blend ratio is approaching the 50/50 value;
- (iii) the minor SBR-phase does not exhibit a separate damping signal until the phase inversion region is reached.

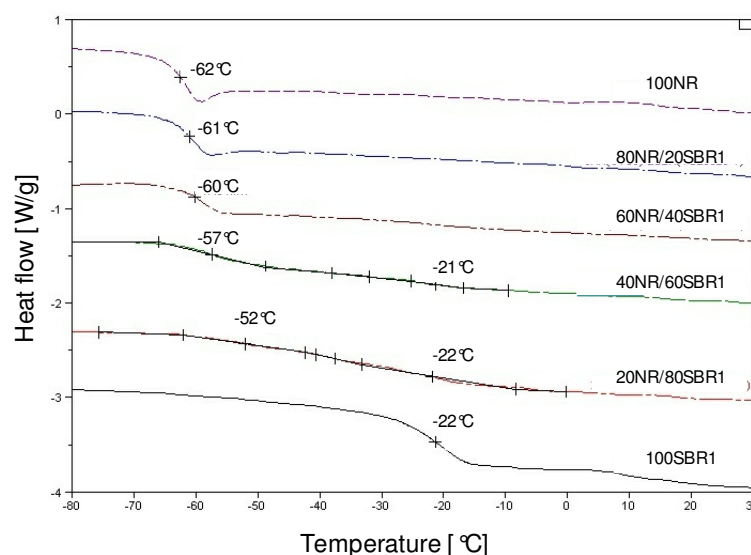


Figure 20: Thermogram of NR/SBR1 at different blend ratio

When the  $\delta$ -parameter difference of a blend becomes smaller, the  $T_g$ -shift of both phases is more pronounced due to a stronger interaction in the interphase. Thus, in some cases, the damping maxima cannot be resolved efficiently by means of mechanic-dynamic spectroscopy. The blend NR/SBR1 is a good example for such a system.

Figure 21 offers a better view on the quantitative  $T_g$ -shift of NR in the two blends analyzed. Only by increasing the content in 1,2-butadiene units from 25 to 50 wt% while keeping the styrene content constant, the polarizability of the chain segments is reduced in SBR1 compared to SBR2. This results in considerable differences in the interaction of SBR towards NR. The higher the degree of compatibility or the lower the  $\delta$ -parameter difference the more pronounced the  $T_g$ -shift. The  $T_g$ -shift of the SBR-phase can also be observed in case of NR/SBR2. Due to the

formation of a bimodal damping maximum, it is rather difficult to assess a quantitative value for this  $T_g$ -shift.

Another important indicator by which the compatibility of blends can be expressed is the half width of the damping peak in the major phase. The analysis of the damping behaviour of the two blends NR/SBR1 and NR/SBR2 provides information about the changing of the half width in those blends. In the order in which compatibility increases, the half width likewise increases by a constant volume fraction of the NR components.

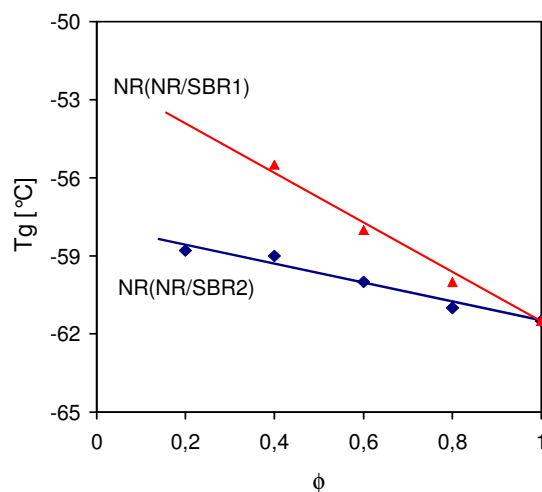


Figure 21: Shift of  $T_g$ (NR) in NR/SBR2 and NR/SBR1 blends (Blend systems are indicated;  $\phi$  is the volume fraction of NR)

However, due to the pronounced  $T_g$ -shift of the SBR1-phase signal in NR/SBR1 the damping peak at a blend ratio of 40/60 demonstrates a bimodal shape. This leads to an overestimation of the half width in Figure 22.

In conclusion, both, the  $T_g$ -shift and the broadness of the damping peaks can be considered as phenomenological criteria for evaluating polymer compatibility.

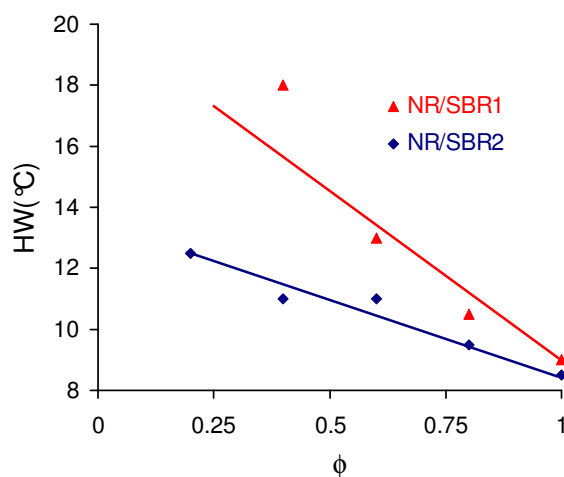


Figure 22: Half width (HW) of the NR damping peaks vs. the volume fraction of NR

When investigating the  $G''(T)$  curves of NR/SBR2 as a function of composition (Figure 19a) more carefully, it can be observed that  $G''$  for SBR2 is very small until a critical concentration (ca.  $\phi = 0,35$ ) is reached. The SBR2-phase does participate insignificantly in the entire mechanical behaviour. Above this critical concentration, an exponential increase in the damping maximum can be observed. This behaviour is related to the phenomenon of phase inversion. Below the critical concentration, the minor SBR2-phase is dispersed as more or less glassy domains in the amorphous and rubbery NR matrix. The mechanical response of such dispersed glassy domains should correspond to that of hydro-dynamical reinforcing effects. Above the critical concentration the increase in  $G''$  can be attributed to the formation of a co-continuous phase morphology in which the predominant mechanical contribution is controlled by the glassy polymer. However, the limiting value is reached when the glassy polymer becomes the continuous phase at even higher concentrations. The critical concentration indicates the "phase inversion" where co-continuous morphology is formed. In the entire system, the formation of the interconnected rigid branches of the glassy polymer forms plays a major mechanical role [11].

In case of NR/SBR1 with a higher degree of compatibility, this special feature is also observed (Figure 19b), even if the formation of a broad bimodal damping peak makes it more difficult to assign the individual mechanical contributions of the blend constituents. Up to a 40% concentration of SBR1, only the damping maximum of NR is observed. Above this concentration, the SBR1 phase forms a discrete and exponentially increasing damping maximum. The mechanically observable critical concentration threshold for the formation of co-continuous phase morphology is shifted to higher concentrations of SBR. For the less compatible blend NR/SBR2 the appearance of a discrete SBR-phase signal becomes evident at much lower concentrations. This can be also understood by the fact that the volume fraction of SBR-chains involved in an intimate interaction with NR is smaller. The evolution of the damping maximum of the high  $T_g$ -phase as a function of the blend composition is shown for both blend systems in Figure 23.

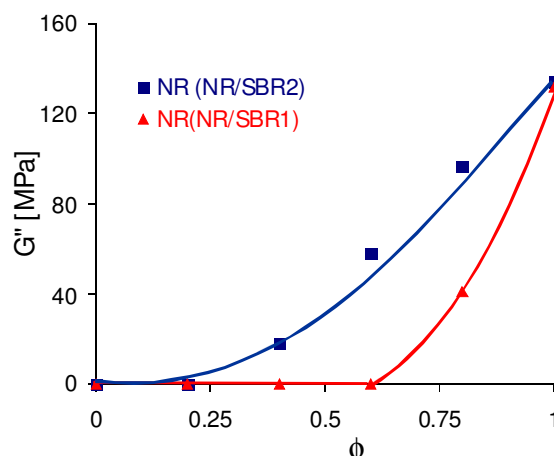


Figure 23: Inverse of the damping signal of the SBR-phase in NR/SBR2 and NR/SBR1 blends (Blend systems are indicated;  $\phi$  is the volume fraction of SBR)

Transmission Electron Microscopy gives essential information about the morphology of the blends. In the micrographs obtained, the NR phase appears as bright domains while the SBR phase forms the dark ones due to higher electron density. In order to evaluate the influence of the  $\delta$ -parameter difference and the interfacial tension the blend ratio of 20/80 was chosen. By this, the dispersed domains of the minor phase can be determined more precisely, because the interpenetrating phase network has not yet been formed.

Figure 24 shows the phase morphology at constant mixing time (10 min) for the three blends under investigation.

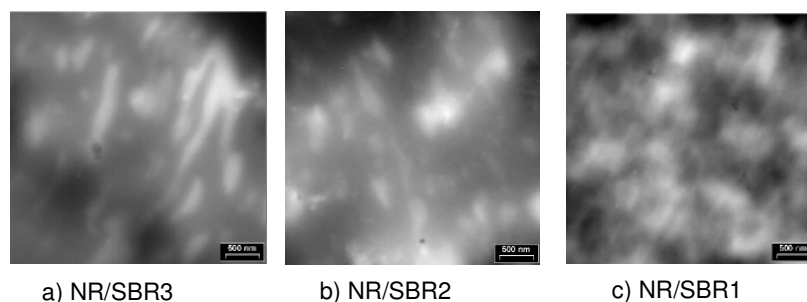


Figure 24: TEM micrographs of NR blends with: a) SBR3; b) SBR2; c) SBR1 at (20/80)

It can be observed that by increasing the content of 1,2-butadiene units in SBR (from SBR3 to SBR1), the dispersed NR domains become smaller and their shape is less elongated and more ellipsoidal or even spherical. In addition, the size distribution becomes narrower. This means also that the blends become more homogeneous. The improvement of the blend homogeneity also should lead to better processing behaviour and improved physical properties of the crosslinked material. Considering the equivalent sphere diameters for the dispersed domains, it has been found that the average domain size increases linearly with increasing the  $\delta$ -parameter difference (Figure 25).

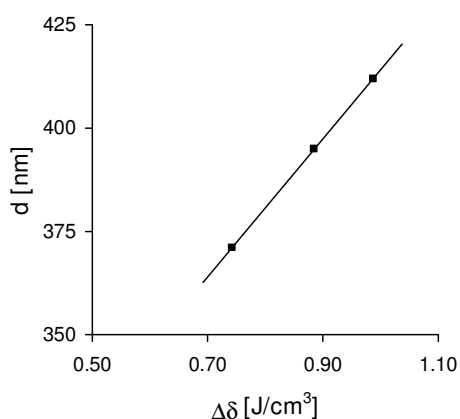


Figure 25: The average domain size vs. solubility parameter difference

The observed dependency is confirming the theoretical considerations that require proportionality between the average domain size of a blend system and the interfacial tension, which is approximated in this work by the  $\delta$ -parameter difference.

### Blends with epoxidized rubbers

As expected from the predictions based on the  $\delta$ -parameter concept, among the blends with epoxidized rubbers studied the best compatibility was observed for the ENR/EpSBR with a low  $\delta$ -parameter difference. The dynamic mechanical analysis of the blend provides one discrete damping peak over the entire concentration range (Figure 26). However, this result is not unquestionable since the difference of the  $T_g$ 's of the blend constituents is rather small (Table 2) and the half width of the damping peaks increases strongly for blend ratios between 40/60 and 60/40. Therefore, one question concerning the compatibility of this blend system is whether the blend system consists of a single phase or not.

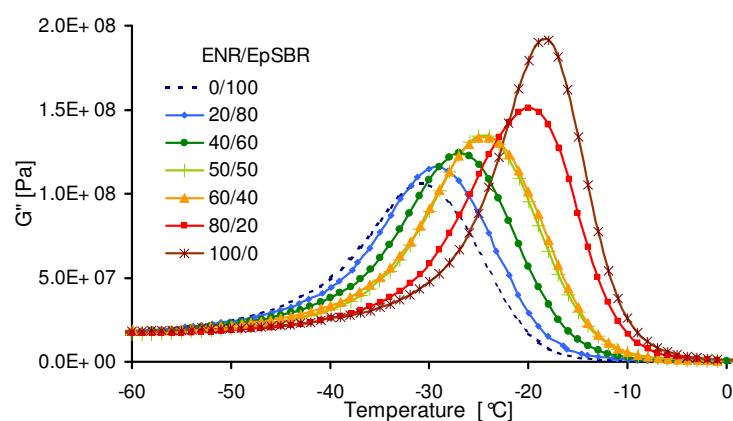


Figure 26: Loss modulus vs. temperature for different compositions of ENR/EpSBR blends.

The quantitative description of this behaviour was studied by means of Flory-Fox equation [91] where the  $\phi_1$ ,  $\phi_2$  are the volume fractions and  $w_1$ ,  $w_2$  are the weight fractions of the component.

$$\frac{1}{T_g} = \frac{\phi_1}{T_{g1}} + \frac{\phi_2}{T_{g2}} = \frac{w_1}{T_{g1}} + \frac{w_2}{T_{g2}} \quad \text{Equ. (65)}$$

The results presented in Figure 27 show a reliable phenomenological description of the single-phase behaviour of the ENR/EpSBR blend.

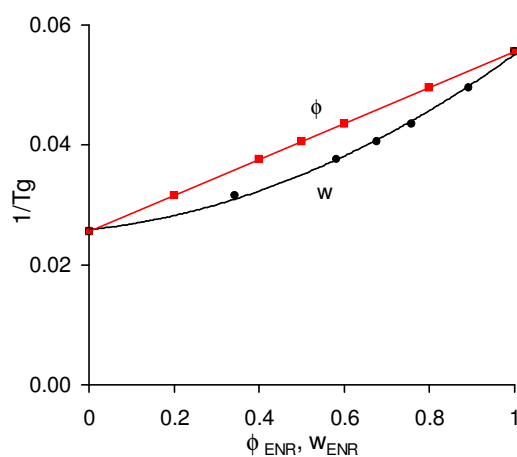


Figure 27: Variation of  $1/T_g$  versus volume fraction of ENR



Due to the limited resolution of the dynamic-mechanical spectroscopy and the observation that half width of the damping maxima increases significantly the morphology of this blend as well as the others containing the epoxidated polymers were investigated by ESI-TEM. This method (Figure 28 delivers valuable information concerning the phase morphology. The presence of two distinct phases was noticed in all the blends under consideration. The presumed phase separation for ENR/EpSBR was demonstrated by TEM. The optical contrasting procedure facilitates a better insight in the material by exploiting different electron densities. The sensitivity of the TEM method was of advantage for investigation.

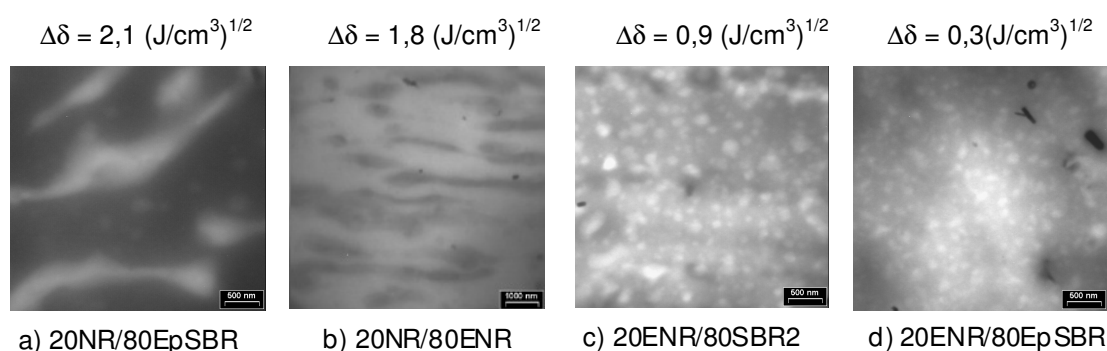


Figure 28: TEM micrographs of various blend systems

The polarity gap between the blends constituents is higher for NR/EpSBR due to the presence of both the polar oxirane rings and the styrene segments in the EpSBR (Figure 29a). The phase separation that occurs in this system was demonstrated also by the dynamic mechanical investigation (Figure 29 a and b). Considering the non-polar system NR/SBR2 as a reference, the average size of the bright NR domains is smaller than those shown for ENR/SBR2. The presence of epoxy groups in polyisoprene chains increases considerably the solubility parameter and reduces the thermodynamic dissimilarity in the ENR/SBR2 blend.

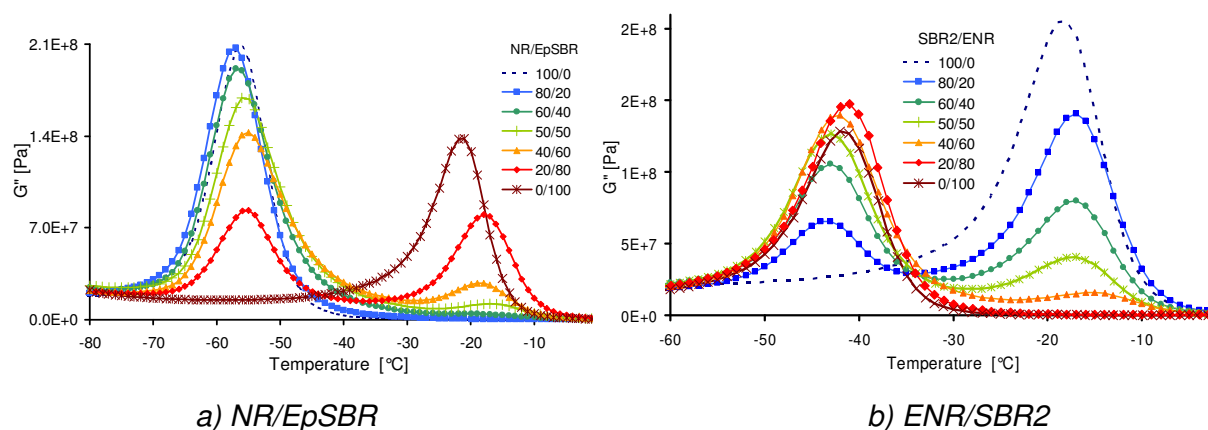


Figure 29: Loss modulus vs. temperature for different compositions of NR/EpSBR and ENR/SBR2 blends

Epoxidation of 30% of the butadiene units of SBR leads in NR/EpSBR to even larger NR domains with a broad size distribution and poor blend homogeneity. Compared to NR/SBR2 the majority of the NR domains present an elongated shape, preserving to some extent the influence of the shear field during the mixing process (Figure 29). The elongated shape of the NR domains can also be observed for NR/ENR, however the NR domain size is slightly smaller in comparison to those of NR/EpSBR.

Further, the study of the influence of viscosity on the blend morphology of the two systems consisting of ENR and SBR2 with different blend concentrations is summarized in Figure 30.

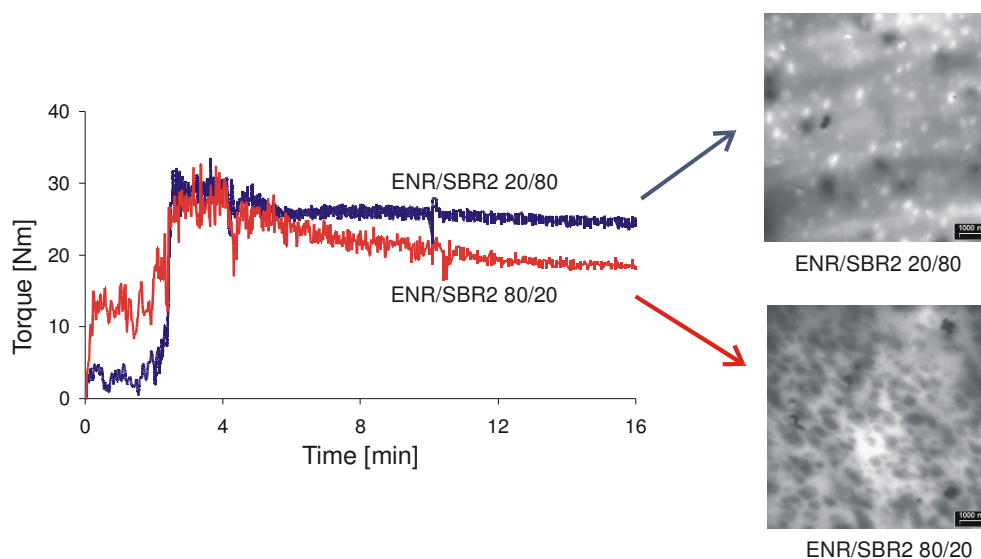


Figure 30: Influence of the viscosity on the morphology of ENR/SBR2 blends

The TEM micrograph of 20/80 ENR/SBR2 shows small white NR domains dispersed in the dark SBR matrix meanwhile when the 80/20 ENR/SBR2 investigated the dark SBR domains are larger being dispersed in the NR matrix. The size of the larger domains is dependent on the used mixture energy, which decreases with increasing of the torque that means that the 20/80 ENR/SBR2 has a higher viscosity compared to 80/20 ENR/SBR2.

#### *Blends with nitrile rubbers*

If a rubber blend consists of two rubbers with different polarity, i.e. NR and NBR, the  $\delta$ -parameter difference is high, leading to strongly phase separated blends. The influence of the acrylonitrile groups on the blend morphology was investigated by using NBR with an increasing content of acrylonitrile groups (Table 2 and Figure 31).

The comparison of the raw polymers demonstrates that the acrylonitrile content has a significant influence on the glass transition temperature of the rubbers. An increase of the ACN content results in a shift of the  $T_g$  to higher temperatures (Figure 31a). The dynamical mechanical investigation of all NR/NBR rubber blends shows two discrete glass transitions for both rubber

phases (Figure 31b). The  $T_g$ 's of the blend are the same as the  $T_g$ 's of the rubbers in the pure state.

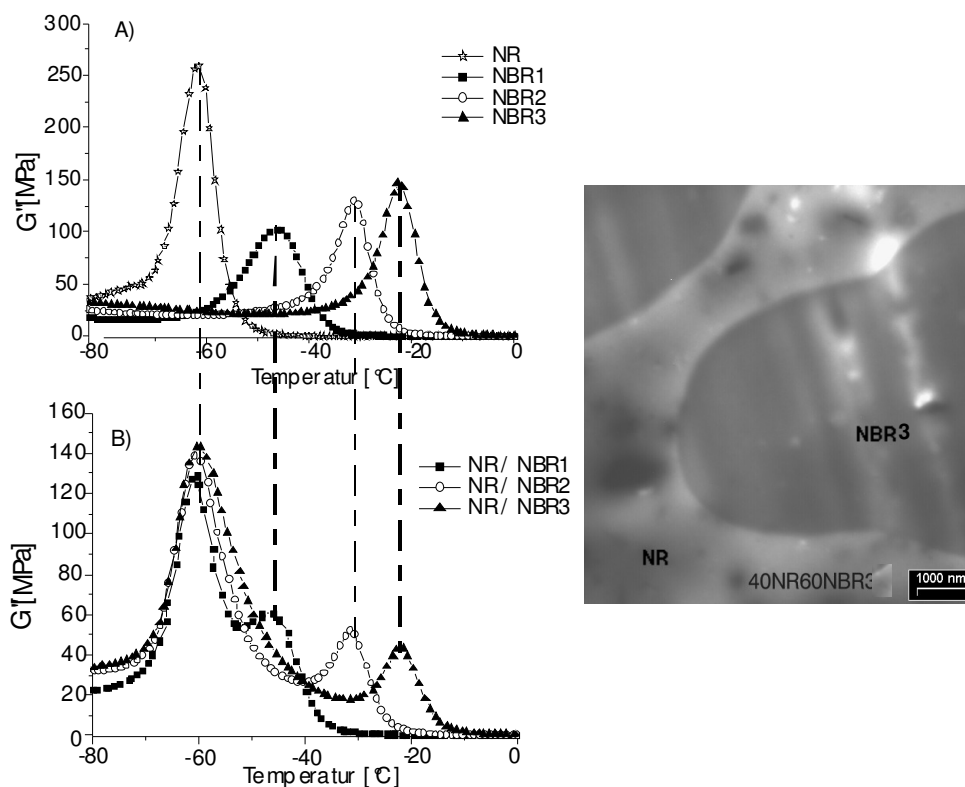


Figure 31: Phase morphology investigations of: A) NR and NBR rubbers in pure state; B) the NR/NBR blends with different ACN content

The large differences in the solubility parameter are responsible for the large domains size found by TEM investigations. The domains formed by mixing of the two rubbers are very large, to more extends considering that the magnification used was 1000 nm, when comparing with NR/SBR. By NR/SBR system the magnification used was 500 nm. This result suggests how large the domains in NR/NBR are and emphasises the incompatibility of those NR/NBR systems. The DSC measurements summarized in Table 6 confirm the dynamic mechanical measurements as well as the TEM investigation.

Table 6: DSC investigation of NR/NBR blends

Blend	$T_g$ [°C]							
	100/0		50/50		30/70		0/100	
NR/NBR1	-62	-	-63	-47	-62	-46	-	-45
NR/NBR2	-62	-	-62	-31	-62	-31	-	-31
NR/NBR3	-62	-	-62	-21	-62	-21	-	-22

The findings obtained by the three methods indicated that NR/NBR systems are incompatible in comparison with NR/SBR and BR/SBR blends. Higher difference between the solubility

parameters of the rubbers leads to a higher interfacial tension, which is responsible for this behaviour.

Another example for an incompatible blend is the NBR3/SBR4 blend. The variation of the loss modulus with temperature is presented in Figure 32.

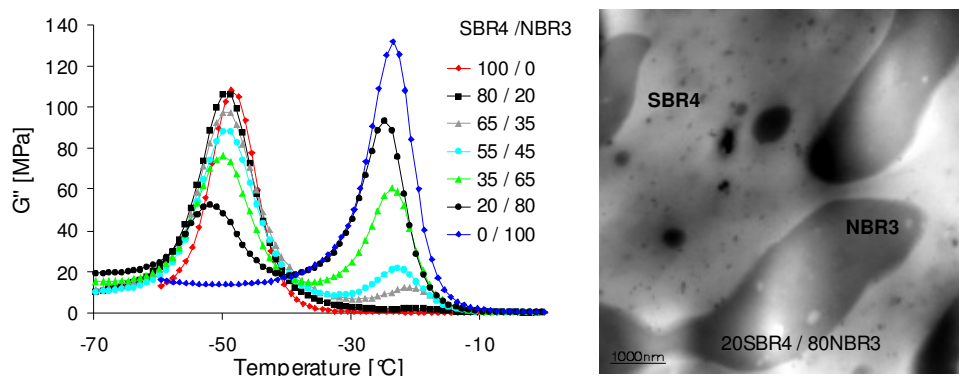


Figure 32: Phase morphology analysis of SBR4/NBR3 blends

Two different glass transitions could be observed, for the SBR-phase there is a slight shift of the glass transition temperature to a small value respectively to higher temperatures for the NBR-phase as the concentration of the minor component increases. Therefore, a phase separation occurs in this system and leads to an incompatible system. These findings were observed also by the thermal characterization displayed in Table 7.

Table 7: DSC investigation of SBR4/NBR3 blends

Blend ratio SBR4/NBR3	$T_g$ [°C]	
	100/0	-49
80/20	-49	-19
65/35	-49	-20
55/45	-50	-20
35/65	-50	-20
20/80	-51	-23
0/100	-	-23

This second example, SBR4/NBR3 underlines again that a higher difference in the solubility of the two rubbers plays a major role in the compatibility of the rubber blends. The higher the difference in the solubility parameter the less compatible blends is obtained. However, an even small interaction leads to small  $T_g$ -shifts in the phase inversion phase.

### Interphase

For an estimation of the interphase volume fraction in rubber, blends the information derived from dynamical mechanical investigations can be exploited. From universal considerations of energy conservation it becomes evident that in a composite system each phase contributes to the mechanical modulus ( $G'$  or  $G''$ ) with a value that is proportional to both the local deformation of the phase under consideration and the volume fraction of the phase. Because the micromechanics of polymer blends are not well known and the local deformation of particular phases is difficult to be measured, the evaluation of the interphase was performed by a fitting procedure [11, 13]. It was assumed that the experimentally measured loss modulus of the blend components comprises the sum of the relaxations of all phases present in the blend. The contribution of the interphase formed by interdiffusion of unlike chains should demonstrate its mechanical response in the temperature range between the two glass transition temperatures of the blend constituents. Further on, the fitting procedure [11] was performed so that the curves  $G''$  vs.  $T$  of the original (pure) polymers were fitted for the blend ratio under consideration and adjusted for a temperature shift. After these operations the curves were summed up by taking into consideration that the sum should result exactly in the front and rear profile of the experimental curve  $G''(T)$  below the lower and above the upper damping maximum.

Examining several rubber blends and considering the variation of the vinyl amount in styrene butadiene rubber or by introducing epoxy rings interesting results about the study of interphase were encompassed.

#### *BR/SBR blends*

The fitting procedure used to describe the loss modulus as a function of the temperature has been applied by modifying the three spline fit parameters (the amplitude, the temperature shift and the width of the damping maxima) of the two components of the blend for the best fit to the experimental curves. As a result, the calculated curve fits very well the area below the low  $T_g$ -peak and above the high  $T_g$ -peak, but does not fit the curve in the temperature range between the two damping maxima. The difference of the blends signal and the two-phase fit is considered as the mechanical damping signal of the interphase. Irrespective of the local deformations of the interphase present in the blend, the amplitude or more accurately the area of the interphase signal corresponds to the volume fraction of the interphase.

A first blend investigated was BR/SBR where it was intended to see the influence of microstructure of SBR on the interphase. The SBR1, SBR2 to SBR3 were used. A convenient and compact way of comparing systems is by plotting the interphase loss modulus signal against the temperature. From such a diagram, it could be observed which system leads to a higher interphase (Figure 33a). The interphase area obtained was standardized to the area of BR/SBR3 and is plotted as a function of the vinyl content.

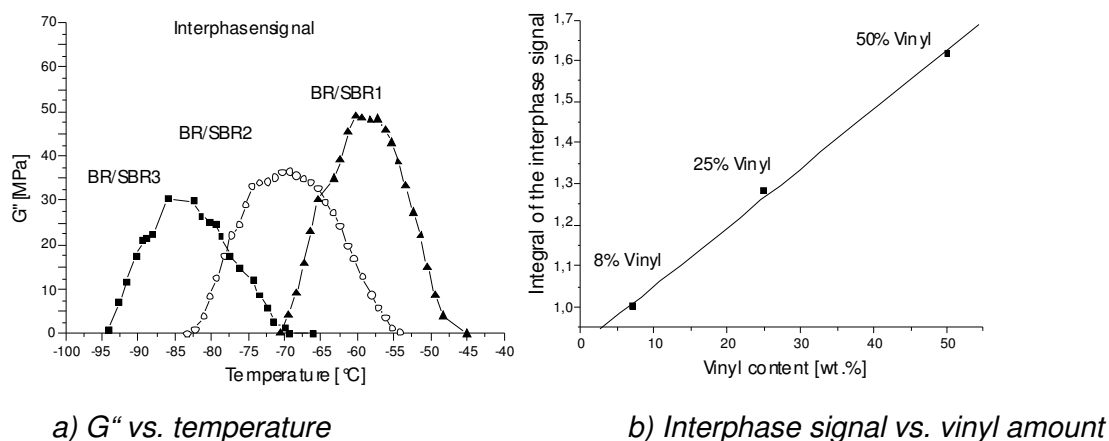


Figure 33: Dependency of interphase signal to the vinyl amount in SBR

Figure 33b provides a linear relationship between the signal of the interphase and the vinyl groups in the range of the errors by using this method in order to estimate the interphase. As can be noticed the amount of the vinyl groups has a great impact on the blend morphology and is responsible for the amount of the interphase that occurs as will be explained in the following section for the system NR/SBR.

#### NR/SBR blends

Figure 34 shows the results obtained from the investigation of the interphase signal in NR/SBR1 and NR/SBR2 systems. It was noticed that the interphase signal increases with the degree of compatibility of the blend constituents. There are several contributions, which have to be considered in order to understand this increase. The one contribution is certainly the smaller difference in the  $\delta$ -parameters that corresponds to a smaller interfacial tension.

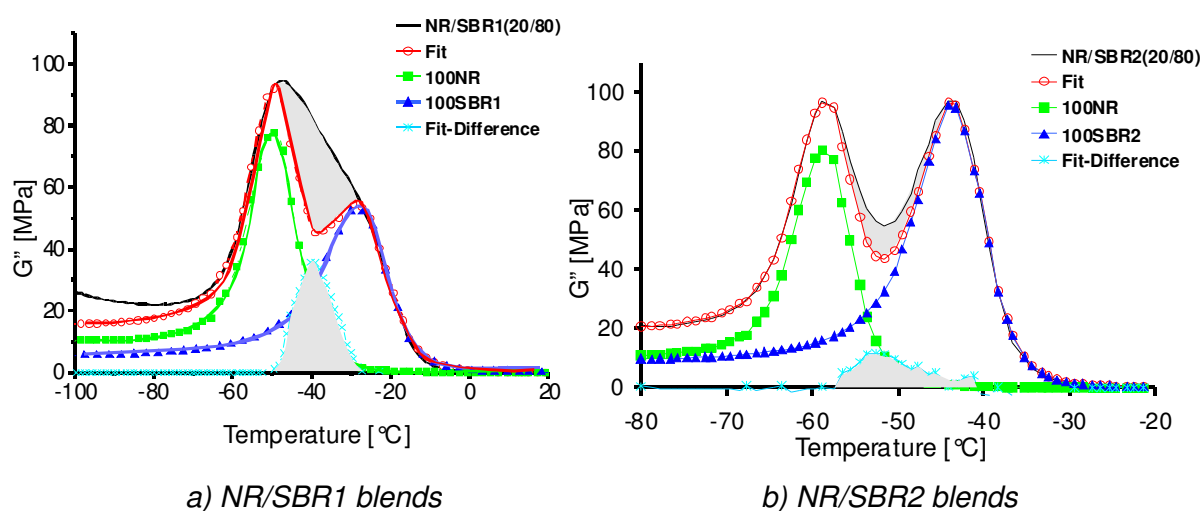


Figure 34: Evaluation of the volume fraction of the interphase.

This decrease of the interfacial tension is responsible for a decrease of the average domain size of the phases, which is equivalent to an increase of the number of domains per unit volume. The

other contribution originates also in the interfacial tension but affects the thickness of the interphase that increases inverse proportional to the interfacial tension.

The amount of interphase in NR/SBR blends with different content in 1,2-butadiene units was measured at different blend ratios (Figure 35).

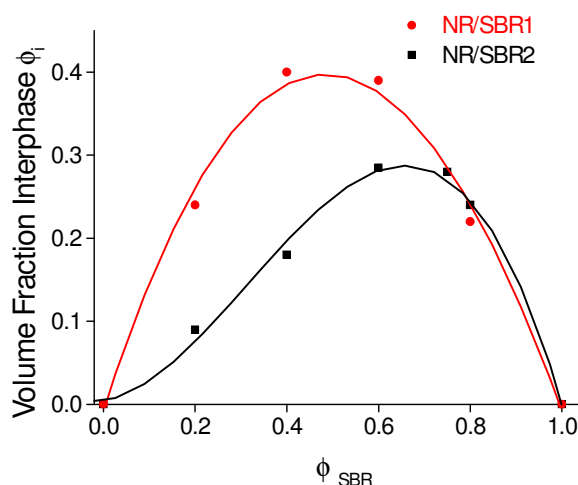


Figure 35: Volume fraction of the interphase as a function of blend composition for NR/SBR blends

It can be noticed that due to the rather high degree of compatibility in the case of NR/SBR1 blend, the volume fraction of the interphase reaches high values of 0,4. If the interfacial thickness in this blend is calculated by applying a simple geometrical core-shell model taking the equivalent shear diameter of the domains into account, a surprisingly high value of ca. 30 - 35 nm is found. It can be concluded that the mechanical method applied to a crosslinked system overestimates the thickness of the interphase and the volume fraction as well. The entire curve has a symmetrical aspect; the maximum value of the interphase signal is achieved at  $\phi_{\text{SBR}} \approx 0,5$ . The less compatible NR/SBR2 blend demonstrates only a volume fraction of the interphase of 0,28 at a SBR concentration of  $\phi_{\text{SBR}} \approx 0,75$ . The observed asymmetry of the curve was found for other blend systems as well (see below). The shape of the curve can be explained by taking into consideration the interaction potentials of the discrete chain segments in SBR and NR. The polarizability of cis-1,4-isoprene units is equal or very similar to that of 1,2-butadiene units. Therefore, the mutual interaction of these two unlike chain segments is providing the highest energy exchange in intermolecular interactions. In comparison, the interaction between cis-1,4-isoprene units and cis-1,4-butadiene units is less favourable. Assuming that the interacting SBR chains present in the interphase can change their coil conformation to some extent, it can be assumed that by effecting such conformational changes more 1,2-butadiene units are placed in the interphase. Thus, they can interact with the cis-1,4-isoprene of the NR chains units placed in the interphase. By increasing the volume fraction of SBR2 (smaller content in 1,2 butadiene

units), the probability that such conformational changes lead to energetically favourable interactions increases. Only at an excess of SBR2 the energetic inside the interphase seems to be similar to those in the NR/SBR1 (50/50) blend.

#### *Blends with epoxidized rubbers*

For blend systems containing epoxidized rubber, the volume fraction of the interphase was determined by using the same procedure.

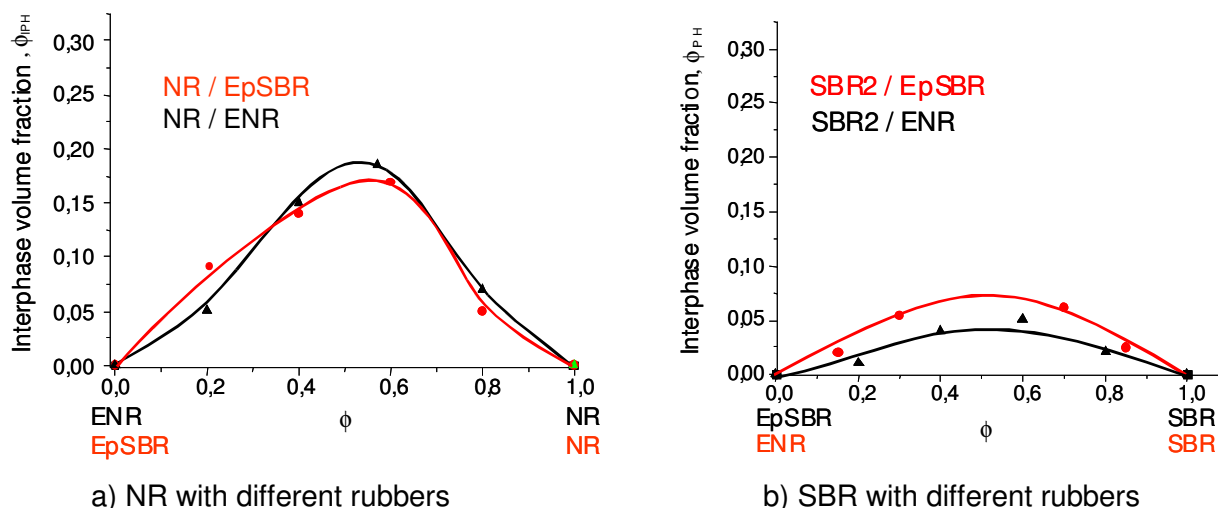


Figure 36: Interphase signal vs. SBR-volume fraction for different rubber blends

The NR blends with ENR and EpSBR display a similar but lower value of the interphase volume fraction than the one of NR/SBR2 taken as a reference.

In Figure 36 b it can be noticed that the maximum of the interphase volume fraction varies 0,07 for the EpSBR/SBR2 blend to 0,05 respectively for the ENR/SBR2 blend. These different maxima of the interphase volume fraction occur because of the interaction between the rubber chains due to the polarity of the epoxidised rubber.

## 4.2 Rubber-additive interaction

Low molecular substances, most of them undefined mixtures, are being employed to improve processing of compounds containing rubber blends. The effects of these mixes, often named as additives, is reaching from lowering the viscosity of polymer blends over modification of low temperature properties to phase compatibilization. Depending upon processing and content of these additives lower energy consumption in the production of raw rubber compounds or a higher level of quality assurance in respect to specified product properties can be achieved by the use of these substances. As raw materials easily accessible substances with a heat of evaporation as low as possible (which means having a high molecular weight) and with a melting point above room temperature, preferably as solid materials, are being employed.



These conditions are a direct consequence from the requirements of practical application of these materials in technical production processes. Furthermore, another condition is the limited solubility of the additives in the target polymers to lower the viscosity of the whole polymer melt by forming phase separated intramolecular gliding films, which contribute to lower energy consumption during procession of rubber compounds.

Though the technical applied additives are mostly mixtures from different substances it is hardly possible to assign observed effects to well defined molecular properties. Having the goal to establish structure-property relations, the following work investigates in detail the effects of well-chosen substances in a commonly used polymer.

The interaction of low molecular components with the polymer will be described considering the variation of the glass transition temperature and the solubility limit at low temperatures.

The solubility at realistic processing temperatures should be investigated by taking the example of a technically used additive. Hereby linear fatty alcohols, -acids and -esters were used as model substances varying in their length of the alkyl chain ( $C_{12}$  and  $C_{18}$ ). Targeted values are glass transition temperature  $T_g$  and solubility by direct comparison of the  $C_{12}$  and  $C_{18}$ -substances.

The functionality as well as the molecular weight has been changed systematically. In addition, an industrial additive has been integrated into the study. The substances have been characterized by means of DSC regarding their melting point and melting enthalpy (Figure 37).

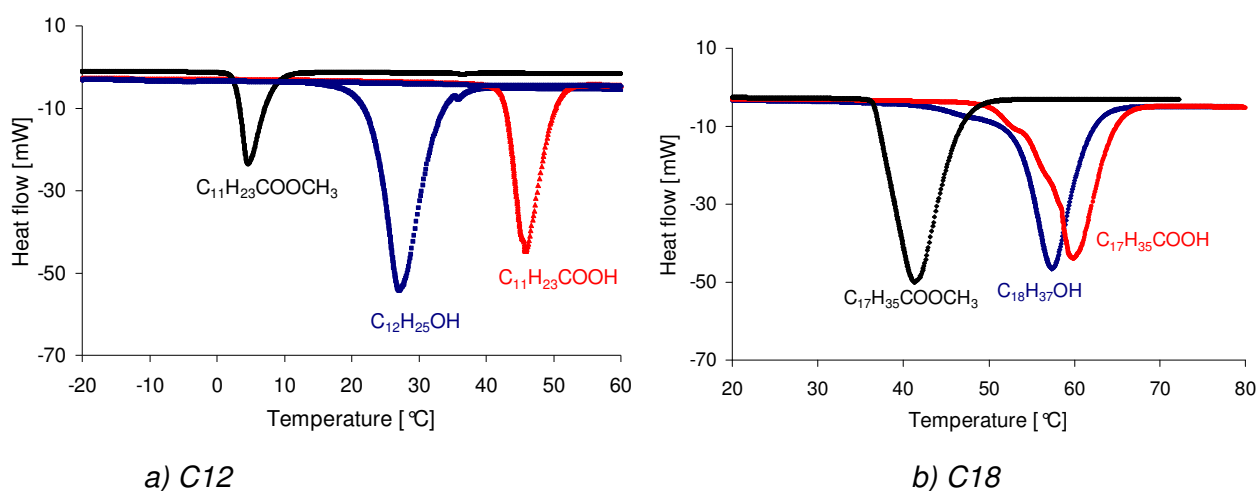


Figure 37: DSC characterization of compounds used as additives

The DSC investigation of the industrial additive is displayed in Figure 38 and shows two melting temperatures (at 78°C and 101°C), which indicates the presence of more components on this product.

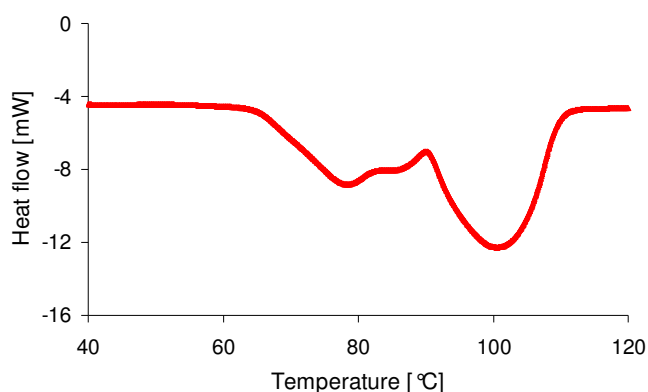


Figure 38: DSC characterization of the industrial additive

To obtain more information about the chemical composition of the industrial additive ATR-FT-IR spectroscopy investigation was done. The results are comprised in Figure 39.

In the spectrum occur the characteristic bands of the symmetric C-H oscillation ( $2849\text{ cm}^{-1}$ ) and the asymmetric C-H oscillation ( $2921\text{ cm}^{-1}$ ), the band for zinc-stearate to  $1538\text{ cm}^{-1}$ , the band for  $\text{CH}_2$ -group at  $1400\text{ cm}^{-1}$  and  $1465\text{ cm}^{-1}$ . The doublet that appears at  $722\text{ cm}^{-1}$  is characteristic for  $\text{CH}_2$ -groups, which are present in a long chain. The interpretation of the relatively simple IR-spectrum leads to the conclusion that the industrial additive is a zinc salt based on fatty acid, mixture of the C16 and C18 saturated and unsaturated chains.

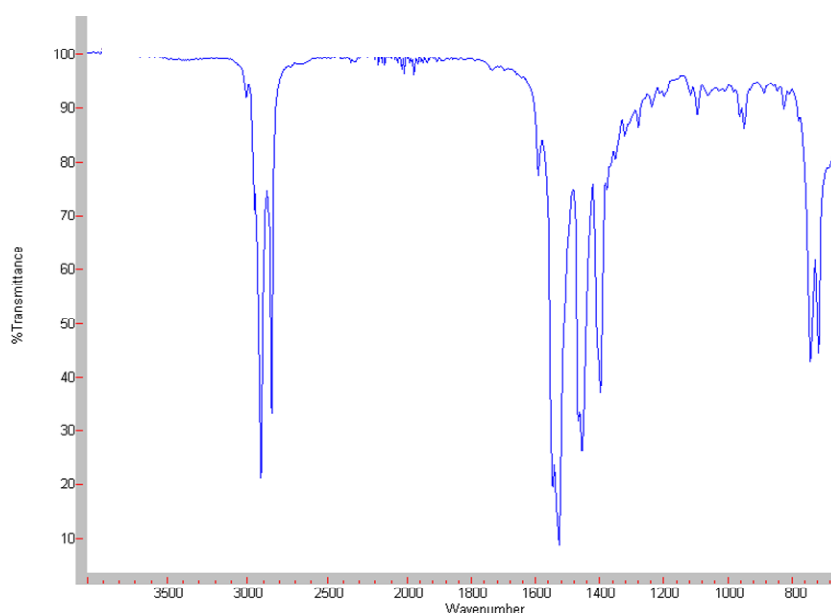


Figure 39: IR-spectra of the industrial additive

The thermal characterization of the model additives and the industrial additive is summarized in Table 8. A comparison of the results obtained with the data delivered by the literature is done.

Table 8. Compounds used as additives

Processing aids	System	T <sub>m</sub> [°C] (Literature)	T <sub>m</sub> [°C]		ΔH <sub>m</sub> [J/g]	
			± 0,1		± 0,36	
C <sub>12</sub> H <sub>25</sub> OH	A	26	27		188	
C <sub>11</sub> H <sub>23</sub> COOH	B	44	45		207	
C <sub>11</sub> H <sub>23</sub> COOCH <sub>3</sub>	C	4,8	5		47	
C <sub>18</sub> H <sub>37</sub> OH	D	61	57		192	
C <sub>17</sub> H <sub>35</sub> COOH	E	68	60		248	
C <sub>17</sub> H <sub>35</sub> COOCH <sub>3</sub>	F	38	41		217	
Industrial additive	G	-	78	101	17	52

It can be noticed that the experimental values obtained for the melting temperatures are in agreement with the ones shown in literature considering small errors, which can be due to the measuring method employed. The C<sub>12</sub>-ester shows a lower T<sub>m</sub> comparing with the data given in literature probably due to the fact that the additive used in this case has a less purity. Generally, the same behaviour considering the melting temperature as well as the melting enthalpy was observed.

The investigations were done on unvulcanised samples using till 6 phr model additive. This concentration range is relevant for technical application.

The sample abbreviation used combines the functionality, the number of C-atoms as displayed in Table 8, and the concentration of the additive as indicated in Table 9. For example A1 represents the mixture of SBR4 with 1,5 phr n-dodecanol.

For the vulcanisation of the samples, sulphur and dithiophosphat (SDT) as accelerator were used.

Table 9. Test recipes used

Materials	System [phr]						
	0	1	2	3	4	5	6
SBR4	100,0	100,0	100,0	100,0	100,0	100,0	100,0
Processing aids	-	1,5	3,0	4,5	6,0	30,0	-
ZnO	-	-	-	-	-	-	4,0
Stearic acid	-	-	-	-	-	-	3,0
Rhenofit SASD (SDT)	-	-	-	-	-	-	5,6
Sulphur	-	-	-	-	-	-	2,0

#### 4.2.1 Impact on glass transition

By the addition of a low molecular component to a polymer, the free volume in the overall system increases. Through this, the translational movements of the polymer chains are favoured and this is expressed by a decrease of the glass transition temperature.

In order to gain more detailed information about the effect of the functional groups and the chain length of the model additives on the low temperature mobility of rubber chains, the systems were investigated by differential scanning calorimetry. As a result it was shown, that even at low

concentrations the additives lead to a decrease of the glass transition temperature ( $T_g$ ) until the phase separation is reached. The plasticizing efficiency ( $\Delta T_g/\Delta c$ ), which is defined as the decrease in  $T_g$  provoked by the concentration unit (in mole %) of a given additive was used for a reliable comparison between the systems under consideration. Above of the concentration where phase separation takes place the  $T_g$  of the polymer-additive mix tends to reach a constant value within the frame of the experimental errors.

By employing pure substances as model additives the phase separation is additionally supported by their crystallization tendency. Therefore, the appearance of an endothermic melting peak indicates phase separation. The area of the peak corresponds to the melting enthalpy of the share of phase separated model. This is exemplarily shown for the system SBR4/ $C_{18}H_{37}OH$  in Figure 40. A discrete phase is formed even at 1,5 phr of the fatty alcohol additive. By further increasing the additive concentration, the melting enthalpy and the melting temperature increase. This indicates that the amount but also the size of the phase-separated crystallites is increasing. As a result both values, the melting temperature and the melting enthalpy, tend to reach the value of the pure additive while the  $T_g$  of the rubber remains constant.

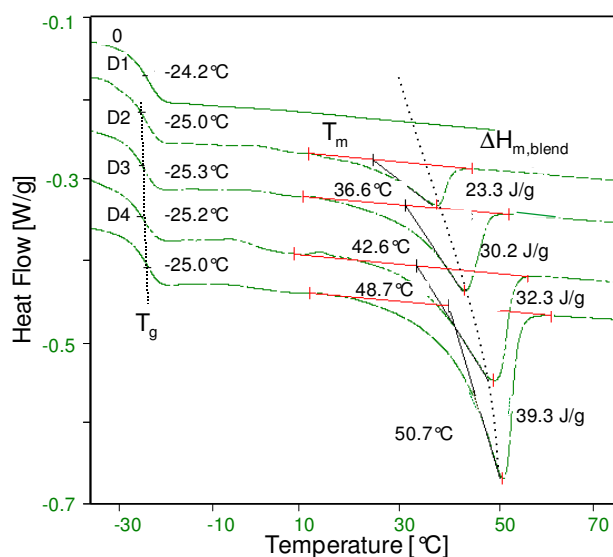


Figure 40:  $T_g$ -concentration phase diagrams for SBR4/ $C_{18}H_{37}OH$

Despite its long hydrocarbon chain the fatty alcohol is practically not soluble at low temperatures in SBR4. A pronounced melting peak of the additive becomes obvious even at concentration of 5 mmole% indicates, that the electrostatic H-bonding interactions of the OH-groups govern the phase separation. The opposite is the case for the methyl ester of the  $C_{12}$  and  $C_{18}$  fatty acids.

Figure 41 shows the case where phase separation of the  $C_{12}$ -methyl ester does not occur in the concentration range considered. The linear decrease of the glass transition temperature indicates a good solubility of the ester in the polymer based on a good interaction. The  $T_g$ -shift of 10 °C for 6 phr of the model additive indicates that by reducing the intermolecular interactions

of the additive to the level of dipole-dipole interactions the tendency for a crystallization driven phase separation is not pronounced, the increase in free volume is higher than for the corresponding alcohol the increase of the low temperature flexibility of the polymer.

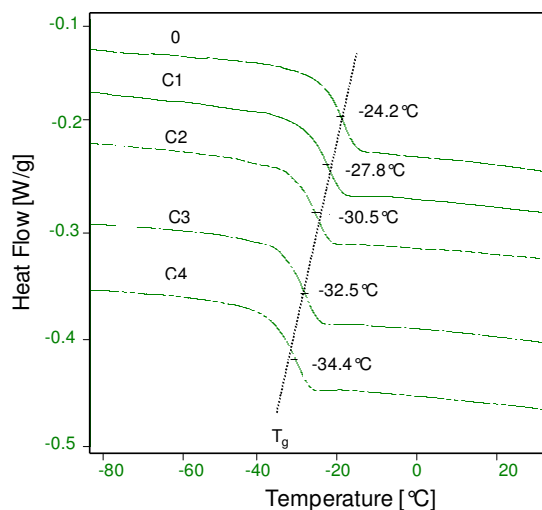


Figure 41:  $T_g$ -concentration phase diagrams for  $SBR4/C_{11}H_{23}COOCH_3$

When comparing the plasticizing efficiency at very small additive concentrations it becomes obvious that both the functional groups as well as the length of the hydrocarbon moiety of the model additive are affecting this parameter (Figure 42 a and b). Irrespective of the molecular weight (C-number) of the additive the methyl-ester demonstrates the highest plasticizing efficiency, whereas the effects exerted by the alcohol and the acid respectively are similarly graded. For the  $C_{12}$ -additive series, the relatively short chain length of fatty alcohol and fatty acid can bring sufficient solubility in order to give the plasticizing effect. The difference in the plasticizing efficiency of the fatty acid ester is not so pronounced as in the  $C_{18}$ -additive series. Beside to the strongly reduced tendency to self-associations, the ester group is able for positive interact with the phenyl groups of SBR. Both causes contribute to the observed shape of the curve. The reduced plasticizing effects as well as the small solubility of the fatty alcohols and the fatty acids can be attributed to the formation of intermolecular clusters based on strong hydrogen bonds. The self-association of the molecules involved in the clustering process reduces the translation movement as well as the rotation of the single molecule. Therefore, clustering contributes to a reduction of the free volume of the additive if compared with the ones not involved in such a self-organizing process.

By comparing the plasticizing efficiency for the  $C_{12}$ - and  $C_{18}$ -model additives it is shown that at the same concentration (mmole %) small size molecules systematically exert a higher influence. On one hand by reducing the chain length, the radius of gyration decreases and the free rotation of the molecule as well as its relative free volume increases.

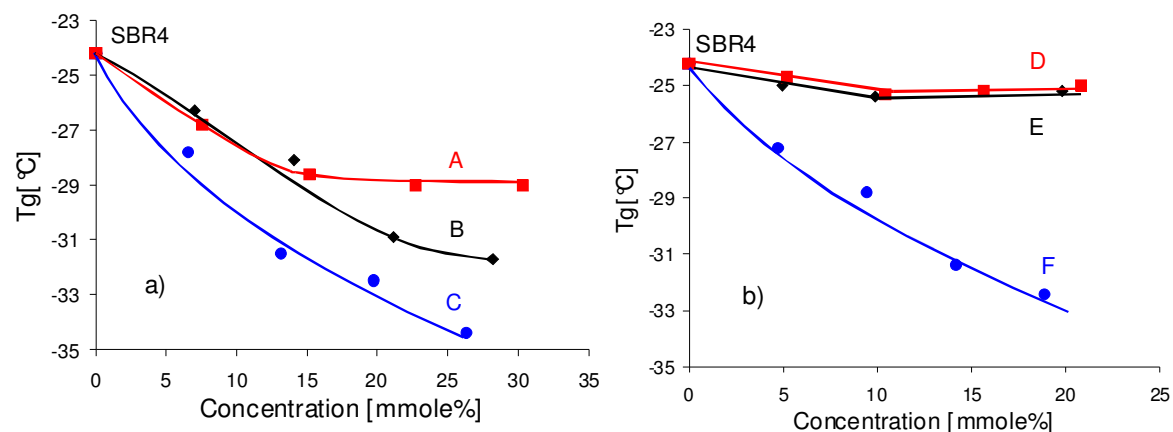


Figure 42: Influence of model processing aid concentration on the glass transition temperature

On the other hand it is shown that molecules with a smaller size and chain length respectively have higher combinational entropy of mixing. Thus, the solubility is increased due to entropic contributions. In addition, if the intermolecular interaction potential is lower, the effect is larger. The presence of these short molecules between the polymer chains leads to an increase of the free volume into the system and consequently the decrease of glass transition temperature is more pronounced in comparison to the longer chains. The values presented in Table 10 are only valid for infinite dilution of the additives in polymer matrix. They are the result of the interactions taking place on a molecular level, which leads to an exchange of free volume in the system.

Table 10. Plasticizing efficiency of model processing aids in SBR4 rubber

System	$(\Delta T_g / \Delta C)_{c \rightarrow 0}$ [°C/mmole%]
A	0,29
B	0,37
C	0,55
D	0,10
E	0,12
F	0,50

It can be concluded that the molecular weight as well as the chemical functionality of the model additives used influence in a certain degree the low temperature mobility of the rubber chains. The  $T_g$ -shift exert a considerably influence on the plasticizing efficiency which was observed to decrease in the sequence: ester > acid > alcohol.

#### 4.2.2 Solubility of model processing aids

Direct information about the low temperature solubility is obtained from the  $T_g$ -concentration diagrams. The concentration at which the  $T_g$  is no more decreasing but remains constant can be considered as the solubility limit at low temperatures. The higher solubility of the  $C_{12}$ -model additives than that of the  $C_{18}$ -ones can be explained by the contribution of two factors. One is the larger increase of the mixing entropy for smaller molecules. The other is the lower melting temperature of the smaller molecules.

At constant C-number of the additive, the chemical nature of the functional group governs the solubility. The best solubility is shown for the methyl-ester, while the acid and the alcohol both with stronger intermolecular interactions between molecules of the same kind, show phase separation at quite low concentrations.

Information about the fraction of phase separated additive in the rubber was derived by using the melting enthalpy  $\Delta H_m$  of the additive as a molecular probe. By normalizing the measured melting enthalpy of the additive in the mixture,  $\Delta H_m^{\text{blend}}$ , to the melting enthalpy of the pure additive,  $\Delta H_m^{\text{pure}}$ , the fraction of phase separated additive in the system is obtained  $\Delta H_m^{\text{blend}}/\Delta H_m^{\text{pure}}$ . In the case of complete phase separation, the normalized melting enthalpy is equal to 1. For the opposite case of total solubility, the normalized enthalpy is equal to 0. Any value between these two extremes indicates the fraction of phase separated additive. The evolution of the insoluble fraction is shown to be exemplarily for the systems A and B, where low temperature phase separation occurs (Figure 43).

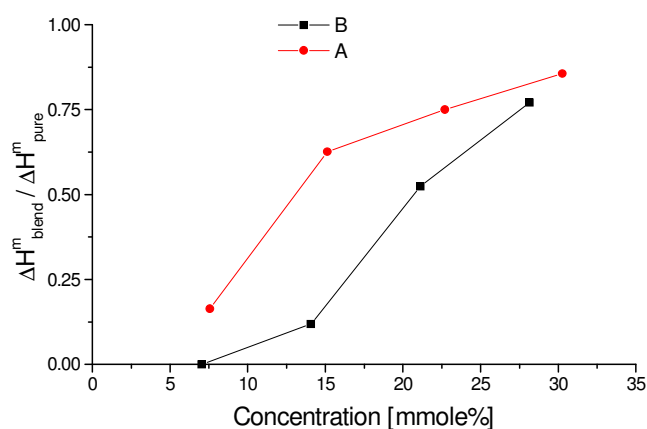


Figure 43: Insoluble fractions for system A and B in SBR4

The results show that the  $C_{12}$ -acid (System B) is dissolved in the rubber matrix by a higher amount than the corresponding alcohol (System A). Increasing the concentration of additive the total amount of un-dissolved additive is increased. The limiting values at 6 phr additive are of ca. 0,85 for A and 0,77 for B. The entire evolution proves that the lower solubility of the alcohol can be compared to the acid.

Comparing the soluble fraction,  $1 - (\Delta H^m_{\text{blend}} / \Delta H^m_{\text{pure}})$ , for the  $C_{12}$ - and the  $C_{18}$ -additives the influence of the molecular weight of the additive becomes more evident (Figure 44). Systematically the acid is more soluble than the corresponding alcohol. The best solubility is shown by the ester. While the  $C_{12}$ -ester is completely soluble (System C) the  $C_{18}$ -one shows a significantly reduced solubility above 9 mmole%.

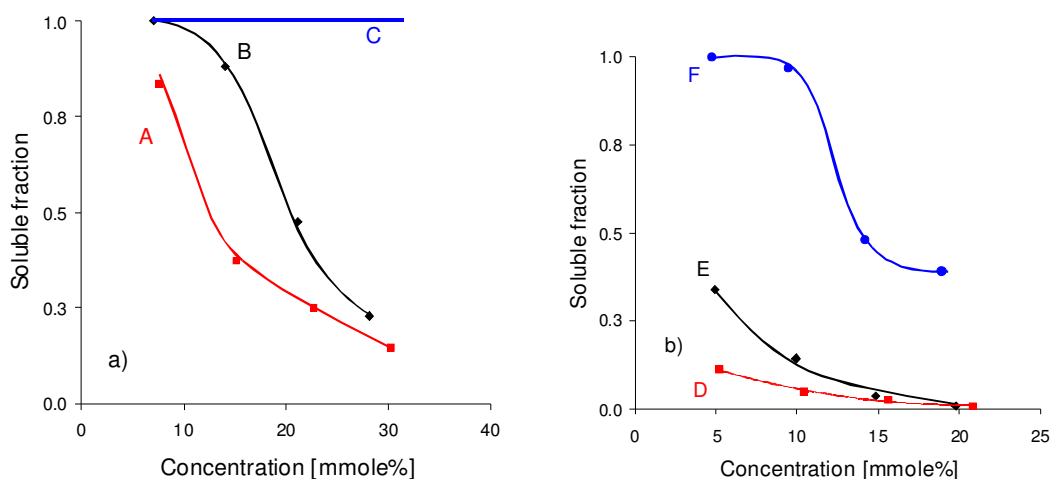


Figure 44: Soluble fractions for  $C_{12}$ - and  $C_{18}$ -additives in SBR4

Technically used processing aids often consist of more than one substance. Therefore, it was also interesting to investigate the solubility of such a material and to see whether or not it dissolved in the polymer at processing conditions and to determine the solubility range of the selected industrial additive. In order to do this, DSC, turbidity measurements and optical microscopy were employed.

Figure 45 depicts the evolution of the melting process of a technically used processing aid in S-SBR (system G5). The sample placed on a heated plate, shows temperature dependency changes in morphology initially around 100 °C. It can be seen that parts of the additive begin to melt and are dissolved in the rubber phase. By increasing the temperature further, the morphology is transformed steadily to that of a homogeneous system. The process is completed at 130 °C. When the system has cooled down to room temperature, the homogeneous morphology of the system is unchanged. This indicates that the crystallites of the processing aids formed by recrystallization during cooling are reduced in size. However, being distributed more homogeneously, they produce less scattering contrast to be monitored with the optical microscope. If the temperature is kept constant at 100 °C where heterogeneous phase morphology still exists for a period of one hour it can be seen that the morphology of the system changes slightly but still demonstrates the existence of two phases. This indicates that at least one component of the technical product remains un-dissolved at this temperature (Figure 46).



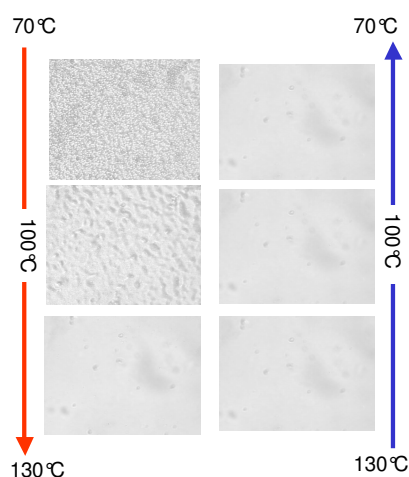


Figure 45: Light microscopy pictures of SBR4/industrial processing aid

The turbidity analysis performed on this system offers additional information about the solid-liquid phase separation. From Figure 47 it can be seen that with an increase in temperature the relative intensity of the transmitted light ( $I/I_0$ ) increases in a first step ranging from ca. 80 to 102 °C and in a second step, which ends at 120 °C.

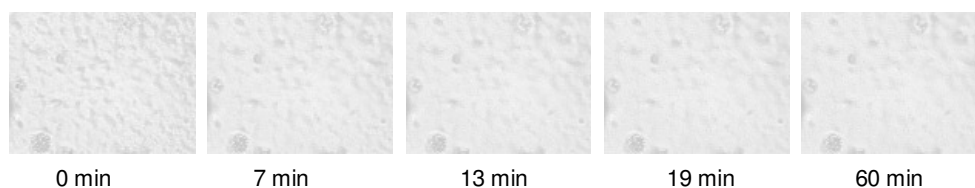


Figure 46: Influence of storing time on morphology of industrial additive in SBR4 at 100 °C

Above 130 °C the relative intensity  $I/I_0$  remains constant. During cooling the relative light intensity is decreasing more than in the heating cycle. The higher opacity is attributed to the formation of a high number of randomly distributed small crystallites. It was proven that the additional heating and the cooling cycles follow the same turbidity-temperature curve as for the cooling cycle indicated in Figure 47. This indicates that once the technical processing aid is completely dissolved into the rubber it becomes well distributed and remains in this state.

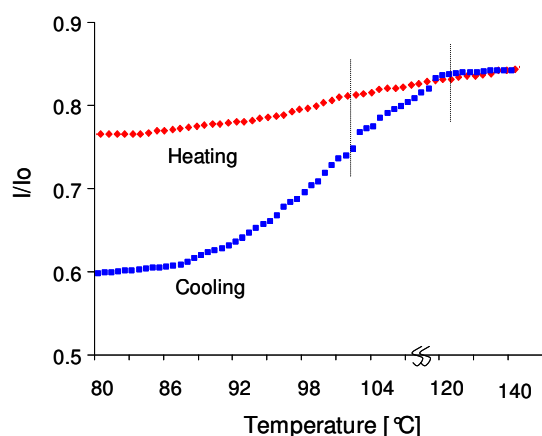


Figure 47:  $I/I_0$  vs. temperature for SBR4/industrial additive from turbidity analysis

An additional confirmation of this mechanism was derived from thermo-analytical investigations. As shown in Figure 48 the system demonstrates a major melting peak exactly in the region where the pronounced step is in the turbidity curve (ca. 81-102 °C) followed by a small melting at 115 °C. Due to the relatively rapid cooling of the system the corresponding two peaks for re-crystallization of the two components in the processing aid are shifted towards lower temperatures.

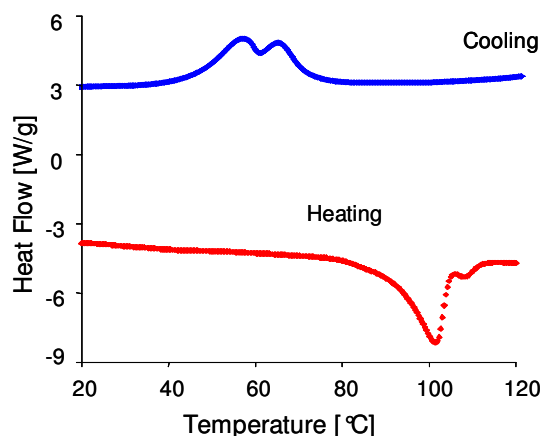


Figure 48: DSC diagram for SBR4/industrial additive

The investigations done concerning the solubility of the industrial additive in S-SBR emphasize the phase separation that occurs on this additive until a temperature of 120 °C is reached. Above 130°C the technical processing aid is completely dissolved into the rubber in less than 5 min, it becomes well distributed and remains in this state. This prevails valuable information for the processability of this product in industry.

#### 4.2.3 Relationship between swelling and plasticizing efficiency

The thermodynamic interaction between the rubber and the model additives was investigated through equilibrium swelling measurements performed on crosslinked SBR4 (system 6). In order to compare the solvent uptake on a molecular base one has to consider the moles of model additives taken up from the mass unit of rubber network at equilibrium. The swelling measurements were done at the processing temperatures of about 120 °C.

Using this base for comparison, it was observed that in general the C<sub>12</sub>-model additives are able to swell the rubber to a larger extent than the C<sub>18</sub>-ones. In other words, even at high temperatures the smaller molecules interact better with the rubber.

Besides that, it was observed that for each group of model additives the molecular solvent uptake correlates well with the plasticizing efficiency, indicating once again that the interaction intensity between the additive molecules and the polymer segments plays a key role in both phenomena (Figure 49).

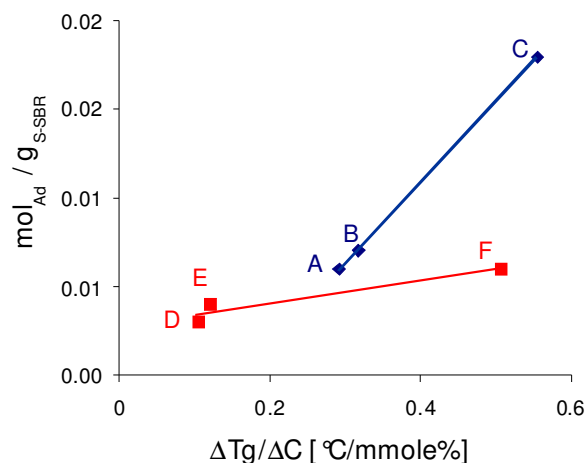


Figure 49: Relationship between the swelling degree (at 120 °C) and plasticizing efficiency

The result underlines also the effect of functional groups. That both esters are showing the largest effect might be related to the ability of the polar ester group to establish dipole-dipole interactions with the styrene units of S-SBR.

#### 4.2.4 Viscoelastic properties

Valuable information about the viscoelastic properties ranging from constrained flow (terminal zone) to the transition zone into the dynamical glass state was obtained by applying the frequency-temperature superposition principle to construct mastercurves.  $G'(T)$  and  $G''(T)$  curves were recorded in a plate-plate configuration in the frequency range permitted by the testing instrument. Figure 50 shows exemplarily the obtained master-curves for SBR4 as a reference and for system F4. The frequency dependency of the  $G'$  and  $G''$  of both systems deviates from the scaling behaviour demanded theoretically by the tube model derived for melts of monodisperse polymers ( $\log G' \sim -2 \log \omega$  and  $\log G'' \sim -\log \omega$ ) [101].

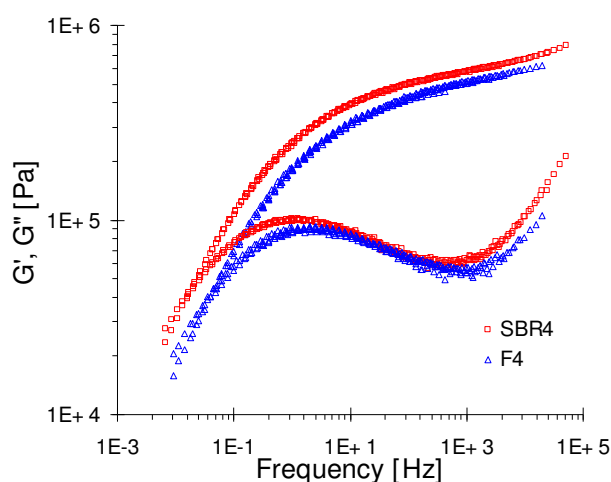


Figure 50: Dynamical moduli as a function of frequency for SBR4 and F4

According to the relatively broad molecular weight distribution the observed slopes are 0,72 for  $\log G'$  and 0,53 for  $\log G''$ . The deviations from the theoretical predictions can be traced back to the disproportional effect of short polymer chains [101] and the softening effect exerted by the model processing aid. They indicate non-linear viscoelastic behaviour. The major effect of the processing aid is observed in both the shift of the crossover of the  $G'(\omega)$  and  $G''(\omega)$  curves and the shift of the frequency at which the  $G''(\omega)$  curve passes through a maximum. For simplicity the reptation time,  $\tau_{rep}$ , was calculated from the frequency at the maximum of  $G''$ . By comparing the changes in reptation time for all model additives, significant but system specific decrease is observed (Figure 51). Additionally, the industrial product was also investigated and it was observed that the reptation time is decreasing and is higher comparing with the model additives used. This indicates a better chain mobility by its incorporation on SBR4, a better plasticizing efficiency when used in formulation with SBR4.

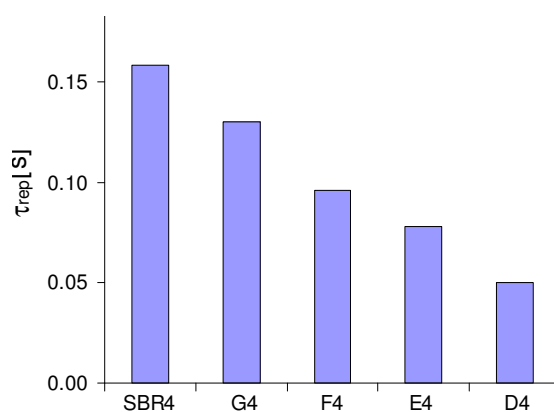


Figure 51: Influence of the functionality group on the reptation time ( $\tau_{rep}$ ) for SBR4,  $C_{18}$ -model processing aids and industrial additive (G4)

Therefore, the processing aid contributes, at ambient temperatures, to a decrease of the entanglement density and acts as an internal lubricant. At frequencies where  $G''$  passes a minimum the plateau zone is reached.

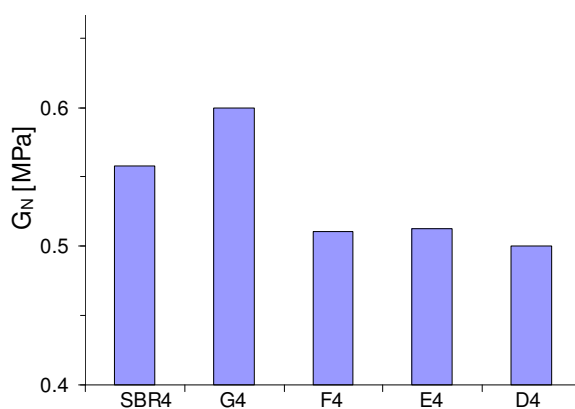


Figure 52:  $G_N$ -plotted for SBR4,  $C_{18}$ -model processing aids and industrial additive (G4)

The corresponding modulus  $G'_N$  depicts the properties of a temporary network based on entanglements that cannot be released in the period of oscillation. Figure 52 shows the results obtained at the investigation of the model additives and the industrial additive. It can be seen that the  $C_{18}$ -additives lead to similar graded reduction of  $G'_N$  while the industrial product increases the plateau modulus. This means that this additive is still solid at the measurement temperature of about 80°C. This additive melts in a range of 80°C - 100°C as the DSC investigations showed.

Summarising the effects it can be stated again that the strongest effect is obtained by the fatty esters. [219, 220].

### 4.3 Diffusion and Permeation of the low molecular components

In this chapter the transport process of well defined plasticizers ( $C_{12}$ - and  $C_{18}$ -hydrocarbons) and a substituted benzene component (t-butyl benzene) as representative constituent in fuel in rubbers with different chemical structure and rubber blends was studied. The aim was to investigate the influence of the chain length of the alkyl group of the diffusant, the content of the nitrile and vinyl groups in the matrix, the unsaturation of the rubber, the crosslinking density of the matrix, the temperature, the filler, the phase morphology and plasma treatment on diffusion coefficient and permeation rate.

An important issue discussed in this chapter was the construction and validation of a permeation measuring apparatus (the direct connection of a gas chromatograph with a permeation unit via an automatic multidirectional valve with specimen loop). The determination of the diffusion coefficient from permeation experiments as well as the permeation rate of low molecular components in rubber and rubber blends was examined.

#### 4.3.1 Determination of the diffusion coefficient by means of ATR-FT-IR-Spectroscopy

Provided the precondition of sufficient chemical compatibility of the plasticizer with the polymer matrix is met, the effect of the plasticizer rests on a reduction of the interaction between individual polymer chains occurs. Generally, this results in (i) an increase of the free volume in the plasticized rubber matrix [103], (ii) a decrease of the entanglement density [221,222] or (iii) a diluting effect of interchain dipole-dipole interactions [223]. To meet the requirements for a good compatibility in the system, polar and mostly synthetic ester- or ether- and thioester-based plasticizers are used for polar rubber types whereas mineral oils with different compositions (paraffinic, naphthenic or aromatic) are used for plasticizing non-polar polydienes (NR, BR, SBR) or polyolefines (EPDM, IIR) [224]. One major requirement is an equal and homogeneous distribution of the plasticizer in the rubber phase.

The objective of this chapter is focused on the structure-property relationships regarding the diffusion process of a homologous series of phthalates and t-butyl benzene (t-BuPh) in NBR, SBR and HNBR. The influence of the ACN and vinyl content as well as the saturation and the crosslink of the rubber matrix on diffusion coefficient are emphasized.

The analytical determination of the diffusion coefficient was pursued for all systems by using the “time-lag” method based on the ATR-FT-IR spectroscopy technique (see Chap. 3.3.2.1). For the system DOP/NBR4 and DOP/HNBR1 the “concentration-distance” method that consists of a special microscopy-FT-IR-spectroscopy coupling was employed in this study.

#### 4.3.1.1 Plasticizers

The work in this chapter was concentrated on the determination of the diffusion constants of phthalates with increasing chain length in rubbers (Table 11).

The calculation of the diffusion coefficient by means of ATR-FT-IR-spectroscopy requires the evaluation of the time lag ( $\tau$ ). The time from covering the one face of the elastomer film with the phthalate until the phthalate penetrates the film is considered as „time-lag” and is recorded on the other face by means of the characteristic IR-absorption band of the ester group ( $1726\text{ cm}^{-1}$ ).

Table 11. Plasticizers used

Sample	Abbreviation	Chemical formula	Molecular weight [g/mol]
Di-methyl phthalate	DMP	$\text{C}_6\text{H}_4[\text{COOCH}_3]_2$	224
Di-ethyl phthalate	DEP	$\text{C}_6\text{H}_4[\text{COOCH}_2\text{CH}_3]_2$	250
Di- butyl phthalate	DBP	$\text{C}_6\text{H}_4[\text{COO}(\text{CH}_2)_3\text{CH}_3]_2$	284
Di-octylphthalate*	DOP	$\text{C}_6\text{H}_4[\text{COO}(\text{CH}_2)_7\text{CH}_3]_2$	344
Di-decyl phthalate	DDP	$\text{C}_6\text{H}_4[\text{COO}(\text{CH}_2)_9\text{CH}_3]_2$	464

\*Common abbreviation for di-ethylhexyl-phthalate “DEHP”

An example of the time-dependent evolution of this band is shown in Figure 53 for DBP/NBR2. It can be observed that for a period of more than 100 minutes there is no signal recorded. After the signal appears the intensity increases linearly in time because of a continuous increase in DBP concentration in the NBR film at the margin of the Ge-crystal.

It was observed that the diffusion coefficient of the phthalate, it was taken into account that during the diffusion process the concentration of NBR on the surface of the Ge-crystal is decreasing while the concentration of the phthalate is increasing.

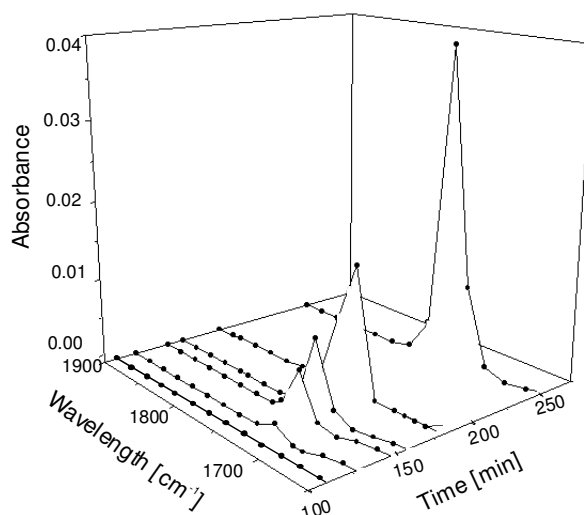


Figure 53: Variation of the ester band absorbance as a function of time for DBP in NBR2 by RT

Therefore, the absorbance of the ester group was normalized to the absorbance of the nitrile group stretching vibration band ( $2237\text{cm}^{-1}$ ). The relative absorbance ( $A_{\text{rel}} = A_{1726}/A_{2237}$ ) plotted vs. time delivers typical plots from which the “time-lag” is determined from the intersection of initial  $A_{\text{rel}}$  with the linearly increasing  $A_{\text{rel}}$  (Figure 54).

As a matter of fact, the slope ( $dA_{\text{rel}}/dt$ ) of the linear time dependence of  $A_{\text{rel}}$  is also directly related to the diffusion constant. A higher slope should indicate a higher diffusion coefficient.

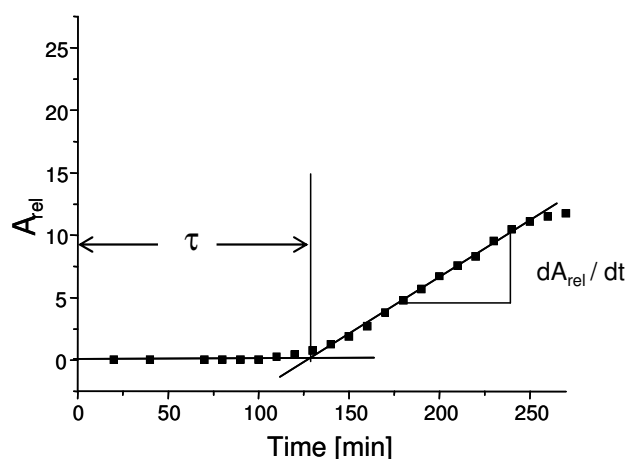


Figure 54: Determination of time-lag of DBP in dependency on time in NBR2

Measurements on films with different thickness were carried out. The investigation revealed a linear proportionality between the time of penetration ( $\tau$ ) and the square of the film thickness ( $l^2$ ) which is presented in Figure 55.

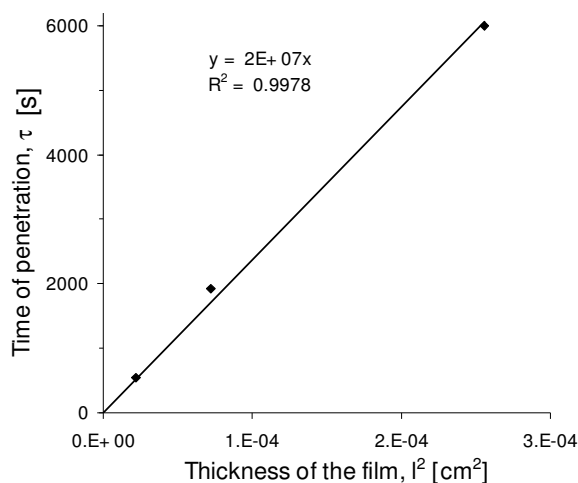


Figure 55: Influence of the film thickness on the penetration time of DBP in NBR1

This result represents an experimental proof that the diffusion coefficient does not depend on the sample geometry. The average diffusion coefficient of DBP in NBR1 derived from the data given in Figure 55 is  $8,3 \cdot 10^{-9}$  cm $^2$ /s.

#### *Influence of the alkyl chain length and acrylonitrile (ACN) content in NBR*

The experimental results of spectroscopic measurements are shown in Table 12. The data presented indicate the influence of the alkyl chain length of the phthalates and the ACN content in NBR rubbers on the time lag and  $dA_{rel}/dt$ .

The mass transport of the diffusant through a polymer (uncrosslinked or crosslinked) is connected with the size and the volume requirement of the moving species. If a homologous series of molecular species is used, the radicals with increasing bulkiness trigger the changes in the mass transport. However, it has to be taken into account that the precision for the determination of the “time-lag” decreases if the molecular weight of the diffusants increases.

Table 12. The “time-lag” ( $\tau$ ) and the slope ( $dA_{rel}/dt$ ) for the diffusion of phthalates in NBR rubbers (Film thickness  $85 \pm 10$   $\mu$ m)

Phthalate	NBR1		NBR2		NBR4	
	$\tau$ [min]	$dA_{rel}/dt$	$\tau$ [min]	$dA_{rel}/dt$	$\tau$ [min]	$dA_{rel}/dt$
DMP	9	2,00	17	1,200	46	0,6000
DEP	11	1,50	35	0,730	123	0,4000
DBP	32	0,26	117	0,090	248	0,0090
DOP	65	0,11	190	0,003	1787	0,0004
DDP	94	0,02	638	0,001	2160	0,00009

For the phthalates under consideration a quasi-hyperbolic decrease of the diffusion coefficient with increasing alkyl chain was observed. This is shown exemplarily for NBR1 in Figure 56. The diffusion coefficient  $D$  decreases from  $2,2 \cdot 10^{-8}$  cm $^2$ /s for DMP to  $2,1 \cdot 10^{-9}$  cm $^2$ /s for DDP. The



decrease of  $D$  with the bulkiness of the diffusant is in accordance with the theoretical expectations. However, the effect of alkyl chains is less pronounced when the chain length increases.

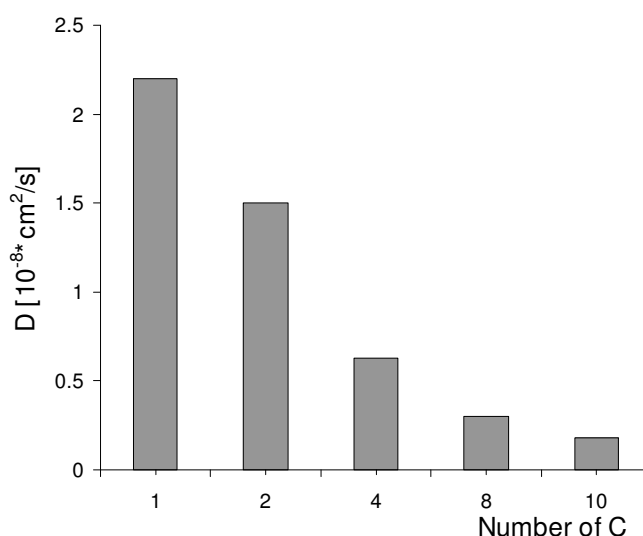


Figure 56: Influence of the alkyl chain length of phthalate on  $D$  in NBR1

The explanation for this evolution is related to the changes in the configuration of the alkyl chain. With an increasing number of C-atoms the alkyl chains tend to adopt a coil-like configuration. Therefore, the radius of gyration of the diffusant molecule increases nearly with the square root of the number of C-atoms and consequently  $D$  is non-linearly decreasing with the alkyl chain length of the phthalates.

At constant nitrile content of the rubber a characteristic power law (Equ. (52), Chap. 3.3.1.4.2) describes the relation between the diffusion coefficient and the molecular weight of the phthalate. From the slope and the intercept of the linear relationship  $\log D$  vs.  $\log M$  the two constants  $K$  and  $\alpha$  were determined. The results are given for the NBR1, NBR2 and NBR4 in Table 13.

Table 13. Influence of the ACN content on the exponent  $\alpha$  and  $\log K$

ACN content [wt.%]	$\alpha$	$\log K$
18	3,4	0,5
28	4,0	1,4
39	5,2	3,7

By fitting the two constants vs. the ACN content by a polynomial function, the dependency of the diffusion coefficient  $D$  can be expressed by a general equation with the acrylonitrile content and

the molecular weight of the phthalates as variables. The values for the two parameters, K and  $\alpha$ , are given by the following expressions:

$$\log K = (0,0059 * C_{ACN}^2 - 0,1808 * C_{ACN} + 1,8473)$$

$$\alpha = (0,0023 * C_{ACN}^2 - 0,0475 * C_{ACN} + 3,4982)$$

where  $C_{ACN}$  is the concentration of the ACN groups.

A comparison between calculated values of D and the experimental data demonstrates only small deviations in the range of experimental errors. For example, the diffusion coefficients of DEP in NBR with a different content of acrylonitrile (18-39% ACN) show a deviation from  $1,2 \cdot 10^{-8}$  to  $1,5 \cdot 10^{-9}$  [cm<sup>2</sup>/s]. Thus, the average deviation of the theoretical prediction is in the range of 1 to 3%. For the other phthalates investigated the obtained values are comparable when low molecular weight diffusants are used and slightly increased when diffusants with higher structure were employed.

#### *Influence of the alkyl chain length and vinyl content in SBR*

The variation in the time lag and the slope with increasing the alkyl chain length of the phthalate and the vinyl content in SBR is illustrated in Table 14. As it was shown in Chap. 4.1 a higher amount of the 1,2-butadiene units leads to a change of the morphology in the system. The transport process of a diffusant through a polymer matrix depends on the polymer morphology, which controls the propagation of a molecule from one site to another. If the structure or the flexibility of a polymer chain is modified it is expected a change of the diffusion through it. However, the time lag is increasing with increasing the 1,2-butadiene units in SBR because the flexibility of the chains decrease which leads to a higher phthalate resistance. The diffusant needs a longer time to penetrate the matrix.

*Table 14. The "time-lag" ( $\tau$ ) and the slope ( $dA_{rel}/dt$ ) for the diffusion of phthalates in SBR rubbers (Film thickness  $85 \pm 15 \mu\text{m}$ )*

Phthalate	SBR1		SBR2		SBR3	
	$\tau$ [min]	$dA_{rel}/dt$	$\tau$ [min]	$dA_{rel}/dt$	$\tau$ [min]	$dA_{rel}/dt$
DMP	64	0.0010	14	0.0057	7	0.0075
DEP	25	0.0063	6	0.0160	4	0.0250
DBP	41	0.0040	10	0.0030	5	0.0200
DOP	50	0.0022	35	0.0018	13	0.0100
DDP	95	0.0015	61	0.0014	18	0.0085

The experiments show that the diffusion coefficient increases in a first stage go through a maximum and afterwards decrease as the alkyl chain length of phthalates increases. An example of this course of D is highlighted in Figure 57.

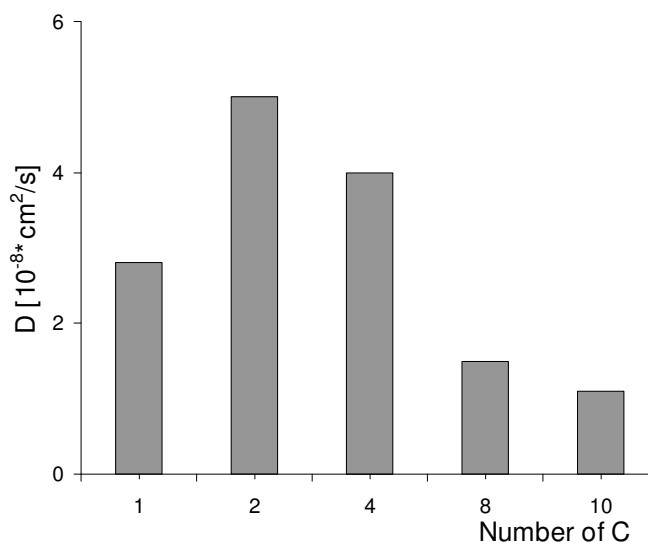


Figure 57: Influence of the alkyl chain length of phthalate on  $D$  in SBR3

On one hand, the increase of the diffusion coefficient when using DEP may be due to a better interaction between SBR with phthalate that is supported by the unpolar units introduced into the system. Further, the diffusion coefficient of DBP in SBR3 decreases, but still has a higher value compared with DMP and as the chain length of the phthalate increases, the diffusion coefficient drops significantly.

On the other hand, this behaviour can be explained by considering the viscosity of the diffusant molecules. The viscosity reflects the effective radius of the molecule. The lower the viscosity the higher the swelling and this effect can explain the correlation between the diffusion coefficient and the liquid viscosity (Figure 58).

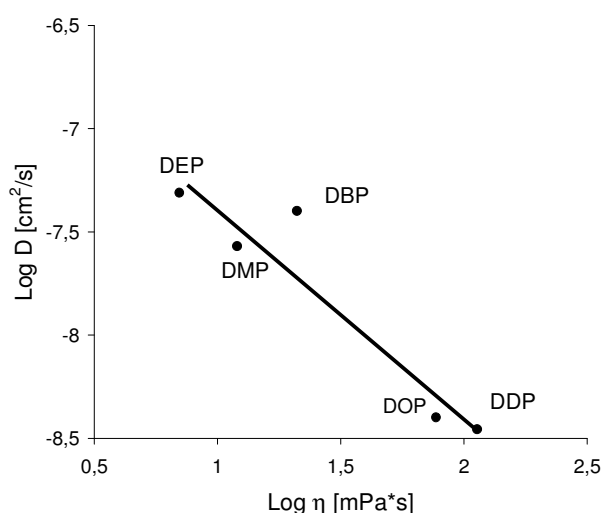


Figure 58: The variation of  $D$  with viscosity (at 20 °C) of plasticizers with different alkyl chain length in SBR3

This behaviour was also observed by Tinker and co-workers [222] who investigated the diffusion of several plasticizers through which DMP, DEP, DBP, DOP in natural rubber and epoxidised

rubber. They showed a similar trend of  $D$  with increase the alkyl chain length of the phthalates. The diffusion coefficient increases first and then decreases continuously. A similar correlation between the  $D$  and viscosity was also noticed by Southern and Thomas [225] in their work by studying the diffusion of a wide range of liquids in natural rubber.

In NBR the nitrile groups exert strong intra- and inter-chain interactions, which lead to a reduction of the chain mobility and the free volume. This is expressed by an increase in the glass transition temperature as well as the characteristic chain relaxation time. As a direct consequence, the diffusion process is affected by the ACN content. From the data listed in Table 12 it becomes obvious that increasing the nitrile content reduces the diffusion coefficient of each particular phthalate. It points out that the diffusant mobility is steadily hindered by the increasing amount of the CN-CN interactions (Figure 59a).

The influence of the nitrile content is reflected quantitatively in a reduction of both values the exponent  $\alpha$  and especially the pre-exponential factor  $K$  in Equ. (52), Chap. 3.3.1.4.2. From Table 13 it can be seen that  $\alpha$  and  $K$  increase when the ACN content increases. A general description of the entire diffusion process of phthalates in NBR is available, because the dependency of both values  $\alpha$  and  $K$  from the ACN-content of the matrix is now determined.

The influence of the vinyl content in SBR and the alkyl chain length of the phthalate on the diffusion coefficient are presented in Figure 59b.

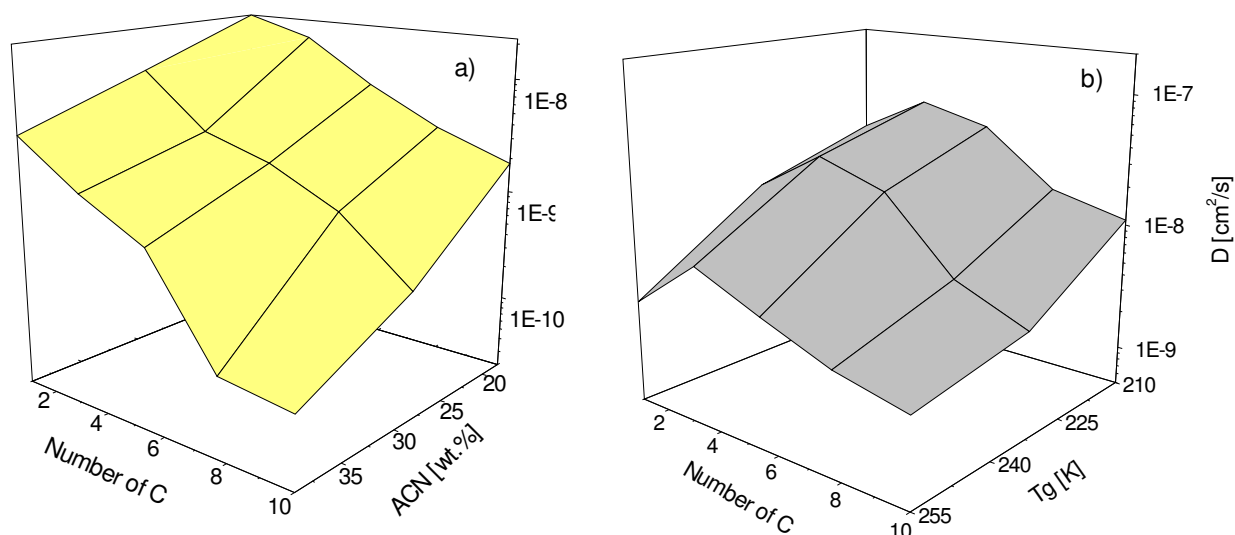


Figure 59: Influence of the alkyl chain length of phthalate, the nitrile content of the NBR (a) and the vinyl content of SBR (b) on the diffusion coefficients

The vinyl content in SBR influences the diffusion coefficient in the same manner as the acrylonitrile content in NBR. An increase of the vinyl content leads to a reduction of the chain

mobility, which is reflected in higher values of the glass transition. Therefore, the diffusion constants decrease.

However, these results indicate that the diffusion process of phthalates in NBR and SBR follows a different mechanism than that of linear aliphatic esters with  $\text{CH}_2$ -units between 13-98 in Poly(ethylene) [118].

#### *Influence of the crosslinking density*

The results concerning the influence of crosslinking density on diffusion transport processes of DMP through SBR2 and NBR3 rubber on  $85 \pm 11 \mu\text{m}$  film thickness are presented in Figure 60. It can be noticed that a linear behaviour of  $D$  as a function of the crosslinking density was obtained. An increase of the crosslinking density results in a reduction of the diffusion coefficient due to lowering the mobility of network chains and of the crosslinks which are restricted regions for the transport process of the low molecular weight substances.

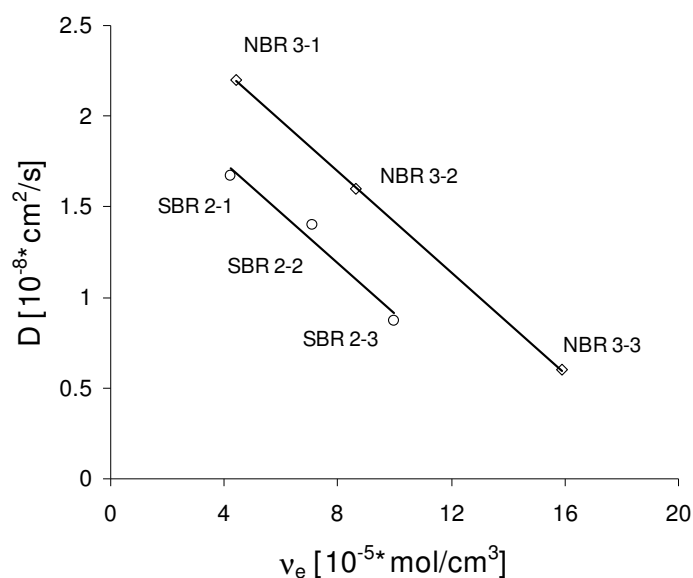


*Figure 60: Influence of the crosslinking density on the diffusion coefficient of DMP*

Tinker demonstrated in his work the influence of crosslinking density on partition coefficients of DMP between different rubbers [226]. The higher the crosslinking density formed in the system the lower the diffusion process respectively the partition coefficients. In another work [227], by investigating the volume fraction of NBR in the toluene-swollen gel with varying the acrylonitrile and increasing systematically the network chain concentration (peroxide vulcanization) was demonstrated that the diffusion process is slower.

Figure 60 presents a general trend of the low molecular component diffusion in favour of the rubber is close in solubility parameter to that of the plasticizer. DMP has a solubility parameter  $\delta$  around  $21,9 \text{ (J/cm}^3)^{1/2}$ , NBR3 has  $\delta$  around  $20 \text{ (J/cm}^3)^{1/2}$  and SBR2 has  $\delta$  around  $17,6$

$(\text{J}/\text{cm}^3)^{1/2}$ . The lower the difference between the solubility parameters of the plasticizer and the rubber the better the compatibility between the components is. This explains the higher swelling of NBR in DMP.

#### 4.3.1.2 Fuel component

In this chapter the diffusion of *t*-BuPh through thin specimen films based on NBR with varying ACN content or SBR with a constant styrene and variable vinyl content was studied.

Figure 61 provides an example for the time-dependent development of the characteristic band of *t*-BuPh in NBR2. It can be noted that no signal is detected for 25 min when the thickness of the polymer film is about 260  $\mu\text{m}$ .

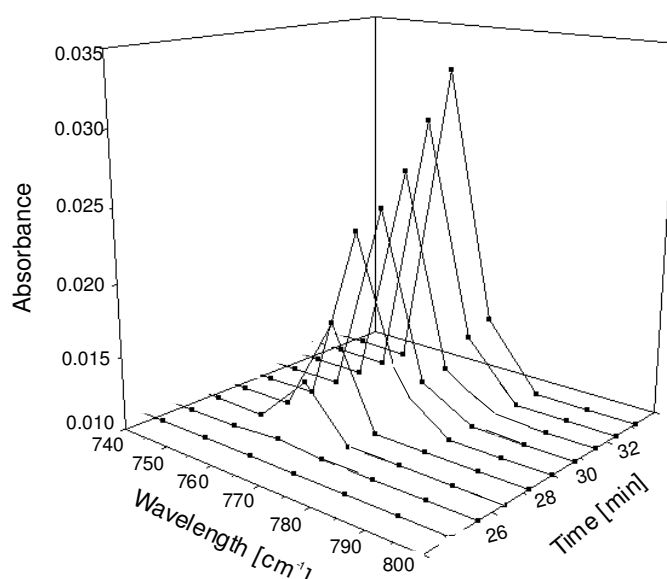


Figure 61: Increasing of the band intensity as a function of time (*t*-BuPh in NBR2 at RT)

To calculate the diffusion coefficient, the dilution of the polymers on the surface of the Ge-crystal and the intensity ratio between the characteristic band of *t*-BuPh and NBR ( $A_{\text{rel}} = A_{768}/A_{2237}$ ) used as variable was taken into account. The “time-lag” was determined from the intersection of linear increasing  $A_{\text{rel}}$  with the abscissa (Figure 62).

Table 15 shows the diffusion coefficient calculated from the time-lag and the slope in the linear range for the NBR and SBR vulcanizates studied. It can be observed that with increasing the ACN content in NBR rubbers the diffusion coefficient decreases.

This is on one hand due to the solubility of weakly polar bindings in *t*-BuPh that is reduced proportionally to the frequency of the nitrile groups in the sample volume. At the same time, the share of non-polar butadiene units (cis-1,4, trans-1,4 and 1,2) that can dissolve *t*-BuPh decreases. This influence seems to affect particularly the saturation concentration of *t*-BuPh.

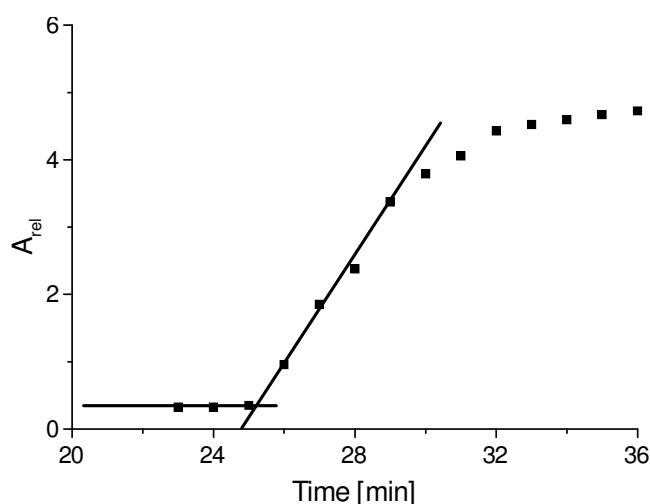


Figure 62: Determination of the time-lag for *t*-BuPh in NBR2 by RT

On the other hand, through strong inter- and intramolecular dipol-dipol interactions, nitrile groups form a physical crosslinkage superimposed over the chemically crosslinkage. Its density, in turn, increases proportionally to the ACN concentration.

Table 15. The time-lag ( $\tau$ ) and the slope ( $dA_{rel}/dt$ ) for the diffusion of *t*-BuPh in NBR und SBR vulcanizates (film thickness:  $270 \pm 40 \mu\text{m}$ )

System	$\tau$ [min]	$dA_{rel}/dt$	D [ $10^{-8} \text{cm}^2/\text{s}$ ]
NBR1	7	1,060	$20,0 \pm 2,51$
NBR3	27	0,510	$6,50 \pm 0,55$
NBR4	157	0,380	$2,10 \pm 0,29$
SBR3	8	0,048	$23,4 \pm 3,19$
SBR2	12	0,030	$18,8 \pm 6,78$
SBR1	14	0,012	$15,2 \pm 1,89$

The free volume in the whole system is reduced by the thermo-reversible physical crosslinkage whereby the transport process of a low molecular compound is restricted. The increase in the glass transition temperature occurs with increasing the ACN content or the characteristic relaxation time in case of a non-crosslinked melting sample can be traced back by the same cause (Figure 63).

In the SBR vulcanizates group, the diffusion coefficient of *t*-BuPh is reduced by the presence of the vinyl groups. Due to the better solubility of *t*-BuPh in SBR, the diffusion coefficient of this compound is higher in SBR than in NBR.

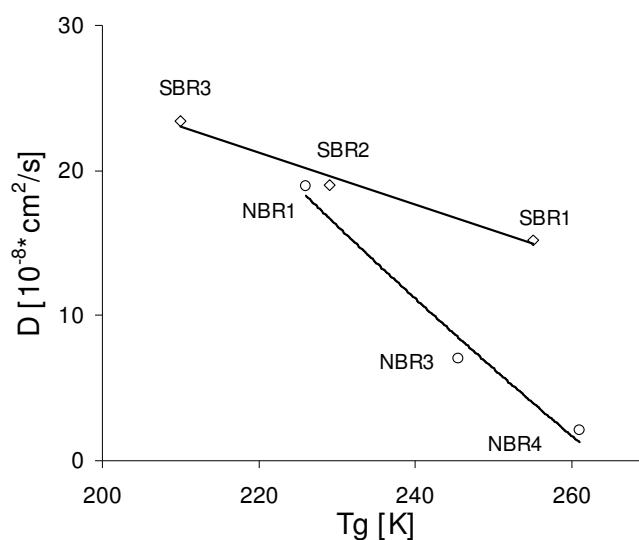


Figure 63: Influence of the polymer constitution

In both vulcanizate groups,  $D$  decreases in different ways with the glass transition temperature, i.e. with the free volume. The solubility of *t*-BuPh in SBR decreases slightly with increasing the vinyl content because of the minor polarizability of these groups. In case of NBR, the decrease in solubility is much more pronounced and specific.

#### 4.3.2 Determination of the diffusion coefficient with the concentration-distance analysis

In order to gain more information about the diffusion process on a microscopic length-scale, the systems DOP/NBR4 and DOP/HNBR1 were investigated by means of the “concentration-distance” analysis. A special arrangement of two layers was prepared. One layer contained the rubber and the diffusant, the second was prepared in the same way without containing the diffusant. The two layers are placed in contact with each other taking care to avoid trapping air bubbles. At different time intervals thin samples (10  $\mu\text{m}$ ) were cut and investigated with FT-IR microscope at various distances (25, 50, 100, 150, 200  $\mu\text{m}$ ) from the borderline between the two layers that is shown in Figure 64.



Figure 64: Test specimen used for the “concentration-distance” analysis (layer 2 contains DOP)

Using the procedure described in the experimental part the diffusion coefficients were calculated according to Equ. (46), Chap. 3.3.1.3. Different concentration profiles versus distance were obtained. For the reproducibility of the method three measurements of each sample were done.



An example of  $D$  determination is illustrated in Figure 65 for DOP/HNBR1 system after two days.

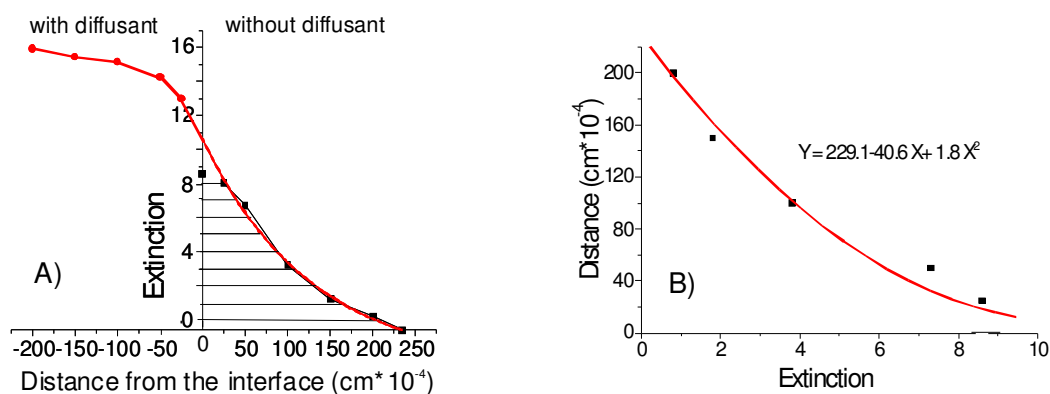


Figure 65: Evaluation of the diffusion coefficient from a “concentration–distance” curve for DOP/HNBR1 at RT

The diffusion coefficients obtained by this method are systematically lower than those obtained by the “time-lag” method. A possible reason for that may be the dependency of  $D$  on the concentration of the diffusant [111]. On the other hand it can be assumed that the mutual contact of the two different polymer layers on the molecular level is less good as the contact between the liquid phthalate and the rubber film formed in the “time-lag” method. Having more void between the two domains under consideration, the materials flux should be significantly reduced, therefore leading to a lower value of the diffusion constant.

Another contribution to this different range of values could be the crosslinking density of the thin film. The determination of the real crosslinking density on the 10  $\mu\text{m}$  thin films was not carried out. However, the general tendency of decreasing diffusion coefficients with increasing nitrile content of the rubber is fairly the same. The comparison between the results of the two methods is summarized in Figure 66. It is evident that with an increase of the ACN content in the polymer the inter-chain interactions experience a reduction of the diffusion coefficient of DOP.

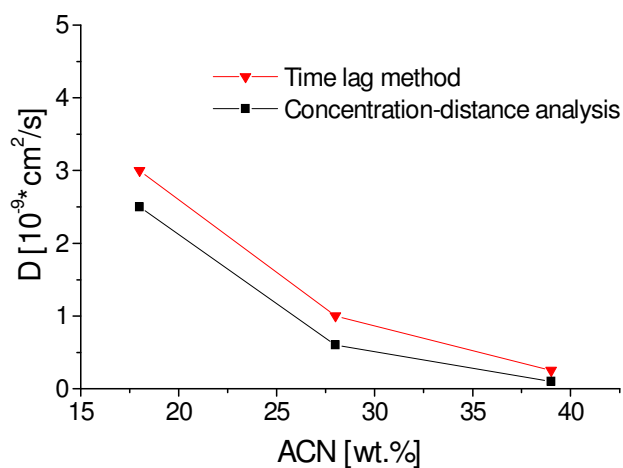


Figure 66: Comparison of the diffusion coefficients determined by the two methods

In conclusion, it can be summarized that the diffusion profiles acquired allowed a determination of the diffusion coefficients. These profiles showed that a significant amount of the diffusant readily migrated across the rubber interface. As expected, the change in diffusant concentration increases with increasing the storage time and the temperature and decreases with increasing the distance from the interface.

The analogy with the time-lag method underlined that even between the two methods small differences occur, the concentration-distance analysis employing the preparation method proposed could be used for the evaluation of the diffusion coefficient.

#### *Influence of unsaturation and temperature*

The temperature dependency of diffusion coefficients of DOP in NBR4 and HNBR1 was investigated at different temperatures.

If comparing the diffusion coefficient for DOP in the two polar rubbers it becomes obvious that the mass transport of DOP is systematically more rapid in HNBR1 than in NBR4 (Figure 67). This striking result seems to be generated by two contributions. On one hand, HNBR1 contains a smaller amount of ACN groups per volume unit than NBR4. This generates a weaker diffusion barrier in HNBR1 if compared to NBR4. On the other hand, a different cure efficiency of the CBS/S system in HNBR1 and NBR4 could also contribute to the higher diffusion rate in HNBR1. Different degrees of unsaturation of the rubbers under study could affect the diffusion. The residual bonds by HNBR are less than 9 wt.% while by NBR the double bonds in the main chain is 56 wt.%.

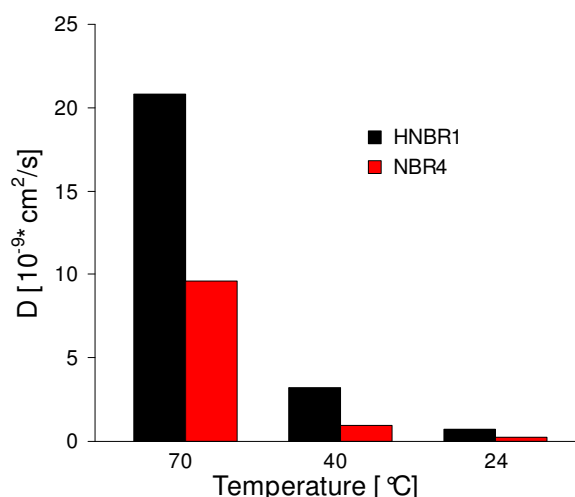


Figure 67: *D* of DOP in NBR 4 and HNBR1 at different temperatures

By investigating the influence of the polymer structure on diffusion using a radioactivity counting method based on tagging with carbon-14, Auerbach showed that the extent of unsaturation in the polymer backbone which is lowered by hydrogenation leads to a decrease of diffusion. He

reported a three fold decrease in  $D$  for octadecane through polyisoprene when the residual unsaturation was decreased from 100 to 37% by hydrogenation [228].

The temperature dependency of the diffusion coefficient is comprehensively expressed by the activation energy calculated with Equ. (53), Chap. 3.3.1.4.3. The experimental results show that the activation energy for the diffusion of DOP in NBR (40 KJ/mol) is higher than that in HNBR (33 KJ/mol). By increasing the temperature, the dipole-dipole interactions in both rubbers are strongly reduced by the contribution of thermal energy, especially above of ca. 60 - 65 °C. Thus, more free volume or holes respectively are formed in the polymer matrix. However, the change should be more pronounced in the NBR matrix with a higher density of CN groups.

#### 4.3.3 Determination of the diffusion coefficient by swelling

Investigations of the swelling kinetics allowed the determination of the diffusion coefficient on crosslinked rubbers. The time-dependent swelling of thin rubber plates corresponds to one of the simplest mathematical solutions of Fick's 2<sup>nd</sup> law (Chap.3.3.1). The diffusion coefficient is obtained from the slope of the linearly plotted reduced mass absorption  $M_{(t)}/M_{(\infty)}$  vs.  $t^{1/2}$ . Figure 68 shows the mass absorption of *t*-BuPh in NBR vulcanizates with different acrylonitrile content. The same kind of measurements was conducted with SBR specimens with variable vinyl content and constant styrene content.

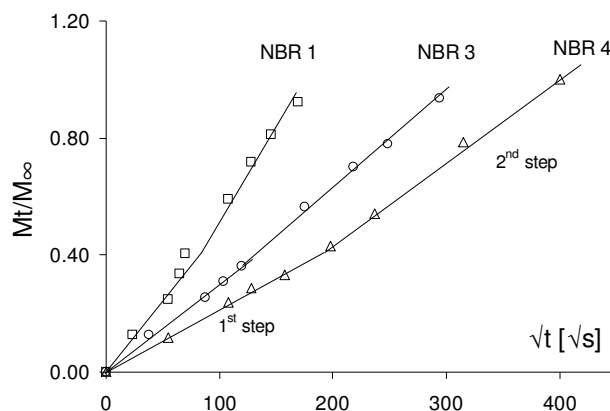


Figure 68: Relative mass absorption of NBR1, NBR3 and NBR4 by swelling in *t*-BuPh by RT

In accordance with the theoretical requirements, the mass absorption rises linearly in the initial segment of the process with  $t^{1/2}$  (Chap.3.3.1). Approaching from the two surfaces of the plate, the solvent fronts the rubber plate and this represents the first stage of swelling (corresponding to the „time-lag”). Further solvent absorption that occurs from this moment takes place in the “softened” matrix at a higher speed (2<sup>nd</sup> stage). Only the first stage of the process was used for determining the diffusion coefficient.

As can be seen from Figure 69, the duration of the first swelling stage is already dependent on the rubber's ACN content. A similar phenomenon is seen in the swelling of SBR plates with

constant styrene content and a variable share of 1,2-butadiene units. With increasing 1,2-unit content, the gradient of the mass absorption is decreasing.

Due to the swelling of rubber, the proportion of the specimens changes as a function of time. In order to obtain reliable results, a correction of the dimensional change was done which consist of an additional multiplicative factor taking into consideration the geometrical changes during swelling ( $Q^{1/3}$ ,  $Q$  is the degree of volume swelling) [111]. Figure 69 shows an example of the relative mass absorption of NBR1.

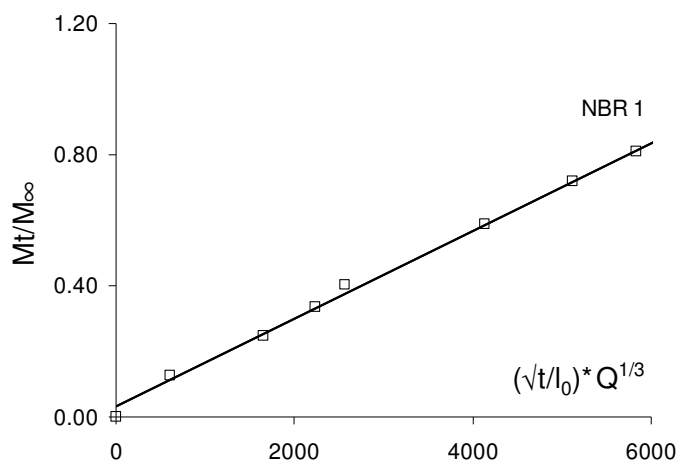


Figure 69: Relative mass absorption of NBR1 in *t*-BuPh with correction

A linear dependence results from the graphical representation of the reduced mass absorption versus the product of  $t^{1/2}$  and  $Q^{1/3}$  results which deliver the diffusion coefficients that numerically correspond to the values obtained from the first stage of the uncorrected curves. The determination of diffusion coefficient by means of swelling investigation takes in consideration this correction.

#### *Influence of the polymer constitution*

The values of diffusion coefficients of *t*-BuPh for NBR, HNBR and SBR rubbers are given in Table 16. It was observed that an increase of the ACN groups in NBR and the 1,2-butadiene units in SBR provoke a decrease of the diffusion coefficient. The chain mobility of the rubber matrix is hindered by the increasing concentration of CN-CN interactions, which lead to an additional physical crosslink in the matrix that determinates the decreasing of the diffusion constant. A similar behaviour is observed for SBR due to the presence of the vinyl groups in a higher amount that restrict the penetration of *t*-BuPh. The solubility of the diffusant can influence in a large extend the value of the diffusion coefficient. This effect can be seen if comparing the diffusion constants of *t*-BuPh in SBR and NBR. *T*-BuPh is an aromatic hydrocarbon substance with a high solubility in non-polar rubbers. This can explain the higher values of  $D$  when diffusion of *t*-BuPh through SBR takes place.

From Table 16 it was also noticed that the diffusion coefficient increases if the unsaturation in the main chain is reduced. The HNBR1 shows a higher  $D$  in comparison with NBR3, both rubbers having fast similar ACN content but different unsaturation grades and crosslinking densities.

Table 16: Diffusion coefficients of *t*-BuPh in polymers

System	D [ $10^{-8} \cdot \text{cm}^2/\text{s}$ ]
NBR1	$22,0 \pm 1,38$
NBR3	$7,78 \pm 0,48$
NBR4	$3,08 \pm 0,83$
HNBR1	$11,4 \pm 1,23$
SBR3	$25,0 \pm 2,56$
SBR2	$19,2 \pm 6,78$
SBR1	$16,1 \pm 3,89$

For both crosslinked polymers a comparison of  $D$  values obtained in swelling measurements with those determined by IR-spectroscopy (Figure 63 and Figure 70) shows that the diffusion coefficients obtained in swelling investigation are slightly higher than the values obtained by spectroscopic experiments by means of “time-lag method”.

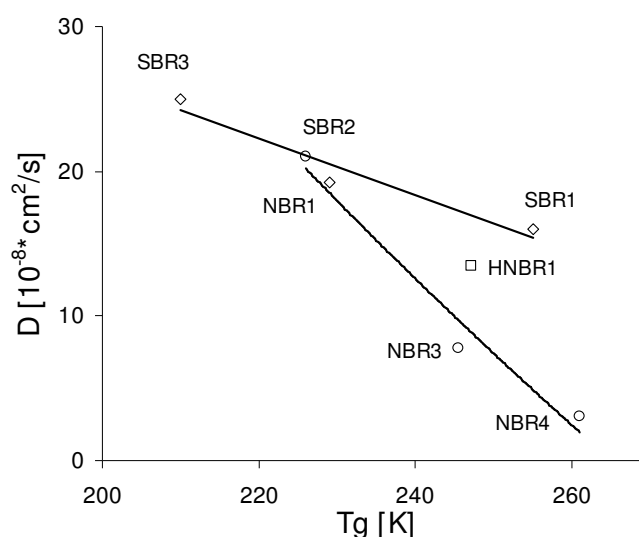
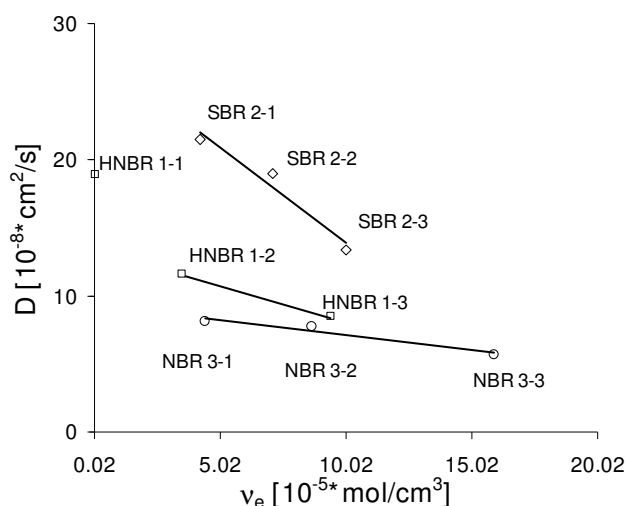


Figure 70: Influence of the polymer constitution

These negligible differences can have their roots on one hand on the different crosslinking density of the polymer thin film and membrane and on the other hand on the different preparative methods used for the calculation of the diffusion coefficient.

### *Influence of the crosslinking density*

The experimental result shown that the more strongly crosslinked a rubber matrix is, the more drastically the mobility of the rubber chains is reduced and the more emphatically the transport of the diffusante through the membrane is hindered. These effects lead to a decrease in the diffusion coefficient, as shown in Figure 71 for SBR2, NBR3 and HNBR1.



*Figure 71: Influence of the crosslinking density on the diffusion coefficient of t-BuPh*

From Figure 71 it was observed that the diffusion coefficient varies in the order SBR2-1 > SBR2-2 > SBR2-3, a similar behaviour being noticed for the other polymers too. This decrease of  $D$  is attributed to the formation of the additional networks in the matrix by increasing the crosslinking density. The dependency of diffusion coefficient versus  $v_e$  reveals a linear behaviour in the case of SBR2 and NBR3. HNBR1 indicates the same trend for higher crosslinking densities while HNBR1-1 evidences a high  $D$  due to the fact that its crosslinking density is very low. For this is responsible the less double bonds rest in the main chain (9 wt%) available for the crosslinking of the polymer.

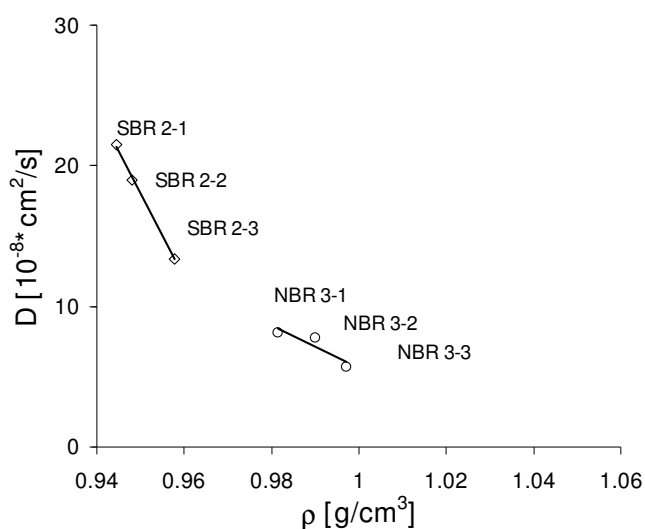


*Figure 72: Dependency of the diffusion coefficient versus the density for SBR2 and NBR3 rubbers*

The crosslinking density is related to the density. An increase in the crosslink networks causes an increase in the density of the material. In order to evaluate the influence of the density on diffusion process, a correlation between D and density was done (Figure 72).

The results demonstrate a linear relationship between diffusion coefficient and density for SBR2 as well as for NBR3. The rubber with the higher density gives a lower diffusion coefficient. This effect was also observed in a study of diffusion of several gases on different rubbers [229], this effect depending on the strength of the molecular interaction forces.

In conclusion, it can be remarked that the investigation of the transport phenomena of two diffusants with different solubility such as t-BuPh and DMP in SBR2 and NBR3 polymers with the same crosslinking densities (see Figure 60 and Figure 71) demonstrated that the solubility is an important factor that influence the values of the diffusion coefficient. The better solubility in the rubber the higher diffusion constants are reached.

#### *Influence of the filler*

The transport process in filled polymers depends on the nature of the filler and its compatibility with the rubber matrix. For the case when the filler strongly interact with the matrix, the filler will reduce the free volume within the polymer matrix and create a barrier for the transport of the diffusant [230].

The fillers used in this study were precipitated silica (7000GR) and carbon black (N326) that were mixed with NBR3 and SBR4 respectively. Carbon black N375 was used for comparison with N326 using the same rubber formulation. The recipes used are enclosed on Table 17.

*Table 17. Test recipe*

Materials	A	B	C	D	E	F	G	H	I	J	K	L
	phr											
SBR4	100.0	100.0	100.0	100.0	0.0	0.0	0.0	0.0	0.0	0.0	0.0	0.0
NBR3	0.0	0.0	0.0	0.0	100.0	100.0	100.0	100.0	100.0	100.0	100.0	0.0
HNBR1	0.0	0.0	0.0	0.0	0.0	0.0	0.0	0.0	0.0	0.0	0.0	100.0
Ultrasil 7000 GR	0.0	10.0	20.0	50.0	0.0	10.0	20.0	50.0	0.0	0.0	0.0	0.0
N 326	0.0	0.0	0.0	0.0	0.0	0.0	0.0	0.0	10.0	20.0	50.0	0.0
Stearic acid	2.0	2.0	2.0	2.0	2.0	2.0	2.0	2.0	2.0	2.0	2.0	2.0
Sulphur	1.5	1.5	1.5	1.5	1.5	1.5	1.5	1.5	1.5	1.5	1.5	0.0
CBS	1.5	1.5	1.5	1.5	1.5	1.5	1.5	1.5	1.5	1.5	1.5	0.0
DCP	0.0	0.0	0.0	0.0	0.0	0.0	0.0	0.0	0.0	0.0	0.0	1.0
DPG	0.0	0.25	0.5	1.25	0.0	0.25	0.5	1.25	0.0	0.0	0.0	0.0

The sorption curves of E and K mixtures (without and with N326) for t-BuPh are viewed in Figure 73. As expected, as the filler was added to the polymer matrix the solvent uptake decreases and need a longer time in order to reach the equilibrium.

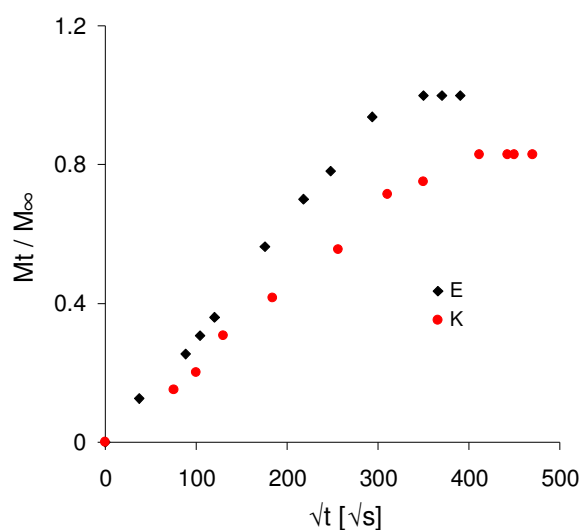


Figure 73: Relative mass absorption of NBR3 with and without filler by swelling in t-BuPh

As it shown before, SBR displays higher diffusion coefficient than for NBR when the swelling takes places in t-BuPh. A drastic decrease of the diffusion coefficient can be observed for SBR when the filler concentration is increased (Figure 74). This decrease originates from the interactions of the polymer with the filler and, on the other hand, by interactions with the solvent.

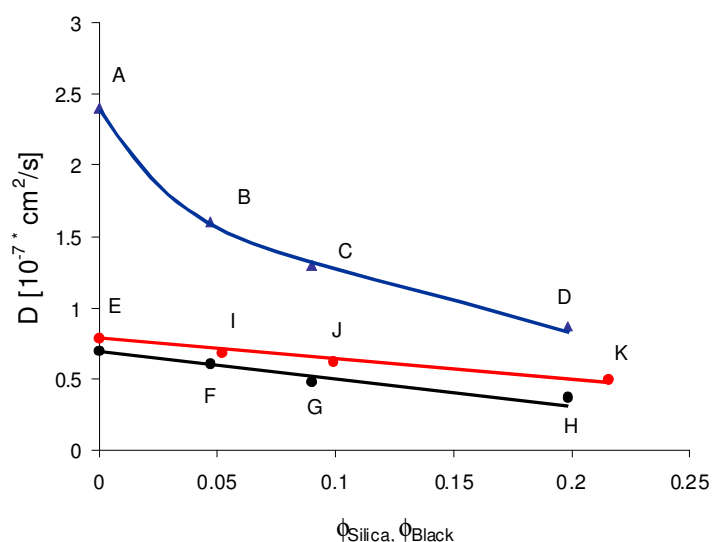


Figure 74: Influence of type and concentration of the filler on the diffusion coefficient of t-BuPh in crosslinked rubbers based on silica filled NBR3 (black), carbon black filled NBR3 (red) and silica filled SBR4 (blue)

Polymer-filler interaction is energetically less pronounced in silica filled SBR than in silica filled NBR and therefore the transport of t-BuPh through the SBR vulcanizate is easier. The heat of



absorption of non-polar SBR with the polar silica (silanol groups) is significantly lower than for NBR [231]. This effect can be observed by the normalization of the diffusion coefficient of filled rubber to unfilled rubber (Figure 75). The results demonstrate that a high concentration of the filler leads to a decrease of this ratio and varies as a function of the polymer used.

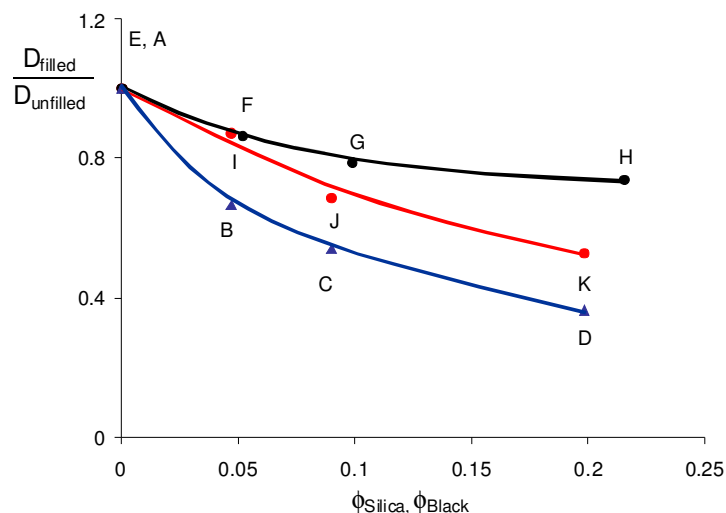


Figure 75: Influence of type and concentration of the filler on normalized diffusion coefficient of *t*-BuPh in crosslinked rubbers based on silica filled NBR3 (black), carbon black filled NBR3 (red) and silica filled SBR4 (blue)

The study of the influence of the filler structure on transport process of *t*-BuPh in crosslinked NBR4 was concentrated on measurements with two carbon blacks with the same structure but different specific surface area employed under the same experimental conditions. The diffusion coefficients of *t*-BuPh in mixture of NBR3 with carbon blacks obtained are similar in range of the errors. When using N326 a diffusion coefficient of about  $5,96 \cdot 10^{-8} \text{ cm}^2/\text{s}$  and for N326 of about  $5,80 \cdot 10^{-8} \text{ cm}^2/\text{s}$  were found. The unfilled NBR3 has a diffusion coefficient of  $7,78 \cdot 10^{-8} \text{ cm}^2/\text{s}$ .

In order to evaluate the diffusion process through the interfacial layer formed at the polymer – filler contact, a model is proposed as presented in Figure 76. A system A consists of 100 g of rubber mixed with 50g filler. The corresponding volumes for rubber and filler were calculated and are  $V_R=106 \text{ cm}^3$  and  $V_F=27 \text{ cm}^3$ . The  $V_{R+IPL}$  represents the volume of the rubber existing in the system and in the interfacial layer. In  $100 \text{ cm}^3$  system A, the calculated volume fractions are  $\phi_F=0,2$  and  $\phi_{R+IPL}=0,8$ . For the calculation of the volume fraction of the interfacial layer ( $\phi_{IPL}$ ) the following equation was considered:

$$\phi_{IPL} = m_F * S_F * d \quad (\text{Eq. 64})$$

where  $m_F$  is the mass of the filler in the  $100 \text{ cm}^3$  system A,  $S_F$  is the specific surface of the filler and  $d$  is the thickness of the interfacial layer.

The volume fraction of the interfacial layer was calculated considering different thickness of the interfacial layer.

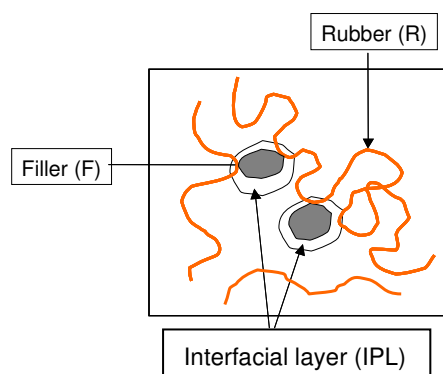


Figure 76: System A contains rubber, filler and interfacial layer

For the determination of the diffusion coefficient in the interfacial layer the following equation was considered:

$$D_{R+IPL} = D_R * \phi_R + D_{IPL} * \phi_{IPL} + D_F * \phi_F \quad (\text{Eq. 65})$$

where  $D_{R+IPL}$  is the diffusion coefficient of the whole system,  $D_R$  is the diffusion coefficient of the rubber,  $D_{IPL}$  is the diffusion coefficient in the interfacial layer and  $D_F$  is the diffusion coefficient of the filler which is zero.

If a thickness of the interfacial layer of 1 nm for the system NBR3/N326 was assumed, the volume of the interfacial layer  $V_{IPL} = 3,13 \text{ cm}^3$  was obtained which leads to a volume fraction of the interfacial layer  $\phi_{IPL} = 0,031$ . As a result, the volume fraction of the rubber in the system was  $\phi_R = 0,765$ . The same assumption was made for the system NBR3/N375. The results are summarized in Figure 77.

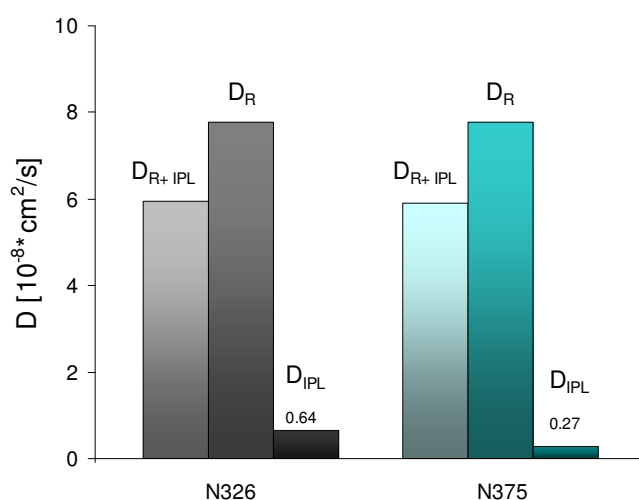


Figure 77: Evaluation of the diffusion coefficients of *t*-BuPh in NBR3/N326 and NBR3/N375 systems if the thickness of the interfacial layer is 1 nm

It was observed for both systems that the diffusion coefficients in the interfacial layer were significantly smaller compared to the diffusion coefficients in the whole system and of the rubber respectively. This result sustained that the diffusion process in the interfacial layer influences to a certain extent the diffusion process of a fluid through a filled rubber. For t-BuPh in NBR/N326 system a  $D_{IPL}$  of  $0,64 \text{ cm}^2/\text{s}$  and in NBR/N375 system a  $D_{IPL}$  of  $0,27 \text{ cm}^2/\text{s}$  were obtained.

A correlation of the diffusion coefficient with the density was shown in Figure 72. From this diagram the densities corresponding to the diffusion coefficients in the interfacial layer can be evaluated. Relatively similar values were obtained, for NBR/N326 system a density of about  $1,036 \text{ g/cm}^3$  and for NBR/N375 system a density of about  $1,041 \text{ g/cm}^3$ . These findings suggest that the thin interfacial layer behave as a glassy one. A comparison of its density with several plastic materials supports this assumption (Table 18).

Table 18: Density and diffusion coefficients of N<sub>2</sub> in plastic materials

Plastic material	Density [g/cm <sup>3</sup> ]	Diffusion of N <sub>2</sub> [10 <sup>-8</sup> *cm <sup>2</sup> /s]
PS (Poly styrene)	1,050	9,60
PET (Poly ethylene terephthalate)	1,370	0,14
PVC (Poly vinyl chloride)	1,520	0,38

When the thickness of the interfacial layer was varied it was noticed that the diffusion coefficient in the interfacial layer increases due to a higher amount of rubber located in the interfacial layer and as a consequence the total amount of rubber in the system decreases (Figure 78).

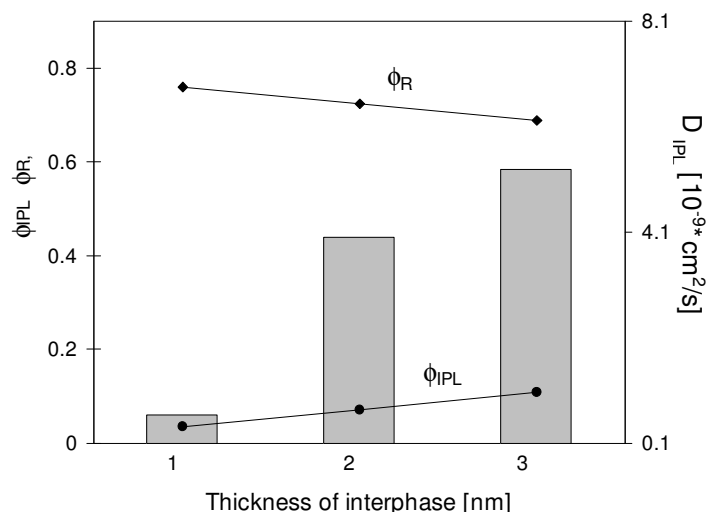


Figure 78: Variation of  $D_{IPH}$  of t-BuPh in NBR/N326 in dependency of the thickness of the interfacial layer

#### Influence of the phase morphology

The transport processes through rubber polymer blends depend upon the compatibility, composition and phase morphology of the blend phases. However, most polymer blends

constitute from components with different polarity forming two-phase heterogeneous systems. Consequently, the effect of diffusion is very dependent on the degree of compatibility of the system. This leads to the question how the phase morphology influences the transport process of the low molecular compounds?

In Figure 79 shows schematically the swelling process through a NBR/SBR blend. It can be seen that at a blend ratio NBR/SBR (20/80) the NBR phase is dispersed in the continuous SBR matrix and at a blend ratio NBR/SBR (80/20) SBR is dispersed in the continuous NBR matrix. At the same blend ratio both NBR and SBR form continuous phase which lead to a co-continuous morphology. By increasing the concentration of SBR from 20 to 80 wt.%, the domains size of SBR increases and it forms the continuous phase. The diffusion process takes place through SBR phase that leads to a high swelling in NBR/SBR (50/50) blend and NBR/SBR (20/80) blend respectively.

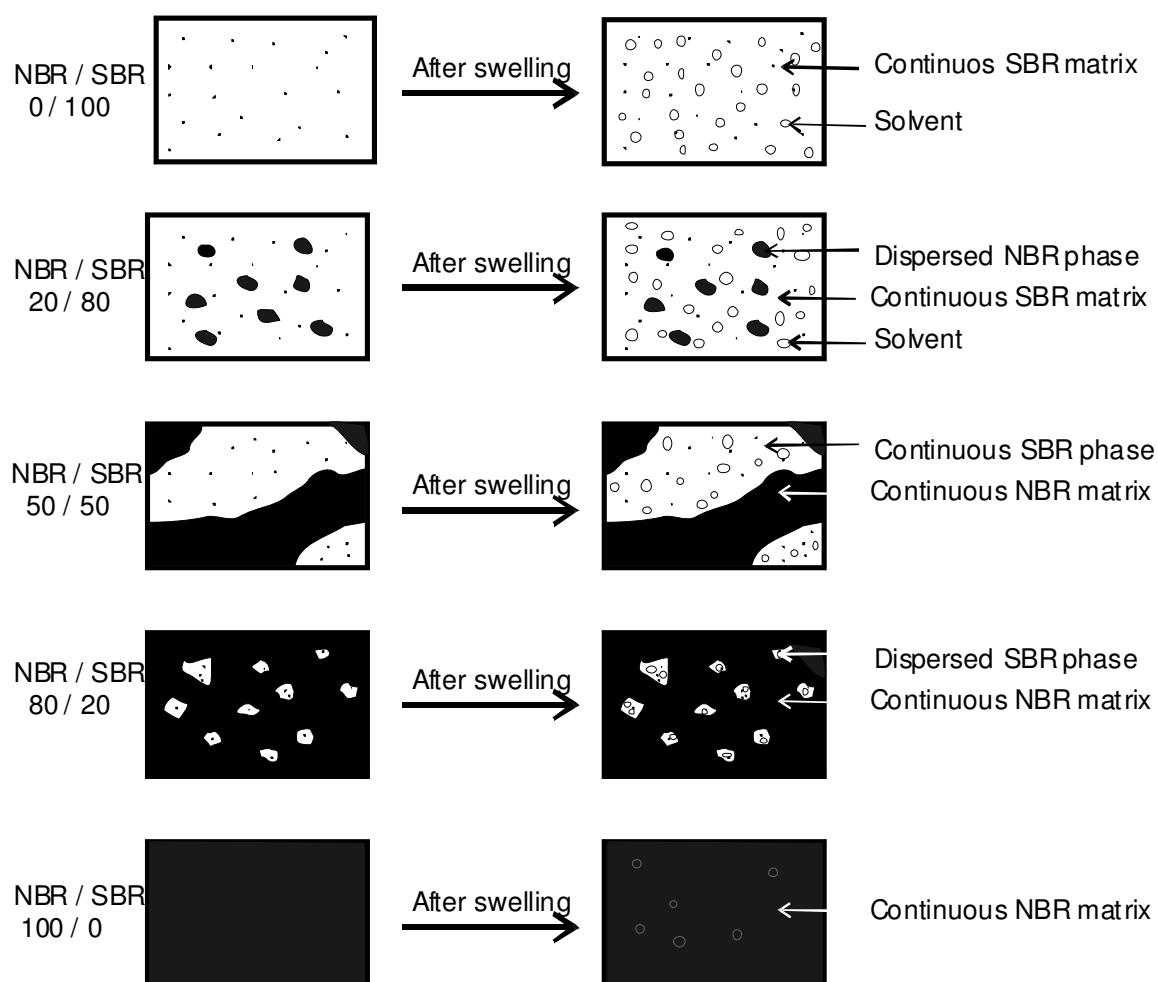


Figure 79: Representation of swelling process in NBR/SBR (different blend ratio)

The influence on the transport process of t-BuPh was analyzed using various blend ratio of SBR/NBR system. Methyl-ethyl-ketone (MEK) was chosen for studying the influence of the

diffusant polarity on diffusion transport in blends. The results are summarized in Figures 80 – 82.

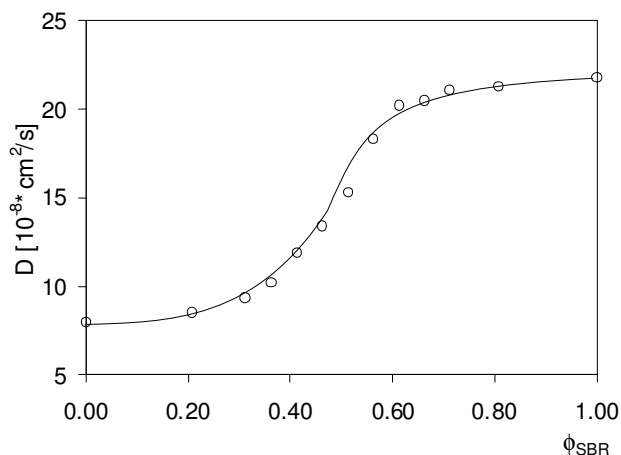


Figure 80: Diffusions coefficients of t-BuPh as a function of volume fraction of SBR for different blend ration of SBR4/NBR3 at RT

The variation of the diffusion coefficient of t-BuPh as a function of the blend composition corresponds to a step function. In the region in which NBR3 forms the continuous phase and SBR4 represents the dispersed phase, the diffusion coefficient only increases slightly. In the phase reversal region the values increase to a level typical for SBR4. In the segment in which only SBR4 forms the continuous phase the diffusion coefficient approaches the typical critical value for pure SBR with a small slope of the curve. TEM pictures, as shown in Figure 81, enable an assignment of values to the corresponding phase morphologies.

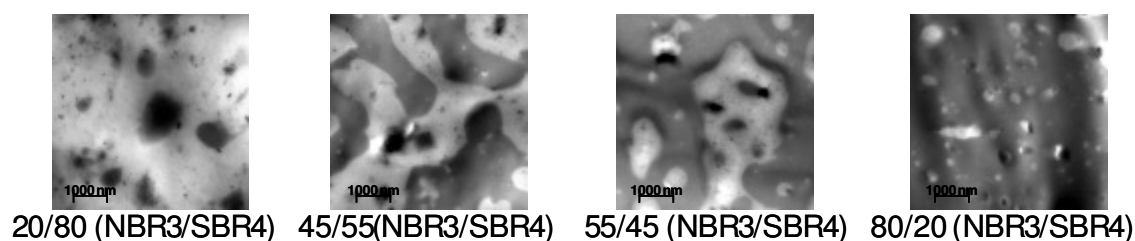


Figure 81: TEM pictures of NBR3/SBR4 blends

The influence of phase morphology on diffusion process was shown in different works [232,233]. The study of the transport process of alkyl benzene in NR/NBR blends demonstrated that increasing the NBR content in blend the diffusion coefficient decreases due to the inherent solvent resistance behaviour of NBR [234].

The behaviour for the diffusion coefficient of MEK in the same blend provides a further indication for the influence of phase morphology (Figure 82).

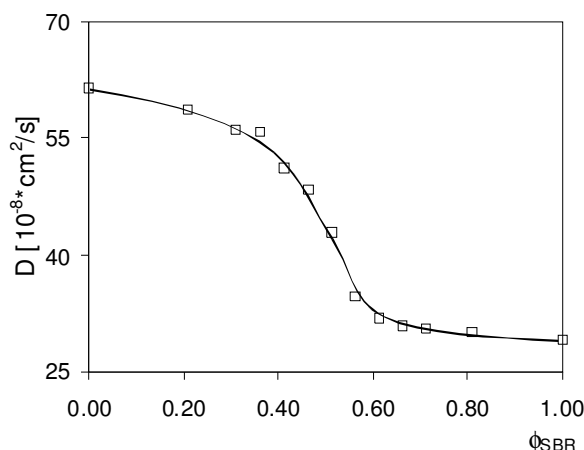


Figure 82: Diffusion coefficients of MEK as a function of volume fraction of SBR for different blend ratios of SBR4/NBR3 at RT

Because of the good solubility and low molecular mass of the MEK in NBR3, the diffusion coefficient is distinctively higher than that of t-BuPh. Here as well a reverse sigmoidal diffusion coefficient curve hints at the pronounced decrease in the phase reversal region.

#### *Influence of the diffusant size and shape*

A comparison of the diffusion coefficient of saturated hydrocarbons with different chemical structures in SBR4 is shown in Figure 83. The diffusion coefficient is higher for substances with short chain length and drops when the chain length is longer due to the changes in the configuration of the alkyl chain. The diffusion coefficient decreases further as the structure of the diffusant is branched (i-Dodecan) due to the increased volume.

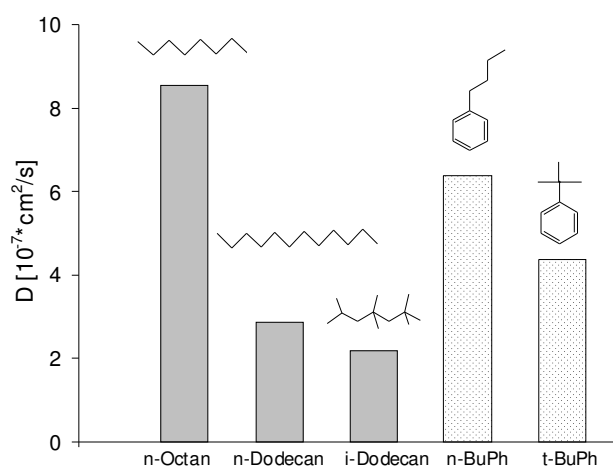


Figure 83: Influence of the diffusant structure on crosslinked SBR4 at 120 °C

The tertiary butyl groups with a high space requirement are responsible for the decrease of the diffusion coefficient. For example, the diffusion coefficient of the bulky tertiary butylbenzene is 30% lower than that of n-butylbenzene.

A decrease in the diffusion coefficient with increase of the size and shape of the penetrant was observed by many investigators [235 - 237]. For instance, the flattened or elongated molecules have a higher diffusion coefficient than spherical molecules of equal molecular volume [238]. This is the case when n-BuPh is compared with t-BuPh. The n-BuPh has an elongated form while the t-BuPh is more spherical.

#### 4.3.4 Determination of the diffusion coefficient with the two-chamber method

A focal point was the setup and validation of an automatic permeation apparatus (two-chamber method) for determining the permeation rate as well as the diffusion coefficient employing the „time-lag” method.

A schematical representation of this equipment is given in Figure 84. The two chambers (1) and (2) have the same volume (80 ml) and are separated by a metal lattice where the polymer membrane is placed. The carrier gas (nitrogen) is introduced with constant flow into the lower chamber through three positions so that after introducing the test fluid, which permeates through the membrane (starts the isobar measurements), the mass flow reaches the six-way valve across a transfer connection (d=1/16").

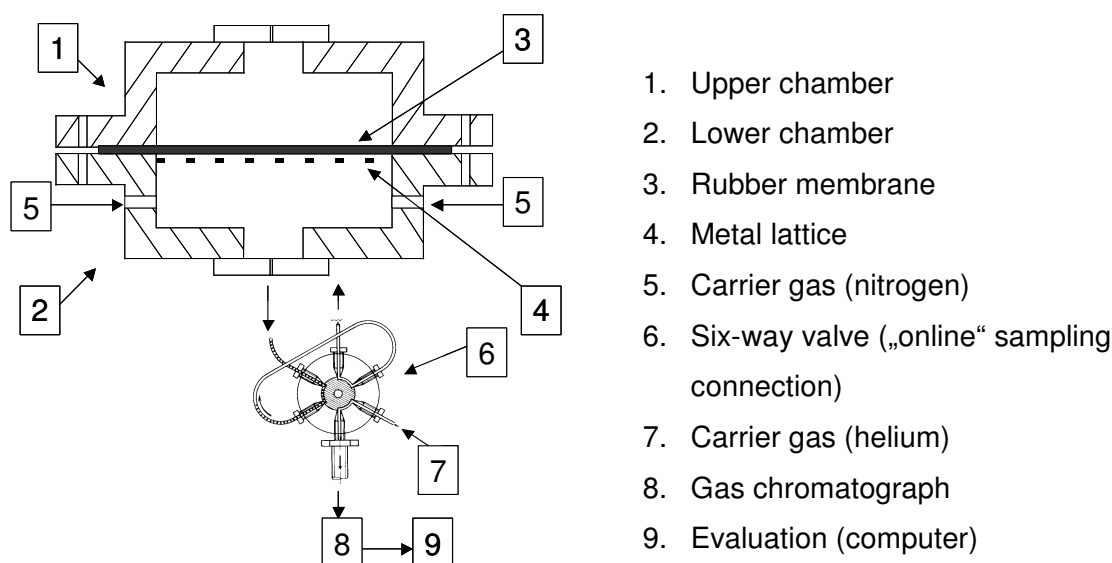


Figure 84: Presentation of the apparatus developed for the permeation analysis

The volume of the sample loop is 0.01 $\mu$ l. Further, using an automatic program for given intervals of time the mass flow is injected into the gas chromatograph. The principle of the six-way valve is presented in Figure 85.

During the whole experiment the transfer connection was heated at 60 $^{\circ}$ C and maintained at this temperature in order to reduce the losses that can occur in this part of the apparatus. The gas sample was introduced through a hot injector (250 $^{\circ}$ C) in the tempered (80 $^{\circ}$ C) capillary column (30mHP5) of a gas chromatograph (HRGC 5300 Mega Series) in order to facilitate the analysing

of mixtures of different test substances using a detector. A recording of the detector response versus time delivers a chromatogram.

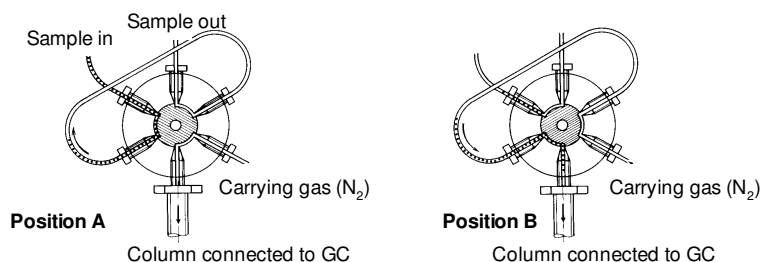


Figure 85: Principle of the six-way valve [239]

Before investigating the influence of different components of permeation and diffusions process the permeation apparatus was calibrated in a range of 0,02  $\mu\text{l/ml}$  to 0,1  $\mu\text{l/ml}$  t-BuPh in nitrogen. In order to work at the same conditions like during the measurements, the samples were preserved at 50°C for a period of 24 h before the calibration. For the calibration, t-BuPh was injected at several concentrations direct in GC and afterwards in the two-chamber apparatus. The calibration curves show a linear behaviour (Figure 86) with a relative standard deviation for the gas chromatographical device about a value < 4,5% and a detection limit of 6,62 ng/ml. For the whole process, the relative standard deviation is about <7,4% and a detection limit of 7,73 ng/ml. The retrieval rate for the small concentration of the test substance is 80%.

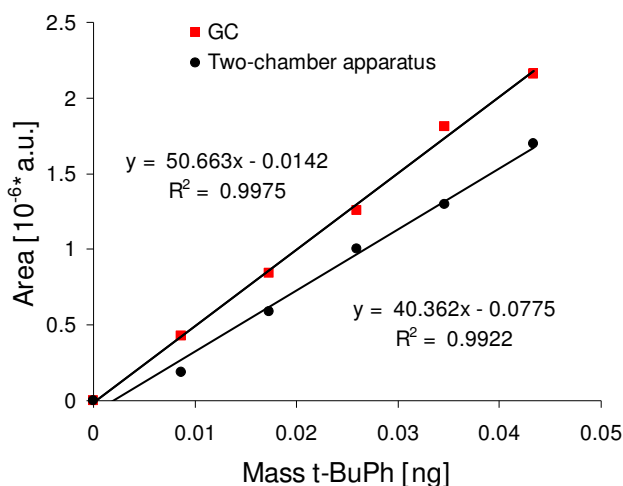


Figure 86: Calibration curves for t-BuPh in GC and two-chamber apparatus

With the permeation apparatus described above the diffusion coefficients and the permeation rates of t-BuPh in different sample plates with different thickness were investigated.

The diffusion coefficients were determined by means of the time lag method. The time dependent linear increase given by the peak obtained by chromatographical detection was extrapolated to the peak area zero. The intersection with the time axis represents the “gross time”. From this value was subtracted the time required for the transport from the lower chamber



to the detector and this was called the “net time lag“ which was used for the calculation of the diffusion coefficient using Equ. (41), Chap. 3.3.1.1. The permeation rates were obtained using the Equ. (34) described in Chap. 3.3.1.

#### *Influence of the polymer constitution*

A direct comparison of the penetrating amount of the *t*-BuPh in time through the plate (2mm) was conducted on NBR vulcanizates with an increasing ACN content (NBR1, NBR3 and NBR4) (Figure 87). Significant differences are evident. These can be related to the constitution of the rubber. The time-lags raise with increasing the ACN content, while the saturation concentration which corresponds to the stationary permeation state decreases.

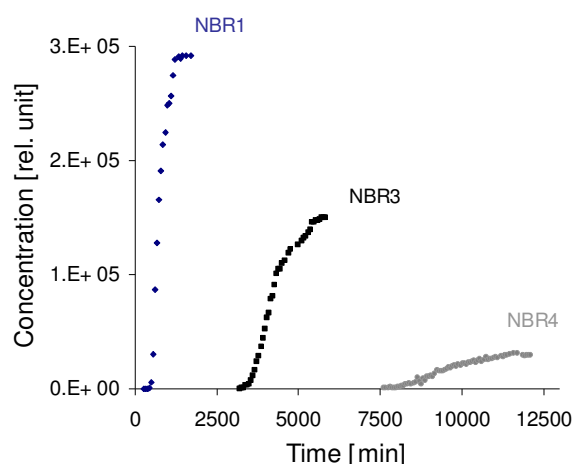


Figure 87: Penetrating amount of *t*-BuPh in NBR1, NBR3, NBR4

Taking into consideration the pronounced differences noticed in the curve characteristics, any influence from the slight variation in crosslinking density could be ignored. What is mainly reflected here is the influence of the polar nitrile groups. The influence of the ACN units already discussed with high consistency confirms the influence of these groups on the transport process of *t*-BuPh through NBR rubber. For the transport processes treated here, this influence was expressed by means of an increase in the time-lags and the concentration gradients ( $dC/dT$ ). It could be observed in all three cases that the time required for attainment of the stationary state increases with the nitrile content (22 h for NBR1; 86 h for NBR3 and 183 h for NBR4).

Table 19: The net time-lag ( $\tau$ ), concentration gradient,  $D$  and  $P$  of *t*-BuPh in NBR crosslinked systems determined from permeation experiments (plate thickness  $2\text{mm} \pm 0.45$ )

Systeme	$\tau$ [min]	$dC/dt$	$D$ [ $10^{-8} \cdot \text{cm}^2/\text{s}$ ]	$P$ [ $10^{-7} \cdot \text{g}/\text{cm}^2 \cdot \text{s}$ ]
NBR1	506	0.0090	19.5	1.170
NBR3	3608	0.0015	5.5	0.217
NBR4	8238	0.0001	1.7	0.014

The permeation rate for the stationary state was determined having the unit  $[g/cm^2s]$ . Table 19 summarizes the values obtained for net time-lags, diffusion coefficient, concentration gradient and permeation rate.

The results demonstrated that the diffusion coefficient and the permeation rate do not decrease in linear proportion to the ACN content. With a high degree of accuracy, a dependency of the permeability rate on the ACN content is determined (Figure 88).

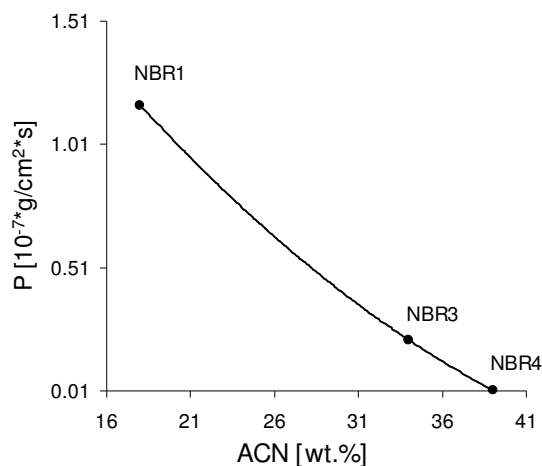


Figure 88: Influence of the ACN content from NBR on the permeation rate of *t*-BuPh at RT

This form of dependency exhibits a certain similarity to the decrease in the swelling degree of the ACN content of NBR crosslinked systems (Figure 89).

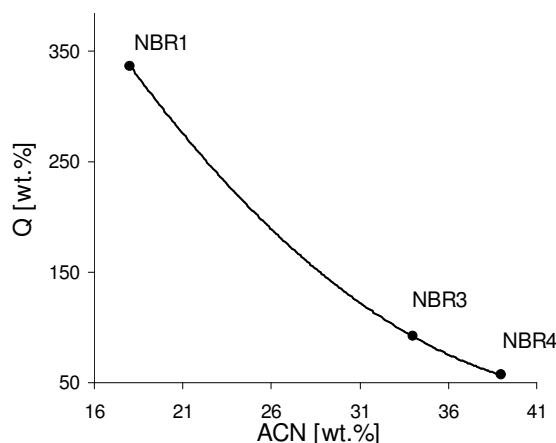


Figure 89: Reception of *t*-BuPh through NBR crosslinked systems with increasing ACN

Since the swelling degree of a crosslinked system qualitatively expresses the magnitude of the polymer solvent interaction, it can be assumed that the sorption of the hydrocarbon has a crucial influence on the decrease of the permeation rate. Furthermore, this is confirmed by the linear relationship between  $P$  and  $D$  (Figure 90), referencing the fact that the permeation process consists of the three stages: a) sorption, b) diffusion and c) desorption.

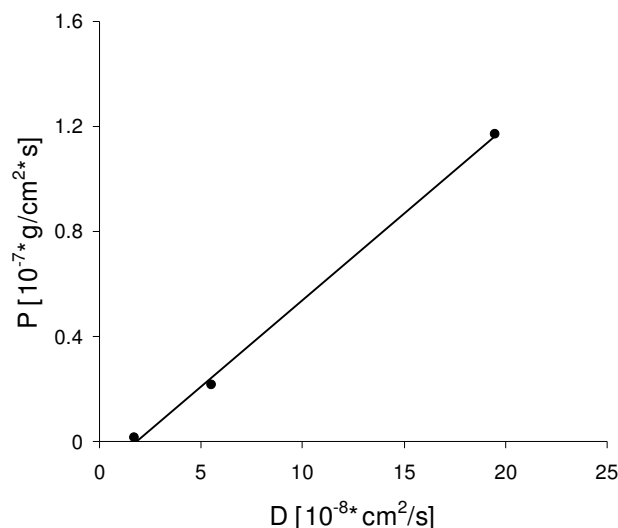


Figure 90: Permeation rate of *t*-BuPh in NBR depending on the diffusion coefficient

The sensitivity and reproducibility of the methods employed for the study of the diffusion coefficient represent an important issue that must be taken into consideration. A comparison between the values obtained for the diffusion of *t*-BuPh in NBR with different acrylonitrile content was done and outlined in Figure 91.

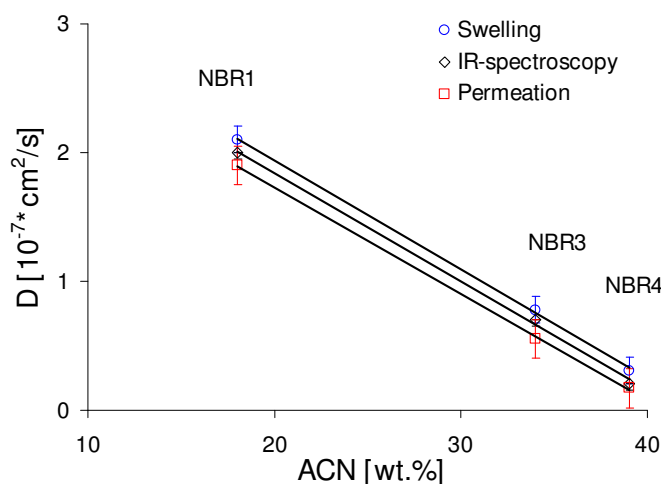


Figure 91: Determination of the diffusion coefficient of *t*-BuPh in NBR by means of swelling investigation, IR-spectroscopy and permeation measurements

The diffusion coefficients using these three methods are roughly the same, the values acquired by swelling measurements are slightly higher than those obtained by the IR-spectroscopy method respectively by permeation. For that behaviour, several reasons can be mentioned: different quality of sample preparations or varying crosslinking densities of the specimens. The relative precision of the methods used is for IR-spectroscopic measurements about 1.6%, for swelling investigations about 2.7% and for the permeation investigations about 7.7%.

Nevertheless, the general trend is similar for all three cases and shows that an increase of the ACN content in NBR leads to a reduction of the diffusion coefficient of *t*-BuPh.

### *Influence of the crosslinking density*

Because of the chemical crosslinking the glass transition temperature of elastomers is shifted to higher values. The concomitant decrease in free volume and chain mobility is reflected in the permeation measurements taken on NBR vulcanizates with increasing crosslinking density (Table 20). In accordance with the explanatory remarks from above, an increase in crosslinking density leads to a decrease in the diffusion coefficient values and permeation rates.

*Table 20: Influence of the crosslinking density on the net time-lag ( $\tau$ ) and the diffusion coefficients of *t*-BuPh in NBR (plate thickness  $2\text{mm} \pm 0.15$ )*

System	XLD [ $10^{-5} \text{ mol cm}^{-3}$ ]	$\tau$ [min]	dC/dt	D [ $10^{-8} \text{ cm}^2/\text{s}$ ]	P [ $10^{-7} \text{ g} \cdot \text{cm}^2/\text{s}$ ]
NBR 3-1	4.5	2604	0.0120	6.9	1.420
NBR 3-2	8.6	3608	0.0015	5.5	0.217
NBR 3-3	15.9	5031	0.0006	3.4	0.068

From this example it is evident that crosslinking density has less impact than the ACN content. An increase of crosslinking density with factor 3 leads to a decrease of the permeation rate to a factor of 20.

### *Influence of the filler*

The incorporation of a volume share of solid particles into the elastomer matrix influences the permeation process being studied for that. The mass transport of permeate cannot take place in a specimen volume proportional to the filler share. Moreover, it can be expected that the filler dispersion and the formation of a polymer layer firmly adsorbed on the filler surface that is a typical phenomenon for active fillers may affect this process.

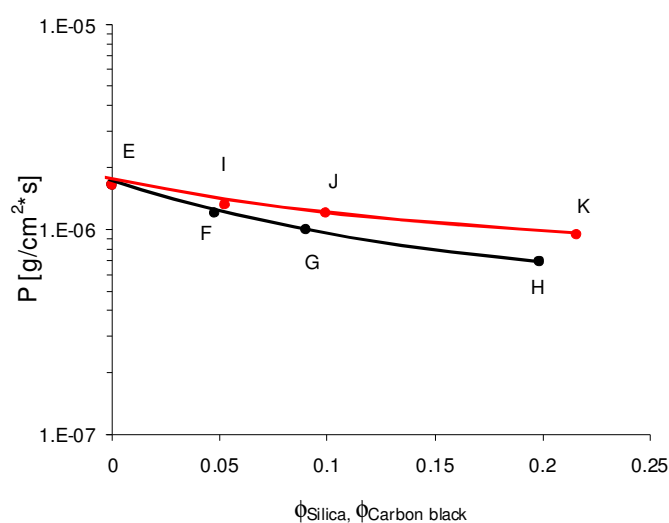


*Figure 92: The influence of the filler type and concentration on the permeation rate of NBR3 (silica filled crosslinked F = 10phr, G = 20phr and H = 50 phr; black filled vulcanizate I = 10phr, J = 20phr und K = 50phr; plate thickness 1mm)*

For a better understanding of these influences, comparative permeation and swelling tests were carried out on NBR3 or SBR4 vulcanizates filled with silica 7000 GR respectively carbon black N326, employing different filler concentrations of 10phr, 20phr and 50phr. The results are presented in Figure 92.

As can be seen from the half logarithmic representation, the permeation rate decreases significantly as the filler volume fraction rises. The fact that the permeation rates of *t*-BuPh in NBR2 vulcanizates containing silica are lower than those in NBR2 vulcanizates containing carbon black is due to a better polymer/filler interaction, which causes a pronounced sorption of the NBR chains on the surface of the silica. This interaction was proven by IR-spectroscopy by the occurrence of a new band as well as a higher bound rubber share and also a large increase of the loss modulus in the glass transition range.

#### *Influence of the plasma treatment*

The influence of thin layers on the specimen surface during the permeation process was investigated in order to verify the sensitivity of the permeation method.

A thin film was applied to a 1 mm NBR3 plate by means of plasma coating with decafluoropentane as precursor. In other coating trials, the composition of the film was analyzed by means of XPS spectroscopy and a layer thickness of 20-50 nm was determined [240]. Assuming a similar magnitude here as well, Figure 93 illustrates the effectiveness of a layer of this nature as barrier for permeation. In literature, it was shown that the film produced by means of this technique can exhibit a high consistency and crosslinking density is increased [241].

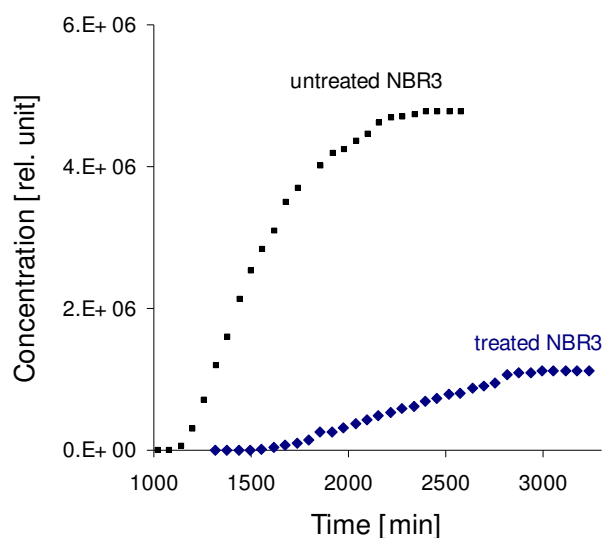


Figure 93: Penetrating amount of *t*-BuPh in untreated and treated NBR3

The thin layer that hardly changes the thickness of the specimen increases the net time-lag and lowers the permeation rate drastically. The stationary state is attained earlier in case of the untreated reference than in case of the treated specimen. The permeation rate of *t*-BuPh is

significantly reduced due to the density and probably also due to the fluorine content of the layer applied. This is a proof for the sensitivity of the measuring method by characterizing the permeation barriers.

The evaluation of the fluorine on the sample surface applied through the plasma treatment was done by AFM, SEM, FT-IR-Spectroscopy and XPS measurements.

By means of AFM investigations, in case of the treated specimen higher homogeneity and less surface roughness ( $4,798 \mu\text{m}$ ) were determined than for the untreated rubber ( $5,740 \mu\text{m}$ ). The SEM measurements confirmed the AFM results (Figure 94).

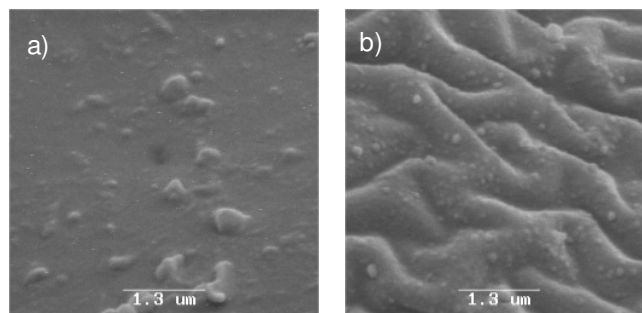


Figure 94: SEM pictures of untreated NBR3 (a) and treated NBR3 (b)

By characterizing the surface with ATR-FT-IR spectroscopy, mainly the oxidative changes of the NBR surface were observed. These changes showed that the coating process with decafluoropentane was done in the presence of air (Figure 95). In the spectrum, the characteristic bands for the carbonyl group in esters ( $1712 \text{ cm}^{-1}$ ) and amides ( $1640 \text{ cm}^{-1}$ ) occur. It is not completely clear whether the band at  $1194 \text{ cm}^{-1}$  corresponds to a C-O vibration or a C-F vibration. The oxidation processes are also indicated by the characteristic O-H bands at  $\sim 3400 \text{ cm}^{-1}$ . In correspondence to these bands, the bands of the symmetric C-H oscillation ( $2849 \text{ cm}^{-1}$ ) and the asymmetric C-H oscillation ( $2921 \text{ cm}^{-1}$ ) decrease.

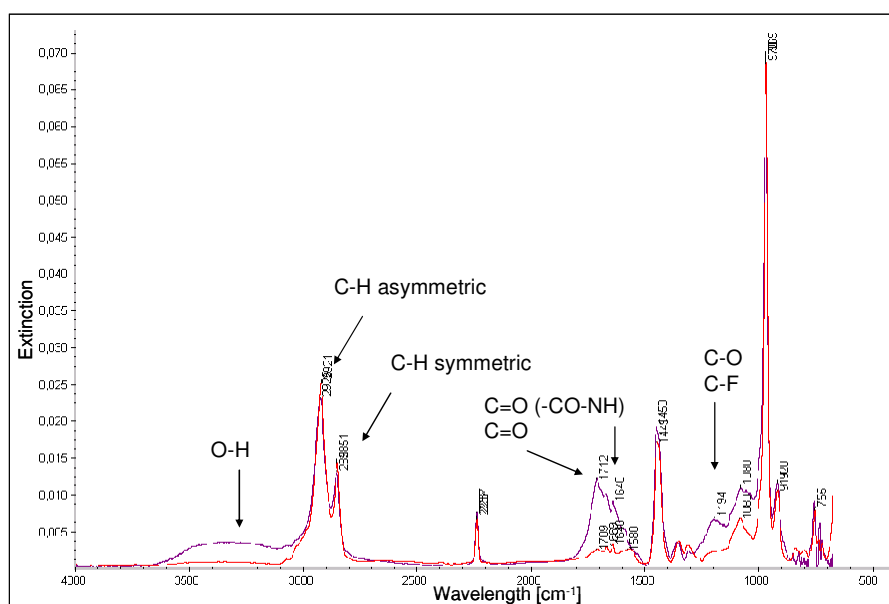


Figure 95: ATR-FT-IR investigation of untreated NBR3 (red line) and treated NBR3 (blue line)

With the XPS investigation of the treated sample several elements were detected and 3,18% fluorine was found (Table 21). These results emphasized that the absorption band at  $1712\text{ cm}^{-1}$  obtained by FT-IR-Spectroscopy measurements point out the presence of fluorine at the surface of the sample.

Table 21. XPS results for untreated and treated NBR3

Element	Untreated NBR3 [atom%]	Treated NBR3 [atom%]
O (1s)	21,58	15,80
N (1s)	1,49	2,38
C (1s)	57,07	69,13
F (1s)	-	3,18
Rest	19,86	9,51

The surface polarity due to the presence of the oxygen groups, the effects of C-F groups as well as the crosslinking density of the matrix could limit the permeation of t-BuPh.

#### 4.4 Relationship of oil exposition and properties

Elastomers have special characteristics, for example, they are flexible, elastic, to some extent impermeable to both water and air. They are classified in two classes: oil-resistance elastomers (nitrile rubber, ethylene-acrylate elastomer, fluorocarbon elastomers) and non oil-resistance elastomers (ethylene-propylene-diene and ethylene-propylene rubbers, natural rubber, butyl rubber, styrene-butadiene rubber).

A correlation between the heat resistance and oil resistance of various elastomers is presented in Figure 96.

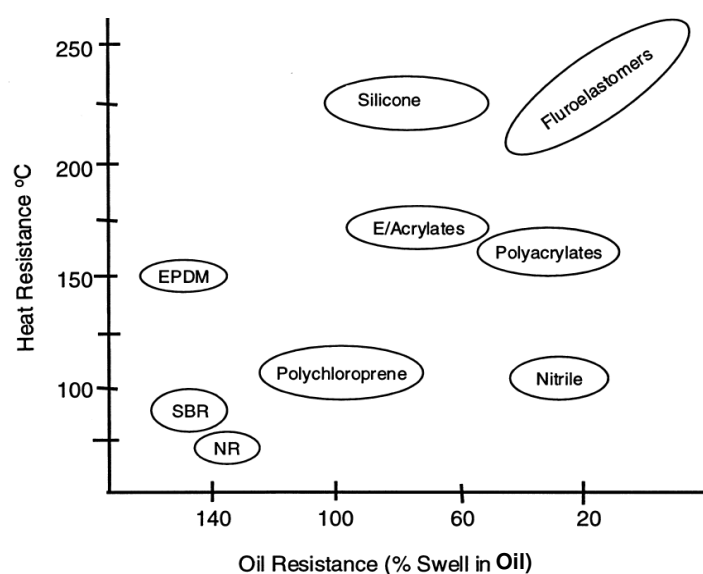


Figure 96: Heat and oil resistance of different elastomers [242]

The resistance to swelling in hydrocarbon oils of elastomers is brought partly by the polar side groups. These groups contain atoms which form covalent bonds with the carbon atoms in the polymer chain, but the electron pair is displaced to the more electronegative atom [243]. The oil resistance is increased, as the electronegativity of the side chain group increases on the polymer. Table 22 presents the resistance of different polymers in IRM903 oil (low viscosity naphthenic oil) at 100°C for 70 hours.

*Table 22. Relationship between structure and oil swell of polymers*

Polymer	Swelling in oil [%]
Fluorocarbon (FKM)	10%
Nitrile (NBR) (33% ACN)	40%
Polyacrylate (PA)	60%
Polychloroprene (CR)	120%
Polyisoprene (IR)	150%

The highest oil resistance is achieved by the fluorocarbons due to the fluorine side group which has the highest electronegativity. Further, the nitrile and polyacrylate have the cyanide and the ester group display lower oil resistance due to lower electronegativity of the side group. The chlorine atom is more electronegative than the methyl group so that the polyisoprene has almost no resistance at all.

This study was focused on investigation of oil exposition on NBR and HNBR rubbers, two elastomers that are classically used in oil applications. The oil resistance of nitrile rubber varies with the acrylonitrile content. Generally, as the ACN content increases the oil and solvent resistance is improved as well as the abrasion resistance. These properties deteriorate when the acrylonitrile decreases but the low temperature flexibility and resilience is enhanced [244].

The study of transport process of oils in elastomers is important for engineering applications [245]. Contrary to the gases that diffuse through polymeric materials with low interaction, the transport process of liquids can cause swell of the polymers. In this work the influence of different types of oils (polyglycol or saturated synthetic-ester oil) were tested on rubbers used in a rotary shaft seals.

Pioneer developments in mechanical engineering field especially by the driving and the fluid technique are often based on improvements in the area of materials and fluids. Important developments with regard to fluids are the improvement of the period of use and the environmental compatibility. Critical components such as dynamical shaft seals have to follow these developments and their efficiency has to be improved with the help of new technologies.



In case of mechanical engineering, especially at stationary and mobile hydraulic aggregates as well as at engines and gear units used in automotive or industrial environment sealing are necessary and are modified to the respect of the working conditions.

A proper sealing over a longer period of time may just be secured by a sufficient chemical resistance against lubricants, their additives and high temperatures, mostly independent from mechanical stress.

The aim of this chapter was to study the influence of oil exposition on rubbers considering the swelling measurements at different temperatures. The effects of those lubricants on mechanical properties were evaluated as well as the damages of the final product that appeared during the dynamical stress. The investigations were done on shafts seals used in industry. In this study the crosslinking density, microstructure of the rubber, the type and the concentration of the filler used in these formulations were considered on the interpretation of the results.

The rubbers used for this investigation were NBR2 vulcanized by a sulphur system and HNBR1 cured with a peroxide system. The formulations contain the other components employed in a rubber compound (fillers, processing aids, antioxidants) used for a rotary shaft seal. For the matrix containing NBR2 the system will be noted with NBR-M1 and for the matrix with HNBR1 it will be used HNBR-M2. For the comparison with the mixtures used in industry, reference mixtures were prepared where the rubbers NBR2 and HNBR1 were vulcanized with the corresponding cured system. The oils used for this study were characterized by means of FT-IR-spectroscopy and gas chromatography; the results are presented in Table 23 and Figure 97.

Table 23. Chemical characterisation of the oils

Oil	Matrix	Additive	Others
Polyglycol 1 (PG1)	Polypropylene glycol, $M_w = 4000$ g/mol	Octane acid methyl ester, Decane acid methyl ester, ODP, „Irganox 1035“, BHT, PPD (Remark: components contain nitrogen, $M_m = 369$ )	Heptane, Toluene, Ethylbenzene, Xylene, Trimethylbenzene, DBP, DEHP
Polyglycol 2 (PG2)	Polyethylene propylene glycol, $M_w = 3300$ g/mol	„Irganox 1035“, ODP, BHT, PPD	Heptane, Toluene, Ethylbenzene, Xylene, Benzaldehyde, Trimethylbenzene, DBP, DEHP
Saturated complex ester synthetic oil (CE)	Ester, (Comparison of IR Spectra epoxidized Soja oil), $M_w = 4700$ g/mol	Octane acid methyl ester, Decane acid methyl ester, (Remark: components contain nitrogen)	Heptane, 2-Methyl-1-butanol, Toluene, Ethylbenzene, Xylene, Trimethylbenzene, DBP, DEHP

Irganox 1035: 2,2'-Thiodiethylen-bis-(3,3'(3,5-di tert. butyl-4-hydroxyphenyl)-propionate)

ODP: Octyl. Diphenylamine

DBP: Dibutylphthalate

DEHP: Di-(2-ethylhexyl)-phthalate, technical also Dioctylphthalate (DOP)

BHT: 2,6-Di-tert.butyl-4-methyl-phenole

$M_m$ : Molar mass

PPD: Paraphenylenediamine

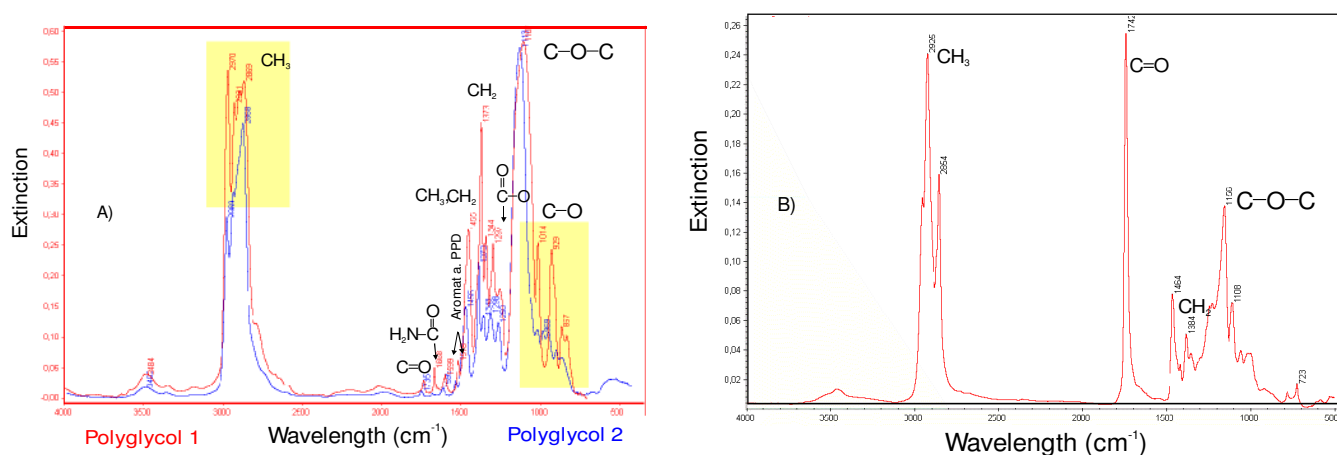


Figure 97. FT-IR-spectroscopy of PG1 and PG2 (A) and CE (B)

The results showed two different types of oils: glycol and ester. Owing to the different polarities of the functional groups different effects in the swelling and mechanical behaviour on the selected elastomer materials are to be expected. The same is valid for the effects of the additives.

#### 4.4.1 General requirements to be met by elastomer materials for rotary shaft seals

Rotary shaft seals are frequently function-limiting components when being used in the area of automotive and mechanical engineering. Thanks to their specific properties, elastomers are especially well suited as materials here as they may cope with the particular exposition conditions and loads of the components [246].

To be sure, predicting the function and service life of the rotary shaft seals used are fraught with uncertainty. This is due, on one hand, to the fact that for technical and ecological reasons the composition of the lubricants used on modern motors, hydraulic systems and gears are constantly subject to changes, especially regarding their constituent additives. On the other hand, there is hardly any detailed knowledge of the wear processes and temperature loads in the zone where the sealing lips get in contact with the shaft (Figure 98).

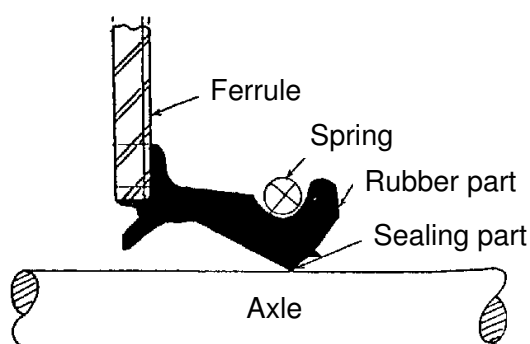


Figure 98: Design and configuration of a rotary shaft seal [247]

This situation is underscored by failures, which may lead to technical and economic consequences in actual practice. When rotary shaft seals suffer a loss of function this usually happens in the form of a leak or the loss of fluids (lubricant) in the adjacent system chamber [246]. To predict the resistance and functional reliability of selected materials for rotary shaft seals, it is thus of the utmost interest – from a chemical perspective as well – to arrive at a comprehensive understanding of aging processes in the elastomer of rotary shaft seals and of the interactions between lubricant, additives and elastomer materials as well as the related consequences for the property profile of the seal.

When used in gears and engines, rotary shaft seals are subject to radically changing operating conditions, such as starting operations, occasional standstill as well as pressure and temperature fluctuations. Rotary shaft seals must provide sufficient resistance over a longer period of use to be able to follow/respond to the radial deviation of the shaft and construction tolerance. In specific cases, this results in high requirements on the materials used. On one hand, these requirements have a mechanical component in form of friction, static compression or dynamic stress. On the other hand, they also encompass physical and chemical factors of influence, such as exposition to lubricants and their additives and the atmospheric oxygen and temperatures in the vicinity of the sealing lip exceeding 140°C, in combination with the sump temperatures of around 80 -100 °C. The high temperatures mostly are due to high peripheral speeds. Besides, a high level of mechanical properties in terms of wear, a compressive set and elasticity, a high resistance to aging and lubricants is thus also required [247]. In actual practice, this complex requirements profile results in the preponderant use of high quality special purpose elastomers on the basis of acrylonitrile rubber (NBR), hydrogenated acrylonitrile rubber (HNBR), fluororubber (FKM) and acrylate rubber (ACM) as well as polyurethanes. Apart from the polymers used, the type of crosslinking and the choice of further compound components such as fillers may have a crucial impact, in chemical terms, on the functional reliability of rotary shaft seals.

#### 4.4.2 Chemical resistance of the rotary shaft seals with respect to different oils

Chemical exposition is of particular significance when it comes to material selection, because physico-chemical interactions between oils and sealing material may lead to swelling, shrinkage and exchange reactions among ingredients, with high temperatures generally favoring these processes. As a rule, the consequence is a drop in the mechanical value level as the elastomer network is brought under tension by swelling processes and secondary reactions leading to premature aging processes because of the elution of anti-aging agents that generally trigger embrittlement of the material with a tendency to cracking. For that reason, the sealing material-lubricant match-ups are to be optimized to achieve the lowest possible physico-chemical

interactions. The interaction between the polymer matrix and a fluid such as oil is exhaustively described in the theory of Hildebrand or by Flory and Huggins.

If the solubility parameters ( $\delta$ ) and the interaction parameter ( $\chi$ ) of the main components involved (polymer, lubricant) are known, a useful instrument for the selection of sealing materials can be done. A chemical resistance, low swelling in the lubricant, is provided only if the solubility parameters between the lubricant and its components and the polymer exhibit the highest possible difference, i.e. if  $\chi$  has a high value.

Table 24 shows the solubility parameters for two glycols, which are present in the oils used for the investigation. Increasing the number of carbon in the chain the polarity of the substance is decreasing. Table 25 presents the solubility parameters of NBR with different ACN contents and shows that increasing the acrylonitrile content the solubility parameter becomes higher. By HNBR, due to the saturation in the chain, a lower solubility parameter occurs.

*Table 24. Solubility parameter of different glycols [248]*

Solvent	$\delta$ [J/cm <sup>3</sup> ]
Ethylene glycol	14.6
Propylene glycol	12.6

*Table 25. Solubility parameter of NBR with different acrylonitrile content [248]*

ACN [wt.%] in NBR	$\delta$ [J/cm <sup>3</sup> ]
18	17.7
20	18.4
30	20.2
39	21.4

On the other hand, care is also to be taken to the other components of the compound like plasticizers and anti-aging agents are wherever possible not soluble in the lubricant. If this is the case, diffusion processes give rise to an elution reaction with undesirable changes in the mechanical property profile (hardening) and to shrinkage. Both processes can also occur in combination in the form of a replacement of low-molecular elastomer constituents with lubricants and lubricant components in accordance with the individual solubility values.

Taking the aforementioned theoretical relationships into account, consideration of the different applications of the mineral oil, polyglycol or synthetic ester based lubricants used yields a broad array of rubber types suitable as polymers for elastomer seals. The basic principle in selecting the rubber is that a polar rubber is suitable for non-polar contact media and vice versa. Examples of polymers frequently used technically for modern seal materials are fluororubber

(FKM), nitrile rubber (NBR, HNBR), acrylate rubber (ACM) and ethylene-propylenediene rubber (EPDM) [249, 250].

Alongside the basic polymer and compound ingredients with a determining influence on the properties like plasticizers and anti-aging agents, crosslink type or crosslinking density is another variable that must be taken into consideration from the chemical perspective.

Crosslinking density has a major influence on the degree of swelling attainable in the case of an interaction between contact medium and material (polymers, filler), with crosslink type (e.g. sulphur, peroxide) determining the stability of the crosslink network. As A. Ismat et al. has shown, using fluoro rubber and machine oil [251] that the chemical exposition to certain lubricant additives leads to a reduction of crosslinking density. A dithiocarbamate has been identified here as harmful additive.

#### 4.4.2.1 Swelling investigations

##### *Swelling in polyglycols*

The first measurements were done in polyglycols at 24 °C, 60 °C and 100 °C. At 24 °C and 60 °C the NBR-M1 showed lower swelling values for both investigated lubricants (Figure 99a). It could be observed that by swelling in PG2 at 100 °C a swelling degree of about 3,5% was reached. In comparison with HNBR-M2, the mass uptake at all three temperatures was noted to be higher (Figure 99b). With a temperature of about 100 °C the swelling degree varied from 3 wt.% for PG2 to 4,5 wt.% for PG1. This behaviour could be explained on one hand by the differences on the formulations employed, for example the NBR-M1 mix had higher amount of filler (50 wt.%) compared to HNBR which had 40 wt.%, different vulcanisation system like for NBR-M1 a sulphur vulcanisation system was employed while for HNBR-M2 a peroxide system was used. On the other hand, a higher amount of ACN in HNBR-M2 (36%) than in NBR-M1 (28%) leads to different solubility of these rubbers in polyglycol oils. HNBR-M2 had a better solubility in polyglycols and in consequence, the HNBR-M2 swelled at different temperatures in both polyglycols in higher amount than NBR-M1.

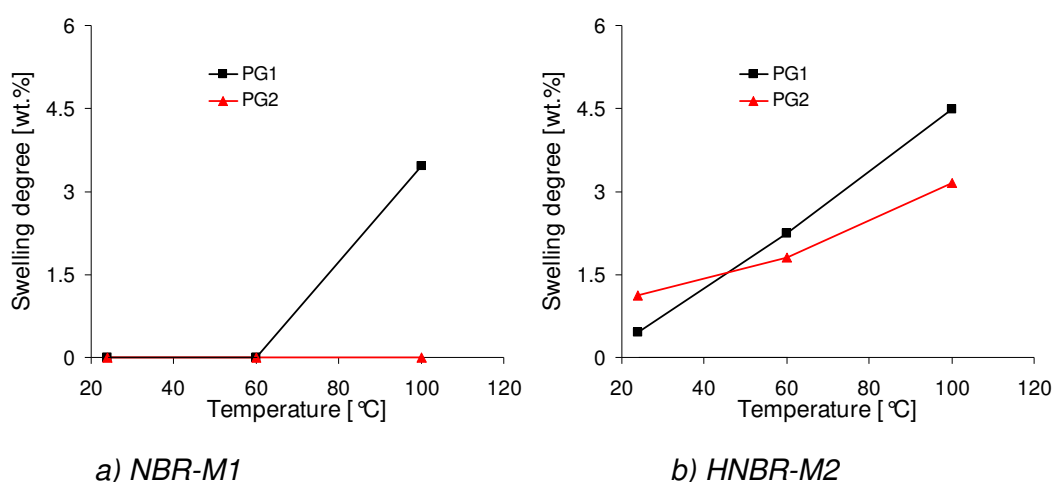
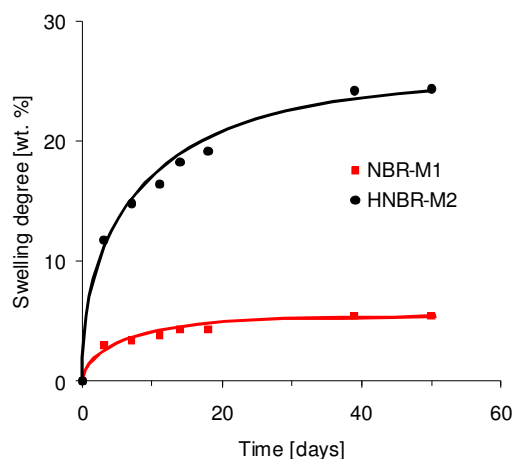


Figure 99: Temperature dependence on the swelling degree

It can be concluded that NBR-M1 and HNBR-M2 showed a relatively slight swelling in PG2. Remarkable was the high temperature dependence of PG1 swelling in HNBR-M2.

#### *Swelling in saturated complex ester synthetic oil (CE)*

Saturated complex synthetic ester lubricant was examined more closely. The following figure showed the results of the swelling of NBR-M1 and HNBR-M2 for 40 days at 140 °C. It was noticed that HNBR-M2 had after 40 days higher swelling degree (of about 25%) than NBR-M1



*Figure 100: Swelling degrees depending on the swelling time for NBR-M1 and HNBR-M2 in complex ester lubricant at 140 °C*

As the lubricant was a saturated complex ester, the small polarity differences between the HNBR rubber and the esters might be explained. That means the smaller the difference in the solubility parameter of the polymer and the oil, the larger the oil swell. For the same reason a similar swelling behaviour should be expected for the relatively polar NBR which, however, was by far not reached with a swelling degree of approx. 6%. A possible reason for this different behaviour was probably due to a higher crosslinking density as well as contribution of the filler content in NBR matrix. Theoretically the tighter the crosslinking density the lower the swell degree.

#### 4.4.2.2 Physical-mechanical measurements

The results obtained from the physical-mechanical characterisation of the materials after swelling in lubricants offered valuable information about the tensile strength and the elongation at break.

With increasing swelling degree the tensile strength decreases for both rubbers as expected whereas the highest effect for HNBR-M2 material was observed (Figure 101).

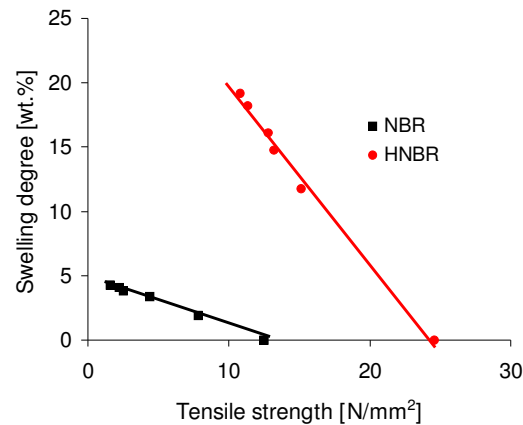


Figure 101: Swelling degrees depending on the tensile strength for NBR-M1 and HNBR-M2 matrixes (Swelling at 140 °C in CE)

Figure 102 shows the dependence of the swelling degree on the elongation at break. The HNBR-M2 material reached values between 370% and about 320%. On the other hand, lower values of the elongation at break were registered for the NBR-M2 material, which probably may be attributed to the high exposition temperature of 140 °C.

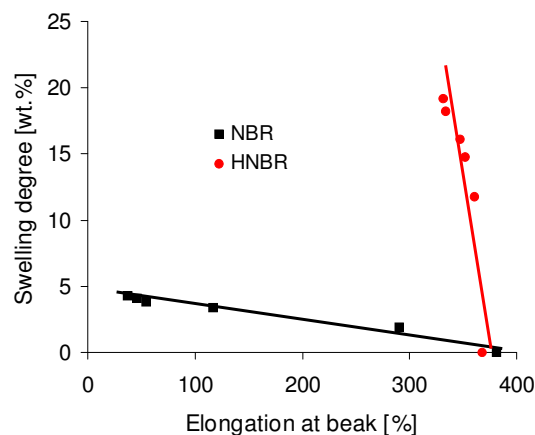


Figure 102: Swelling degree depending on the elongation at break for NBR-M1 and HNBR-M2 matrixes (Swelling at 140 °C in CE)

NBR is a chemically unsaturated rubber with reactive double bonds in the polymer chain and was cured with sulphur. The investigation of the additives influence on rubber exposition to oil showed that the modifications in the polymer structure during the vulcanization, e. g. by reactions of the side groups (acrylonitrile groups), are possible.

#### 4.4.3 Chemical investigation of material damages after dynamical stress

##### *NBR matrix*

Table 26 shows the thermo-gravimetical and swelling results of rotary shaft seals of NBR-M1 basis after dynamic experiments at different running time in CE [252]. It could be noticed that by

increasing the running time the glass transition was shifted to higher values, especially after 1500 hours a shift of about + 5°C was emphasised. A positive  $T_g$  shift first of all means a reduction of the chain mobility of the polymer which was connected with a decrease of elasticity. The  $T_g$  shifts correlates well with the results of the crosslinking density evaluated by swelling. A low swelling degree means an increase in the crosslinking density. In conclusion, the combination of NBR with the complex ester under the chosen experimental conditions was shown that the ageing process leads to a hardening of the material and an increase in the crosslinking density by an oxidative attack in the area of the double bonds of the rubber via peroxy-radicals with formation of cyclic structures or additional crosslink bridges by recombining macro radicals [253 - 256]. NBR was sulphur-vulcanized and additional modifications in the area of sulphur bridges, such as the transfer from flexible polysulphide crosslink knots to more stable and stiff monosulphide crosslink knots, have to be expected.

Table 26. DSC, swelling and extraction investigation on NBR-M1

Sample	$T_g$ after extraction [°C]	Swelling [wt.%]	Extr. Amount [wt.%]
NBR-M1 (damage) ~200h run in CE, sample 1	-29	91	7,7
NBR-M1 (not damage) ~1500h run in CE, sample 2	-24	78	7,4
NBR – reference in CE	-30	89	2,6

The TGA measurements confirmed these results. Figure 103 did not show that by extraction investigation any material modification regarding elution processes or polymer reduction occurs. It was just noted a minimal swelling degree of about 5 wt.% lubricant components if compared with the reference.

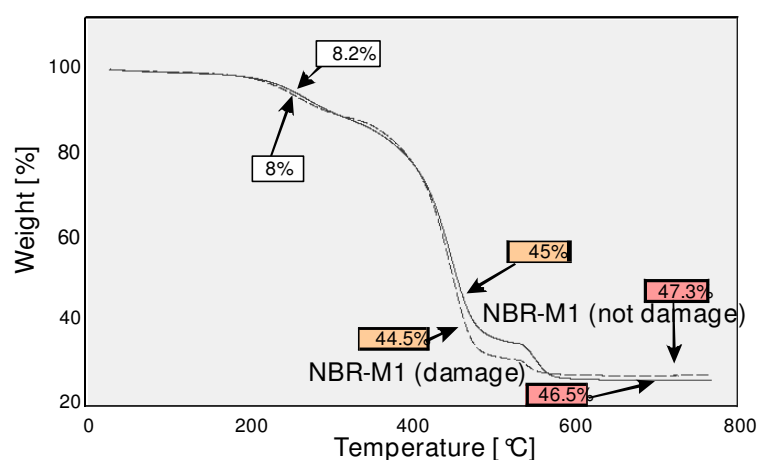


Figure 103: Measuring curves of TGA at damaged and not damaged material



The ATR-FT-IR spectroscopic analysis of the rotary shaft seals NBR-M1 (damaged) and NBR-M1 (not damaged) after extraction shows a carbonyl band (C=O) at a wave length of  $1729\text{ cm}^{-1}$  (Figure 104) which explains the oxidation process, which occurs during the exposition in oil.

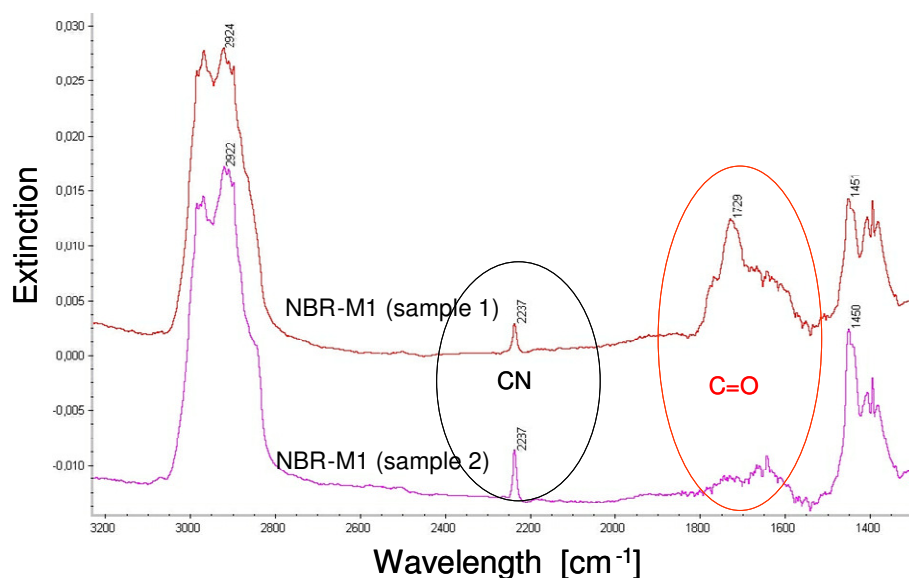
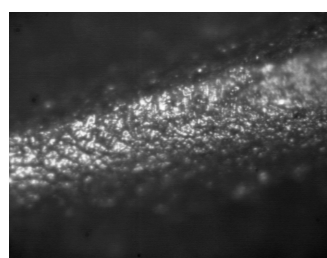
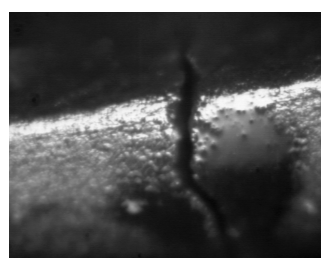


Figure 104: Comparison of the ATR-FT-IR spectrums of extracted NBR-M1 rotary shaft seals after exposition in CE

The band at  $2240\text{ cm}^{-1}$  is typical for the nitrile group of NBR rubber. Due to the analysis and preparation technique quantitative examinations at the ATR-FT-IR spectra were not successful. The following figures showed the results of the light-microscopic analyses of the sealing lips of the rotary shaft seals NBR-M1 (damaged) and NBR-M1 (not damaged):



a) NBR-M1 (sample 1)



b) NBR-M1 (sample 2)

Figure 105: Light-microscopic shots of the sealing lips surfaces of the NBR-M1 rings after dynamical stress in combination with CE

The sealing lip surface of the tight NBR (Figure 105a) shows no cracks, in contrast to the ring run 1500 h turned out to be not tight (Figure 105b). The presence of the damage correlates with the DSC and swelling experimental results. An increase of the crosslinking density leads to the embrittlement of the material, which can favour the formation of the cracks at the sealing surface.

*HNBR matrix*

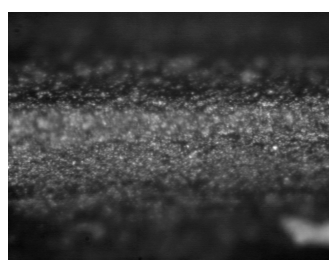
The results obtained after the investigation of the shaft seals of basis HNBR show small differences and are presented in Table 27. For all systems investigated the same glass transition and similar swelling degree after exposition in oil were obtained. The hardening of the HNBR-M2 material for both samples was not observed which suggest that an increase in the crosslinking density did not occur.

*Table 27. DSC, swelling and extraction investigation on HNBR-M1*

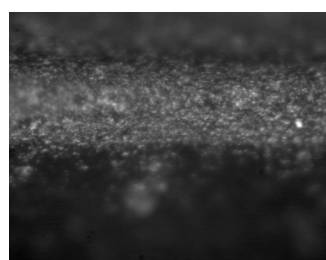
Sample	T <sub>g</sub> after extraction [°C]	Swelling [wt.%]	Extr. Amount [wt.%]
HNBR-M2 (not damage) ~200h run in CE, sample 1	-28	118	11,5
HNBR-M2 (not damage) ~200h run in CE, sample 2	-29	112	11,2
HNBR - reference in CE	-28	107	2,6

In contrast to the NBR, the HNBR contained a saturated main chain with low content of double bonds (less than 9%). The TGA results proved the high chemical stability with a constant proportion between polymer and filler considering the methods error margins. It might be noted from the extraction results that by the combination HNBR with the ester-containing lubricant a higher extractable amount which explains the higher swelling degree.

The light-microscopy pictures of the sealing lips of the above mentioned HNBR-M2 radial rotary shaft seals (Figure 106) did not show any cracks.



*a) HNBR-M2 (sample 1)*



*b) HNBR-M2 (sample 2)*

*Figure 106: Light-microscopic shots of the sealing lips surfaces of the HNBR-M2 rings after dynamical stress in combination with complex ester*

These findings correlated with the results of the above mentioned analyses: DSC, TGA and swelling measurements.

#### 4.4.4 Investigation of additives used in lubricants and their influences

There was a long standing commercial desire for elastomers with a high resistance to oil. The chemical composition of the oils used in automobile industry is very complex; various additives are used as antioxidants. Bhattacharjee and co-workers described the mechanism of oxidation of nitrile rubber where they suggested that the nitrile group is affected during the oxidation process and may be converted to  $-C-C=NH$  as shown in the mechanism described in Figure 107 [214].

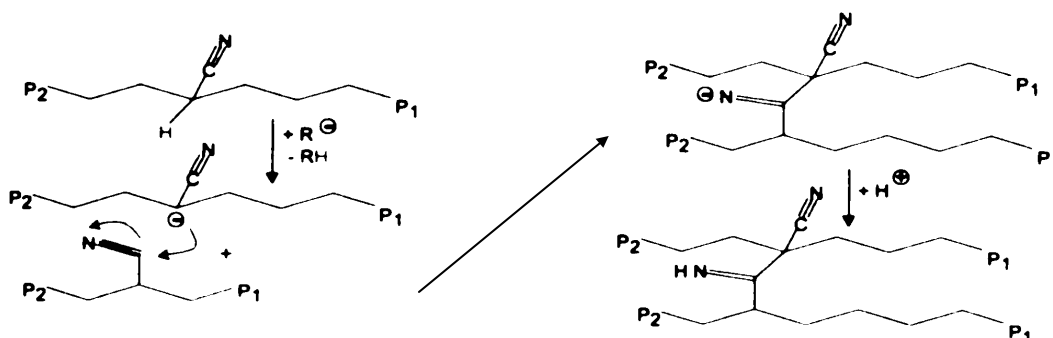


Figure 107: Vulcanisation mechanism proposed by Bhattacharjee [214]

The vulcanisation process can occur after this mechanism when the basic additive react with the nitrile group that leads to a brittle material due to additional crosslinks formed.

#### Additive influence of the lubricants PG1 and PG2 on the NBR-M1 material

The investigation of the swelling behaviour of the NBR-M1 material as well as of a model vulcanizate as reference shows tendentially comparable results to the lubricants PG1 and PG2 with and without additive. However, the swelling degree in presence of additives which are different fatty acid esters, an IRGANOX 1035, 2,6-Bis(tert-butyl)-4-methylphenol (BHT) and an octylated diphenylamine (ODPA) is lower than without additives (Figures 108 a and b).

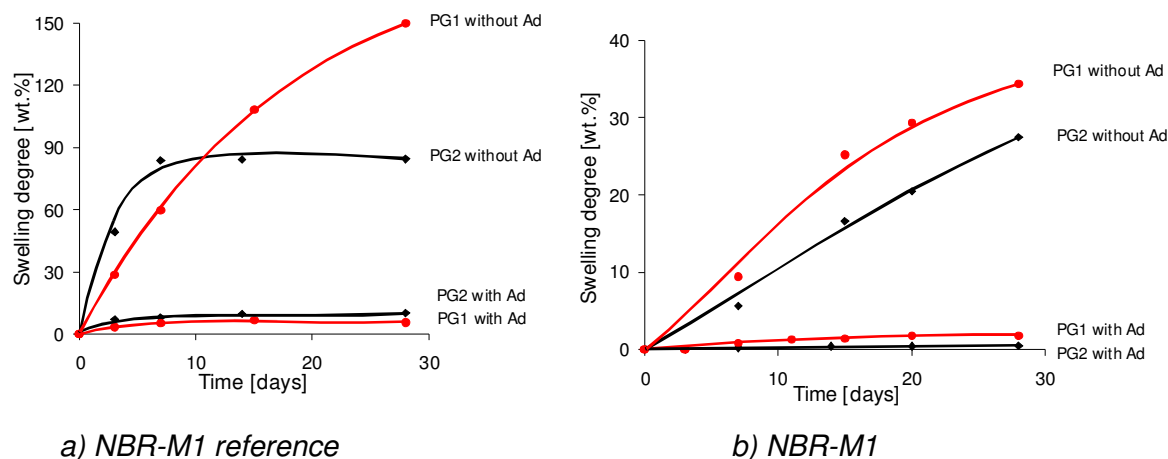


Figure 108: Swelling degrees depending on the swelling time of the reference on the basis NBR in PG1 and PG2 with and without additives at 140 °C

Generally, the increase in swelling degree of the model vulcanizate due to missing fillers and differences in the crosslinking density is much higher than in case of the original material NBR-M1, but the effect of the additives is the same. The reason for the lower swelling degree in presence of additives may on one hand result from the lower chemical tolerability of the additive/lubricant as multi-component mixture compared to the additive-free one in contrast to the NBR-M1 material. On the other hand chemical reactions set off by additive components or thermal-caused aging processes may also lead to an increase in the crosslinking density which again results in a lower swelling degree.

In conclusion, because of its crosslink type and unsaturation, NBR is less temperature resistant than the other examined elastomer. During the vulcanisation process with sulphur S-S and S-C bonds will form. The bond energy of S-S (270 KJ/mol) and S-C (272 KJ/mol) are relative low and this lead to a lower temperature stability of this material. However, the predominant attack of oxygen is on the double bonds with the generation of hydroperoxide-radicals making this rubber less stable over a temperature of about 100 °C.

#### *Additive influence of the lubricants PG1 and PG2 on the HNBR-M2 material*

A comparison of the swelling degrees of HNBR-M2 model vulcanisate and original material without additives in PG1 and PG2 shows analogously to the NBR material. Higher swelling degrees for the model vulcanizate were noticed because above all the fillers are missing.

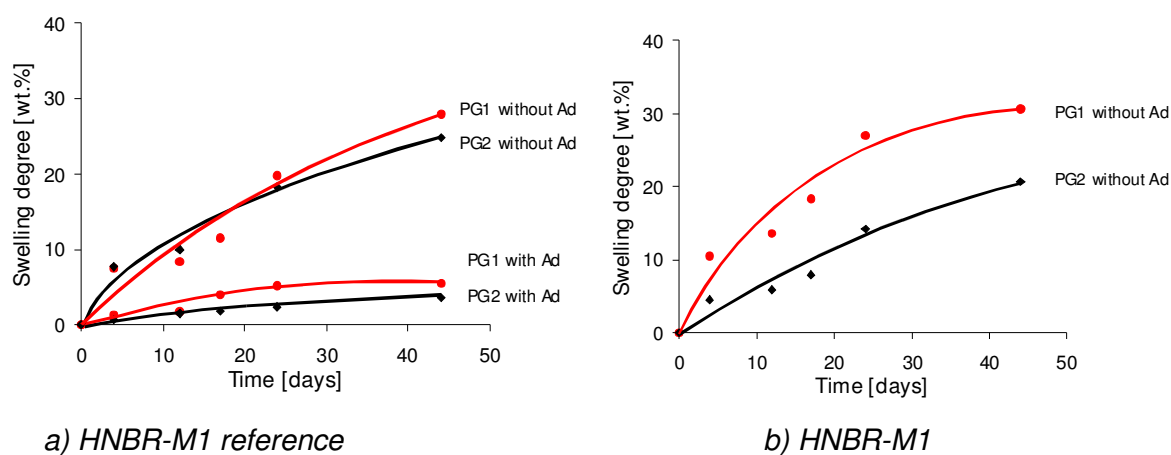


Figure 109: Swelling degrees depending on the swelling time of the reference on the basis HNBR in PG1 and PG2 with and without additives at 140 °C

The study of the exposition against oil of several shaft seals based on NBR and HNBR compounds used in industry demonstrated that the polyglycols and saturated complex ester synthetic oil swell both rubbers to different extent. The experiments showed that there is overall correlation between swelling degree and solubility and that the swelling degree and solubility of nitrile rubbers in the oils investigated increase with increasing polarity.

## 5. Conclusions

This work brings a contribution to the study of the rubber blend compatibility, diffusion and permeation mechanism of the low molecular components in rubber and rubber blends taking into consideration the influence of polymer structure, the crosslinking density, the chain length of the diffusant, the temperature and the nature of filler.

For the characterisation of the phase morphology, dynamic mechanical spectroscopy and transmission electron microscopy were employed. Both the  $T_g$  shift and the broadness of the damping peaks were considered as dynamic-mechanical criteria for the study of the compatibility. Based on the experimental results, it could be established that the presence of vinyl and epoxy groups plays an important role on the influence of phase morphology. Increasing the amount of vinyl groups of SBR phase, a higher compatibility in blend with NR is achieved because the interaction between the vinyl and isoprene units is favoured. By TEM investigation, it was seen that by increasing the vinyl amount in SBR the size of the dispersed NR domains becomes smaller and the shape of the domains appears less elongated. This leads to a better homogeneity of the blend. A linear relationship between the average domain size and the solubility parameter difference was achieved for a series of NR/SBR blends.

By chemical modification of one phase by means of introducing epoxy groups, for example in SBR phase of a rubber blend with NR it was observed that poor blend homogeneity of NR/EpSBR occurs due to the formation of large NR domains with a broad size distribution. On the other hand, if the epoxidation was done in NR phase, the solubility parameter was very much increased which has the effect of reducing the thermodynamic dissimilarity in ENR/SBR. The modification of both phases leads to a considerable improvement in the compatibility of both epoxidized rubber phases (ENR/EpSBR blend).

It was demonstrated that by mixing of two rubbers with different polarity, i.e. NR and NBR or SBR and NBR the  $\delta$ -parameter difference is high, leading to strongly phase separated blends, an incompatible system being obtained.

The volume fraction of the interphase in different rubber blends was estimated quantitatively from dynamic mechanical analysis when the impact of the blend ratio on the  $G''$  (T) in the glass transition region of unfilled blend systems was studied. The determination of the interphase of non epoxidized and epoxidized rubber blends was estimated. Among the systems studied, the best compatibility was observed for the ENR/EpSBR blend.

The efficiency of additives (processing aids) in rubber is strongly related to the constitution of the molecules. It was noticed that at low temperatures, the investigated esters are soluble in SBR matrices at higher concentrations compared to the other additives (alcohols and acids)

studied. The higher plasticizing efficiency was shown by the methyl-ester meanwhile the effects demonstrated by the alcohol and the acid respectively are similarly graded.

It was observed that the molar mass ( $C_{12}$  and  $C_{18}$ ) and the chemical functionality (alcohols, acids and ester) have a high influence on  $T_g$  shift, which influences the plasticizing efficiency considerably.

The investigation of the solubility and the behaviour of a technical product designed to improve processability in rubber demonstrated (through DSC, turbidity measurements and optical microscopy) that more than one component exist in this product and that at 100 °C at least one component of the technical product remains undissolved.

The viscoelastic analysis demonstrated that by incorporation of the model processing aids the plateau modulus  $G_N^0$  is not strongly affected but the reptation time  $\tau_{rep}$  is significantly decreased.

For the study of the transport processes of the low molecular components in rubber and rubber blends four different methods in order to determine the diffusion coefficients were employed. Two FT-IR spectroscopic methods were used such as macroscopic "time lag" method and the "concentration-distance analysis" that has the advantage of the direct determination of the diffusion process at a microscopic scale. By the time dependent swelling measurements a correction after Crank that takes into consideration the geometrical change of the sample during swelling was considered. The time lag method considering the permeation measurements (two chamber method) was used also for the determination of the diffusion coefficient.

The diffusion process of phthalates in NBR, HNBR and SBR was investigated by employing the first two methods. The results showed that the chemical constitutions of the polymer (ACN and vinyl content) as well as the state of crosslinking of the matrix exert a determinant contribution on the value of the diffusion coefficient. It was demonstrated that by increasing the ACN and vinyl content in NBR and SBR respectively the diffusion coefficient was significant lowered. The influence of these parameters was described by a simple empirical model.

The investigation of the influence of the molecular weight of the diffusant on the diffusion coefficients showed that the diffusion coefficient decreases from  $2,2 \cdot 10^{-8}$  cm<sup>2</sup>/sec for DMP to  $2,1 \cdot 10^{-9}$  cm<sup>2</sup>/sec for DDP.

The influence of unsaturation of the polymer and temperature on diffusion process was examined in NBR and HNBR. The results indicated that the diffusion of DOP is faster in HNBR than in NBR. The temperature, which is expressed in terms of the activation energy, demonstrated higher activation energy for the diffusion of DOP in NBR (40 KJ/mol) than in HNBR (33 KJ/mol).

It was shown that the diffusion coefficients obtained by using the "time-lag" method and the "concentration-distance" analysis are not identical. The differences result from the quality of the sample preparation and from the concentration dependency of diffusion coefficient.

For determination of the diffusion coefficients of t-BuPh in NBR, HNBR and SNBR the time lag method using the ATR-FT-IR spectroscopy, swelling kinetics and permeation measurements were carried out.

The study of the transport processes of t-BuPh in NBR, SBR specimens covering the same  $T_g$  range were compared applying the ATR-IR spectroscopic time-lag method. The comparison showed that the influence exerted by the free volume of the rubber matrix as well as the solubility of the low molecular compound in the rubber matrix has a crucial influence on the diffusion coefficient. Both influences are determined by the constitution and the chemical structure of the polymers.

The influence of the filler on transport processes was described on the basis of a comparison of swelling measurements:

- 1) the diffusion coefficient and the permeation rate decrease with filler content;
- 2) differences in the rubber/filler interaction are reflected on diffusion coefficients values for a constant filler volume fraction;
- 3) the influence of the interfacial layer in filled rubber on diffusion process was evaluated considering a proposed model and it was demonstrated that a higher volume fraction of the interfacial layer leads to a higher diffusion coefficient through the interfacial layer.

The influence of the diffusant structure on diffusion process was studied by means of swelling investigation. At the same molecular weight of the diffusant but different isomers a significant reduction of the diffusion coefficient was noticed, i.e. the bulky tertiary butyl benzene showed a decrease of  $D$  with 30% if compared with n-butylbenzene.

An atmospheric-pressure plasma apparatus was used for the surface treatment of a rubber plate using decafluoropentane as precursor. After the treatment the diffusion coefficient as well as the permeation rate was reduced by more than 50%.

In the case of rubber blends, the transport process was clearly shown to be dependent on the phase morphology. In each case the continuous phase determines the value level of the diffusion coefficient.

A permeation apparatus (two-chamber method) was set up and involved the tracing over the time the transport of low-molecular compounds through a rubber plate (with a thickness of 0.3-3mm) that separates a chamber where the solvent is placed from a chamber where a carrier gas with a stationary stream passes. The low molecular component was quantified by means of gas chromatography. The gas chromatographic system allows for a separation of the solvent mixes into single components, so that selective permeation processes can be traced.

The function of the apparatus was tested and validated on unfilled NBR vulcanizates with t-BuPh as the test substance. Comparison of the diffusion coefficients results, which were carried out on NBR specimens with the help of three methods (time lag method, swelling and permeation), pointed out a good agreement of the results.

The tests carried out on NBR with t-BuPh using the permeation apparatus showed that:

- 1) increasing the ACN content leads to a significant increase in time lag and to a lower diffusion coefficient as well as a lower permeation rate;
- 2) the effect of crosslinking density shows the same influence as the ACN content but is much less significant.

In the last part of the work, the study of the exposition against oil of several shaft seals based on NBR and HNBR compounds used in industry was shown that the polyglycols and saturated complex ester synthetic oil swell both rubbers to different extent. The experiments showed that there is overall correlation between swelling degree and solubility and that the swelling degree and solubility of nitrile rubbers in the oils investigated increase with increasing polarity.



## 6. Experimental part

### 6.1 Materials used

#### 6.1.1 Rubbers

Commercially available rubber types (Lanxess) not subjected to further purification were used for this study. A characterization of them is provided in Table 2 (Chapter 4). The epoxidation of SBR was carried out in toluene with hydrogen peroxide in accordance with a previously developed procedure [259]. For this study, Ep-SBR with an epoxidation degree of 30 mol% of the butadiene units was used.

#### 6.1.2 Fillers

The fillers used in this work were silica Ultrasil 7000GR with CTAB surface of 160 m<sup>2</sup>/g (Degussa AG), carbon black N326 with CTAB surface of 83 m<sup>2</sup>/g and N375 with CTAB surface of 96 m<sup>2</sup>/g (Columbian Carbon).

### 6.2. Methods and apparatus employed

#### 6.2.1 Mixing process

The mixes were prepared corresponding to the recipe presented in Table 27, in two steps in an internal mixer when the polymer, zinc oxide, stearic acid and filler were added and mixed for a 15-min period at a temperature of 60°C and a rotor speed of 50 rpm. The vulcanising system was introduced to the mix on a laboratory mill (Troester type WNU 1 with roll diameter of 100 mm, roll length of 250 mm, friction factor of 16 und 20 U/min) and mixed for 4 minutes at 60°C. The mixes were stored over night before further processing.

*Table 27. Mixing recipe*

Mixing steps	Components
First mixing step: Thermo Haake PolyLab System	Polymer
	Zinc oxide
	Stearic acid
	Filler
Second mixing step: Laboratory mill	Vulcanising system

#### 6.2.2 Vulcanisation process

In order to work at the optimal vulcanisation time, rheometer curves were recorded for each mixture using a Rheometer (Monsanto Type MDR 2000 E). The measurements were done at a

temperature of 160 °C, a frequency of 1,67 Hz and amplitude of +/- 0,5 % in accordance with DIN 53 529. To minimize the outside effects, the sample was placed between two foil layers of polyamide und polyethylene terephthalate. The vulcanisation time represents the time  $t_{95}$  (maximum of the torque).

The vulcanisation process of the rubbers was done by 200 MPa in a press (J. Wickert & Söhne Type WLP 63/3,5/3). The enclosed air was removed through different ventilation.

For IR spectroscopy measurements, vulcanised thin plates using a heatable mould (Specac L. O. T. Oriol) under 40KN were prepared.

### 6.2.3 Differential scanning calorimetry (DSC)

The glass transition temperatures and the low temperature solubility limit of the mixtures were determined by DSC measurements (TA-Instruments DSC 2920CE Modulated DSC equipment) at a heating rate of 10 °C/min.  $T_g$  was taken as the maximum of the first derivative of the heat flux as a function of the temperature.

### 6.2.4 Thermogravimetry (TGA)

The thermogravimetric measurements were done with equipment High Resolution TGA 2950 (TA Instruments Corp). During the measurement, a heating rate of 10 K/min was used, starting the measurement at room temperature. In the chamber where the sample was analysed constant nitrogen flow of 60 ml/min was used. After a period of time it was switched over to 550 °C using synthetic air. That means, the burning destruction of the matrix was made under nitrogen, meanwhile the oxidative destruction took place under oxygen.

### 6.2.5 Dynamic mechanical analysis (DMA)

The DMA was employed for the analysis of the phase morphology, the temperature dependency of the loss modulus,  $G''$ , of the blends was recorded over the entire concentration range. Test specimens were deformed in torsion on a dynamic analyzer (ARES 3A5 Rheometrics Scientific) at 1 Hz and 1% strain amplitude and a heating rate of 1 °C/min.

For the investigation of the additives influence on viscoelastic properties, the dependency of the storage modulus  $G'$  and the loss modulus  $G''$  with the deformation frequency was measured at a constant strain amplitude of 0,5 % in the temperature range from 10 to 140 °C using a plate-plate configuration ( $D/H = 30 \text{ mm}/2 \text{ mm}$ ) with a Rheometrics Dynamic Analyser RDA II. By employing the temperature frequency superposition principle [101] a master curve was established.

### 6.2.6 Transmission Electron microscopy (TEM)

Ultra thin cuts (70nm) obtained on an Ultra Cut FC4 (Reichert-Jung) microtome were investigated by using electron spectroscopy imaging (ESI) on a transmission electron microscope (Zeiss EM 902). Contrast was obtained without chemically staining procedures, but merely by simply out-blending the inelastically scattered electrons using energy filters. With this procedure, the phase with the higher electron and carbon density appears as the dark one. The domain size distribution was measured by a computer-aided imaging system, taking into account the equivalent circles of the detected domains.

### 6.2.7 Equilibrium swelling

Equilibrium swelling experiments of crosslinked rubber in selected solvents or additives were performed at different temperatures. After the sample reached the equilibrium the solvent uptake was measured gravimetrically.

### 6.2.8 ATR-FT-IR-spectroscopy

The experimental set up is depicted in Figure 106. The prepared thin films were placed on the horizontal surface of the Ge-crystal at room temperature of 24°C. A reservoir containing the pure diffusant was placed in an open tube on the top of the rubber film.

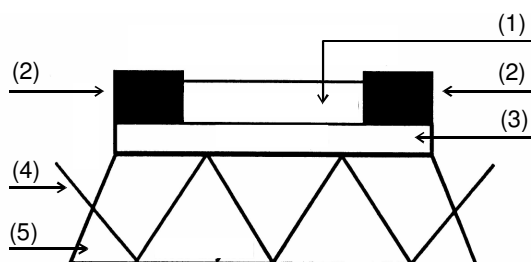


Figure 110: Principle of FT-IR ATR diffusion measurements with (1) reservoir (pure diffusant), (2) sealing rings, (3) rubber film, (4) IR-beam, (5) ATR-crystal

The diffusion process starts when contact between rubber and diffusant is engaged. The time dependent change of concentration of the diffusant at the surface of the Ge-crystal was determined by using the absorbance signal intensity of the diffusant. The measurements were carried out at a temperature of 24°C by means of FT-IR Nicolet 60 Nexus equipped with a horizontal 45° germanium crystal ATR device. For the reproducibility of these measurements three samples were investigated.

### 6.2.9 Concentration-distance analysis

The system used for this study is made up of two separated layers. One layer contained the rubber and the diffusing substance and was considered the reservoir. The other layer was

vulcanized rubber of the same chemical constitution. An inorganic dye was incorporated for increasing the optical contrast between the two layers. By this, the borderline between the two layers could be observed more precisely. The two layers were pressed together at a temperature of 24°C and at a pressure of 100 bar, for different periods of time. Microtome cuts (10 µm) were made perpendicular to the boundary plane of the "sandwich" samples on an Ultra Cut (FC4 Reichert-Jung) microtome. The analysis was carried out by means of an IR-microscope (type: Nicolet Continuum) in the transmission mode coupled to Fourier-Transform-Infrared spectrometer (type: FT-IR Nicolet 60 Nexus).

During the whole process, the condition of the conservation of mass had to be satisfied. This required from the experimental design to measure the concentration along the x-axis from the initial position of the boundary between the two components at the relative precision about  $\pm 0,8 \%$ . The changes in concentration (concentration profiles) were recorded at several times as a function of the distance using the borderline as origin. The concentration-distance curve was plotted for a given time  $t$  of observation and the diffusion coefficient  $D$  was evaluated from the concentration profiles using Equ. (46), Chap. 3.3.1.3.

#### 6.2.10 Turbidity measurements

The transmission of a laser light beam through a thin film cast from a methylene-chloride solution was recorded as a function of increasing or decreasing temperature. The sample was placed on a horizontal sample carrier inside of a metal block thermostat heated with a precision of  $\pm 1^\circ\text{C}$ . Changes in light transmission ( $Tr = I/I_0$ ) caused by phase transitions were observed from changes of the intensity of the transmitted light. Reduced light transmission indicates a phase separated system.

#### 6.2.11 Optical microscopy

To investigate the morphology within thin films an optical microscope (Zeiss-Universal) at a magnification of 125 was used. The samples were placed into a heating chamber (Linkam, THMS 600) and were heated with a rate of  $10^\circ\text{C}/\text{min}$  up to  $150^\circ\text{C}$ . Cooling of the sample was performed at a rate of  $1^\circ\text{C}/\text{min}$ .

#### 6.2.12 Plasma treatment

In a plasma apparatus, PFW20, Plasmatrete, NBR2 plate was treated using as precursor Dekafluoropentan in thin layer under atmosphere pressure. The precursor which is needed for the coating was introduced at the lower part of the plasma zone (Down-Stream Process). The treated sample and the untreated sample were analysed by means of Raster electron microscope (MicroProf) in contact mode in order to study the surface roughness.

#### 6.2.13 Determination of the crosslinking density

The crosslinking density was determined by means of tension-strain measurements using Mooney-Rivlin theory (Equ. (60), Chap. 3.3.1.4.5). The measurements were done in accordance with DIN 53 504 by a deformation speed of 200 mm/min at 23 °C in a universal test apparatus (Zwick 1445), equipped with an optical measuring way. The average of five measurements for each sample was taken into consideration and the results for HNBR1, NBR2 und SBR2 with 2 mm thickness of the test sample are presented in Table 34.

#### 6.2.14 Dispersion measurements

The amount of the filler agglomerates that are not dispersed (macro-dispersion) can be determined by means of Hellfeld-Vertical reflections measurements on vulcanised sliced sample. Dark region dispersed on bright ground define the form and size of the filler agglomerates. The filler dispersion and the surface of the agglomerate ( $\geq 6 \mu\text{m}$ ) are calculated using a picture evaluation program.

#### 6.2.15 Scanning electron microscopy

The sample was covered with a thin sheet of gold in order to minimize the electron beam reflection. The SEM investigations were done on Philips-FEI-apparatus, type XL 30, with a wolfram-hairpin cathode and using a distance of 10 mm.

## 7. Annexes

Table 28. Solvents used

Solvents	Producer, technical data
t-Butyl benzene	Fluka Chemie AG, $\geq 97\%$ (purum), d 0,866
n-Butyl benzene	Fluka Chemie AG, $\geq 98\%$ (purum), d 0,860
n-Dodecane	Aldrich, $\geq 99\%$ (purum), d 0,749
Decanoic acid	Fluka Chemie AG, $\geq 98\%$ (purum), d 0,893
Lauric acid	Fluka Chemie AG, $\geq 98\%$ (purum), d 0,883
Palmitic acid	Fluka Chemie AG, $\geq 90\%$ (purum), d 0,852
Stearic acid	Fluka Chemie AG, $\geq 99\%$ (purum), d 0,845
Toluene	Fluka Chemie AG, $\geq 99\%$ (purum), d 0,865
Cyclohexane	J. T. Baker, $\geq 99\%$ (purum), d 0,779
Methyl-ethyl-cetone	Fluka Chemie AG, $\geq 98\%$ (purum), d 0,805

Table 29. Chemicals used in vulcanisation process

Chemicals	Producer, technical data
Sulphur	Solvay Barium Strontium GmbH, (soluble), $\geq 99,95\%$
Stearic acid	Henkel KG, Edenor ST 4 A, techn., mixture of palmitin- and stearic acid with low amount of oil (stearic iodine number 4), activator
Zinc oxide	Grillo Zinkoxid GmbH, 99,6 %, activator
Vulkacit D (DPG)	Bayer AG, extrusion granulated
Vulkacit CZ (CBS)	Bayer AG, extrusion granulated

Table 30. Silica characterisation

Name	Ultrasil 7000 GR
Primary particle diameter [nm]	5-28
CTAB-surface [ $\text{m}^2/\text{g}$ ]	160
BET-surface [ $\text{m}^2/\text{g}$ ]	175
DBP-Adsorption [ml/100g]	240
Silanol group density [OH groups / nm]	3,3
Sears number [ml NaOH/5g]	15
pH-value	6,8
Dry loss [wt.%]	6,5
SiO <sub>2</sub> amount [wt.%]	98

Table 31. Test recipes (mixes used in chapter 4.1)

Materials	System [phr]
Polymer*	100,0
ZnO	4,0
Stearic acid	3,0
CBS	2,5
Sulphur	1,6

\*NR, SBR, ENR, EpSBR, NBR

Table 32. Test recipes (mixtures used in chapter 4.3.1)

Materials	System [phr]
Polymer*	100,0
Stearic acid	3,0
ZnO	4,0
CBS	1,5
TMTD	2,0
Sulphur	2,0

\*NBR1, NBR2, NBR4

Table 33. Test recipes (mixtures used in chapter 4.3.1.2)

Materials	Layer 1 [phr]	Layer 2 [phr]
Polymer*	100,0	100,0
Stearic acid	3,0	3,0
ZnO	4,0	4,0
CBS	1,5	5,0
TMTD	2,0	2,0
Sulphur	2,0	2,0
DOP	-	10,0

\*NBR4, HNBR1

Table 34. Crosslinking density for different rubbers

Sample	Vulcanization system	Amount [phr]	$v_e$ [ $10^{-5} \cdot \text{mol}/\text{cm}^3$ ]
NBR 3-1	S/CBS	1,0/1,0	$4,5 \pm 0,13$
NBR 3-2	S/CBS	1,5/1,5	$8,6 \pm 0,3$
NBR 3-3	S/CBS	2,5/2,5	$15,9 \pm 0,1$
HNBR 1-1	DCP	0,5	$0,041 \pm 0,003$
HNBR 1-2	DCP	1,0	$0,77 \pm 0,07$
HNBR 1-3	DCP	2,0	$9,4 \pm 0,51$
SBR 2-1	S/CBS	1,0/1,0	$4,2 \pm 0,6$
SBR 2-2	S/CBS	1,5/1,5	$7,0 \pm 0,3$
SBR 2-3	S/CBS	2,5/2,5	$9,9 \pm 0,41$

## 8. Literature

- [1] L. A. Utracki, "*Polymer Alloys and Blends*", Hanser, New York, (1989).
- [2] D. R. Paul, S. Newman, "*Polymer Blends*", Academic Press, New York, (1978).
- [3] F. M. Sweeney, "*Polymer Blends and Alloys: Guide to Commercial Products*", Technomic, Lancaster, PA, (1988).
- [4] Olabisi, L. M. Robeson and M. T. Shaw, "*Polymer-Polymer Miscibility*", Academy Press, New York, (1979).
- [5] K. Solc, "*Polymer Compatibility and Incompatibility Principles and Practice*", Harwood Academic, New York, (1982).
- [6] J. Stoelting, F. E. Karasz, W. MacKnight, *Polym. Eng. Sci.*, **10** (1970) 133.
- [7] G. A. Zabrzewski, *Polymer*, **14** (1973) 347.
- [8] B. Ohm, R. Annicelli, T. Jablonowski, R. Mazzero, *Rubber World*, **8** (2002) 33.
- [9] A. O. Patil, T. S. Coolbaugh, *Rubber Chem. and Technol.*, **78** (2005) 516.
- [10] L. Bohn, *Rubber Chem. Technol.*, **41** (1968) 495.
- [11] C. M. Roland, *Rubber Chem. Technol*, **62** (1989) 456.
- [12] M. Klüppel, R. H. Schuster, J. Schaper, *Rubber Chem. Technol.*, **72** (1999) 91.
- [13] W. Hofmann, H. Gupta, *Handbuch der Kautschuktechnologie*, (2001), Ch. 9.
- [14] B. G. Crowther, *128th ACS-Rubber Division Meeting* Cleveland (OH), Oct. 1985.
- [15] L. Steger, *Kautschuk Gummi Kunststoffe*, **43** (1991) 197.
- [16] G. Thielen, *Kautschuk Gummi Kunststoffe*, **44** (1991) 232.
- [17] B. L. Lee, *Polym. Eng. Sci.* **21** (1981) 294.
- [18] S. A. Groves and A. J. Tinker, *J. of Natural Rubber Res.*, **11** (1996) 125.
- [19] E. Földes, J. Lohmeijer, *Journal of Applied Polymer Science*, **65** (1997) 761.
- [20] H. Schulz and L. Steger, *Kautschuk Gummi Kunststoffe*, **6** (1998) 402.
- [21] R. H. Schuster, H. Geisler, G. Scholz, *Kautschuk Gummi Kunststoffe*, **55** (2002) 653.
- [22] W. Keberle, W. Gobel, *U. S. Patent* 3,637,553 (1972) (assigned to Farbenfabriken Bayer).
- [23] R. P. Kane, *J. Elast. Plast.*, **9** (1977) 416.
- [24] R. H. Schuster, *Angew. Makromol. Chemie*, **202/203** (1992) 159.
- [25] P. J. Corish, *Rubber Chem. Technol.*, **40** (1965) 156.
- [26] P. J. Flory, *J. Chem. Phys.*, **9** (1941) 660.
- [27] M. L. Huggins, *Ann. N. Y. Acad. Sci.*, **43**, 1 (1942).
- [28] M. L. Huggins, *J. Chem. Phys.*, **9** (1941) 440.
- [29] P. J. Flory, "*Principles of Polymer Chemistry*", Cornell Univ. Press., Ithaca, New York (1953).
- [30] R. L. Scott, *J. Chem. Phys.*, **17** (1949) 279.



- [31] H. Tompa, *Tran. Faraday Soc.*, **45** (1949) 1142.
- [32] E. Helfand and Y. Tagami; *J. Chem. Phys.*, **56** (1971) 2591.
- [33] S. Wu, *Polymer*, **28** (1987) 1144.
- [34] R. H. Schuster, J. Schaper and M. L. Hallensleben, *151<sup>st</sup> Meeting of ACS-Rubber Division*, Anaheim (CA), May 1997, paper XII.
- [35] R. Koningsveld, L. A. Kleintjens, *Pure Appl. Chem.* **39** (1974) 197.
- [36] W. Berger, H.W. Kammer and C. Kummerlöwe, *Makromol. Chem. Suppl.*, **8** (1984) 101.
- [37] N. Tokita, *Rubber Chem. Technol.*, **50** (1977) 708.
- [38] H. P. Grace, *Chem. Eng. Comm.*, **14** (1982) 225.
- [39] J. H. Hildebrand and R. L. Scott, "*The Solubility of Non-Electrolytes*", New York (1964).
- [40] M. B. Huglin, D. J. Pass, *J. Appl. Polym. Sci.*, **12** (1968) 473.
- [41] L. H. Sperling, "*Introduction to physical polymer science*", 2<sup>nd</sup> edition, J. Willey & Sons, (1992).
- [42] O. Smidsrod, J. E. Guillet, *Macromolecules*, **2** (1968) 272.
- [43] P. A. Small, *J. Appl. Chem.*, **3** (1953) 71.
- [44] R. F. Fedors, *Polym. Eng. Sci.*, **14** (1974) 147, 472.
- [45] D. M. Koenhen, C. A. Smolders, *J. Appl. Polym. Sci.*, **19** (1975) 1163.
- [46] D. W. Krevelen, P. J. Hoftyzer, *J. Appl. Polym. Sci.*, **11** (1967) 2189.
- [47] K. L. Hoy, *J. Paint. Technol.*, **42** (1979) 76.
- [48] H. Mark, A. V. Tobolsky, "*Physical Chemistry of High Polymeric System*", Willey (Interscience), New York, (1950).
- [49] G. DiPaola-Baranayi, J. E. Guillet, J. Klein H. –E. Jeberien, *J. Chromatogr.*, **166** (1978) 349.
- [50] G. DiPaola-Baranayi, *Macromolecules*, **15** (1982) 622.
- [51] J. E. G. Lipson, J. E. Guillet, *J. Coating Technol.*, **54** (1982) 90.
- [52] M. Magat, *J. Chem. Phys.*, **46** (1949) 344.
- [53] W. Merk, R. N. Lichtenthaler, J. M. Prausnitz, *J. Phys. Chem.*, **84** (1980)1694.
- [54] H-M. Issel; "*Thermodynamische und rheologische Steuerung der Materialeigenschaften von Elastomersytemen durch trans-Poly(octenylen)*", PhD. Thesis, Universität Hannover (1993).
- [55] R. H. Schuster, H. M. Issel, V. Peterseim, *Rubber Chem. Technol.*, **69** (1996) 769.
- [56] M. Matsuo, C. Nozaki, Y. Jyo, *Polym. Eng. Sci.*, **9** (1969) 197.
- [57] J. E. Lewis , H. N. Mercer, M. L. Deviney, L. Hughes, J. E. Jewell, *Rubber Chem. Techno.*, **44** (1971) 855.
- [58] J. Callan, W. Hess, C. Scott, *Rubber Chem. Technol.*, **44** (1971) 814.
- [59] J. D. Moore, *Polymer*, **12** (1971) 478.

- [60] H. Keskkula, P. A. Traylor, *J. Appl. Polym. Sci.*, **11** (1967) 2361.
- [61] M. Blume, C. Rosin, R. H. Schuster, *162nd ACS-Rubber Division Meeting Pittsburgh, (Pennsylvania), Oct. 8<sup>th</sup>-11<sup>th</sup>, (2002).*
- [62] V. R. Landi, *Rubber Chem. Technol.*, **45** (1972) 22.
- [63] R. W. Seymour, S. L. Cooper, *J. Polym. Sci. B*, **9** (1971) 689.
- [64] R. F. Boyer, *Rubber Chem. Technol.*, **36** (1963) 1303.
- [65] S. Krause, *J. Polym. Sci. A*, **3** (1965) 1631.
- [66] M. T. Shaw, *J. Appl. Polym. Sci.*, **18** (1974) 449.
- [67] D. R. Paul, J. O. Altamirano, *Adv. Chem. Ser.*, **142** (1975) 371.
- [68] U. Eisele, *“Introduction to Polymer Physics”*, Springer, Berlin, (1990).
- [69] K. Fujimoto, N. Yoshimiya, *Rubber Chem. Technol.*, **41** (1968) 669.
- [70] D. Feldman, M. Rusu, *Eur. Polym.*, **10** (1974) 41.
- [71] D. W. McCall, *Acc. Chem. Res.* **4** (1971) 223.
- [72] K. Fujimoto, *J. Soc. Rubber Ind. Jpn*, **43** (1970) 54.
- [73] D. G. Legrand, *Trans. Soc. Rheol.*, **15** (1971) 541.
- [74] C. Elmqvist, S. E. Svanson, *Eur. Polym. J.*, **11** (1975) 789.
- [75] C. S. P. Sung, N. S. Schneider, *Macromolecules*, **8** (1975) 68.
- [76] J. K. Clark, R. A. Scott, *Rubber Chem. Technol.*, **43** (1970) 1332.
- [77] S. T. Wellinghoft, J. L. Koenig, E. Baer, Jr., *J. Polym. Sci., Polym. Phys. Ed.*, **15** (1977) 1913.
- [78] J. S. Higgins, *“Polymer Blends and Mixtures”*, Martinus Nijhoff, Dordrecht, (1985).
- [79] C. T. Murray, J. W. Gilmer, R. S. Stein, *Macromolecules*, **18** (1985) 996.
- [80] D. R. Buchanan, *J. Polym. Sci. A*, **9** (1971) 645.
- [81] V. Peterseim; *“Quantitative Betrachtung der Verträglichkeit von Kautschuken und Untersuchungen zur Rußdistribution und -dispersion”*, PhD. Thesis, Universität Hannover (1995).
- [82] R. H. Schuster, J. Meier and M. Klüppel; *Kautschuk Gummi Kunststoffe*; **11** (2000) 663.
- [83] R. S. Raghava, R. W. Smith, *J. Polym. Sci. B*, **27** (1989) 2525.
- [84] T. Reichmann, F. Sommer, T. M. Duc, *Kautschuk Gummi Kunststoffe*, **5** (2004) 252.
- [85] R. H. Schuster, M. Müller, M. Klüppel and J. Ziegler, *159<sup>th</sup> Meeting of ACS-Rubber Division, Providence, April (2001).*
- [86] G. R. Hamed, *Rubber Chem. Technol.*, **54** (1981) 576.
- [87] G.R. Dimeler, *ACS-Rubber Division Ed. Symp.*, No. **9** (1982).
- [88] J. Nieberle, G. Paulus, H. Queins, H. Schoepl, *Kautschuk Gummi Kunststoffe*, **39** (1986) 108.

- [89] A. J. Tinker, A. B. Ahmad and D. W. Aubrey, *Journal of Natural Rubber Research*, **9** (1) (1994) 1.
- [90] A. M. Grazia, A. Sanguineti, *Journal of Polymer Science, Part B: Polymer Physics*, **42** (2004) 1987.
- [91] T. G. Fox and P. J. Flory, *J. Phys. Chem.*, **55** (1951) 221.
- [92] J. Le Bras, *Rubber Chem. Technol.*, **35** (1962) 1308.
- [93] J. B. Class, S. G. Chu, *J. Appl. Polym. Sci.*, **30** (1985) 805, 815, 825.
- [94] P. J. Flory, *J. Chem. Phys.* **18** (1950) 108.
- [95] Y. S. Lipatov, "Advanced in Polymer Science", Springer, Berlin, **26** (1978) 63.
- [96] G. Zachmann, "Kunststoff Handbuch", vol.1, Carl Hanser, München, (1975).
- [97] R. Simha, R. F. Boyer, *J. Chem. Phys.*, **37** (1962) 1003.
- [98] R. H. Schuster, H. M. Issel, H. Geisler, *160th ACS-Rubber Division Meeting Cleveland, (OH), Oct. 16<sup>th</sup>-18<sup>th</sup>*, (2001).
- [99] H. Geisler, "Einfluß der Struktur niedermolekularer Komponenten auf physikalische Eigenschaften von EPDM / Lösungsmittel – Systemen", PhD. Thesis, Universität Hannover, (1988).
- [100] J. J. Aklonis e W. J. MacKnight; "Introduction to polymer viscoelasticity", John Wiley & Sons 2nd Ed. (1983).
- [101] Ferry, J. D., "Viscoelastic Properties of Polymers", 3<sup>rd</sup> ed. New York: Wiley (1980).
- [102] F. Bueche, "Physical properties of polymers", John Wiley & Sons, New York (1962).
- [103] P. Hiemenz, *Polymer Chemistry*, Marcel Dekker, Inc., (1984).
- [104] P. G. DeGennes, *J. Chem. Phys.*, **55** (1971) 572.
- [105] M. Doi and S. F. Edwards, *J. Chem. Soc. Faraday Trans II*, **74** (1978) 1789 .
- [106] I. M. Ward, "Mechanical Properties of Solid Polymers", New York, (1971).
- [107] S. H. Wasserman and W. W. Graesley, *J. Rheol.* **36** (1992) 543.
- [108] B. B. Boonstra and A. I. Medalia, *Rubber Age*, N.Y. **92** (1963) 892.
- [109] J. Deiters, J. Weick, R. H. Schuster, M. L. Hallensleben, *Platic Rubber and Composites*, (1993).
- [110] A. J. Tinker, A. B. Ahmad and D. W. Aubrey, *Journal of Natural Rubber Research* **10** (1) (1994) 1.
- [111] J. Crank, "The Mathematics of Diffusion", Clarendon Press, Oxford, (1956).
- [112] L.G.F. Stuck, *Journal of Polymer Science*, **28** (1990) 127.
- [113] R. E. Kesting and A.K. Fritzsche, "Polymeric gas separation membranes", John Wiley, New York, (1993).
- [114] W. Beckmann, *Kautschuk Gummi Kunststoffe*, **4** (1991) 323.

- [115] J. M. Veranaud: "*Liquid Transport Processes in polymeric Materials*" Prentice Hall, New York, (1991).
- [116] G. Adam, J. Jung, C. Babilas, *Kautschuk Gummi Kunststoffe* **43** (1990) 1067.
- [117] K. Beck, R. Kreiselmaier, V. Peterseim, E. Osen, *Kautschuk Gummi Kunststoffe*, **56** (2003) 657.
- [118] California Environmental Protection Agency Press Release 98-69, 5<sup>th</sup> November (1998).
- [119] M. Geier, W. Thiel, *ATZ Automobiltechnische Zeitschrift*, **98** (1996) 12.
- [120] M. Nulma, A. Olejnik, M. Samuel, E. Fead, G. Rossi, *Society of Automotive Engineers*, Technical series, no. 981360, (1998).
- [121] K. Azaar, R. Grang, I. D. Rosca, J. M. Vernaud, *Gummi Fasern Kunststoffe*, **54** (2001), 236.
- [122] J. Schaube, R. H. Schuster: Vortrag "*Determination of Gas Permeability with New Testing Methods*", International Rubber Conference Nürnberg 7/2003.
- [123] J. Schaube, „*Modeluntersuchungen zur Phasenanbindung in Polymerblends*“, Ph.D. Thesis, Universität Hannover (1993).
- [124] J. L. Graham, R. C. Striebich, K. J. Myers, D. K. Minus, W. E. Harrison, *Energy & Fuels*, **20** (2006) 759.
- [125] J. Bacha, F. Barnes, M. Franklin, L. Gibbs, G. Hemighaus, N. Hogue, D. Lesnini, J. Jind, J. Maybury, J. Morris, *Aviation Fuels Technical Review*, Houston, (2000).
- [126] C. Moses, P. Roets, *Status Report on Semi-Synthetic Jet Fuel and the Development of Syntethic Jet Fuel*. Presented at CRC Alexandria, April 30, (2003).
- [127] K. Beck, R. Kreiselmaier, V. Peterseim, E. Osen, *Kautschuk Gummi Kunststoffe*, **56** (2003) 657.
- [128] J. M. Veranaud: "*Liquid Transport Processes in polymeric Materials*" Prentice Hall, New York, (1991).
- [129] G. P. Streit, M. Achenbach, *Gummi Fasern Kunststoffe (GAK)*, **54** (2001), 816.
- [130] K. Azaar, R. Grang, I. D. Rosca, J. M. Vernaud, *Gummi Fasern Kunststoffe (GAK)*, Jahrgang 54 ,4 (2001), 236.
- [131] P. J. Flory, J. Rehner, *J. Chem. Phys.* **11** (1945) 52.
- [132] K. Muniandy, E. Southern, A.G. Thomas, "*Diffusion of liquids and solids in rubber*" (1978).
- [133] G. J. Van Amerongen, *Rubber Chem. Technol.*, **37** (1964) 1065.
- [134] J. Crank, "*The Mathematics of Diffusion*", 2nd ed., Clarendon Press, Oxford (1975).
- [135] P. Meares, *J. Polym. Sci.*, **27** (1958) 391.
- [136] H. Fujita, A. Kishimoto, K. Matsumoto, *Trans. Faraday Soc.*, **56** (1960) 424.
- [137] A. Fick, *Ann. Phys. Lpz.*, **170** (1855) 59.

- [138] DIN 53536, Bestimmung der Gasdurchlässigkeit.
- [139] R. M. Barrer, “*Diffusion in and through Solids*”, Cambridge University Press, London, (1951).
- [140] S. Glasstone, K. J. Laidler, H. Eyring, “*The Theory of Rate Process*”, McGraw-Hill, New York, (1941).
- [141] R. M. Barrer, *J. Phys. Chem.*, Wash., **61** (1957) 178.
- [142] P Meares, *J. Polym. Sci.*, **27** (1958) 391.
- [143] H. Fujita, A. Kishimoto, K. Matsumoto, *Trans. Faraday Soc.*, **56** (1960) 424.
- [144] F. Bueche, *J. Chem. Phys.*, **21** (1953) 1850.
- [145] H. L. Frisch, *J. Polym. Sci.*, **3** (1965) 13.
- [146] A. T. DiBenedetto and D. R. Paul, *J. Polym. Sci., A*, **2** (1964) 1001.
- [147] J. Crank, G. S. Park, “*Diffusion in Polymers*”, Academic Press, London, (1968).
- [148] V. M. Shah, S. A. Stern, P. J. Ludovice, *Macromolecules*, **22** (1989) 4660.
- [149] K. A. Mauritz, R. F. Storey, *Macromolecules*, **22** (1990) 2033.
- [150] M. H. Cohen, D. Turnbull, *J. Chem. Phys.*, **31** (1959) 1164.
- [151] A. Aitken and R. M. Barrer, *Trans. Faraday Soc.*, **51** (1955) 116.
- [152] M. Sallem, A. F. A. Asfour and D. Dekee, *J. Appl. Polym. Sci.*, **37** (1989) 617.
- [153] G. A. Maria, A. Sanguineti, *Journal of Polymer Science*, **42** (2004) 1987.
- [154] L. B. Georgoulis, *J. Appl. Polym. Sci.*, **97** (2005) 775.
- [155] G. J. Armerogen, *Rubber Chem. Technol.*, **20** (1947) 494.
- [156] G. J. Armerogen, *Rubber Chem. Technol.*, **29** (1955) 821.
- [157] I. Hidec, M. Jasso, M. Cernak, *Kautschuk Gummi Kunststoffe*, **10** (2005) 525.
- [158] P. Chevallier, M. Castonguay, S. Turgeon, N. Dubrulle, D. Mantovani, P. H. McBreen, J. C. Wittmann, G. Laroche, *J. Chem. Phys.*, **105** (2001) 12490.
- [159] R. Dahlmann, IKV – *Berichte aus der Kunststoffverarbeitung*, 124, Aachen, Mainz Verlag, **124** (2002) 1.
- [160] H. Eyring, *J. Chem. Phys.*, **4** (1936) 283.
- [161] H. S. Taylor, *J. Chem. Phys.*, **6** (1938) 331.
- [162] W. Sutherland, *Philos. Mag.*, **9** (1905) 78.
- [163] H. Eyring, R. H. Ewell, *J. Chem. Phys.*, **5** (1937) 726.
- [164] F. Eirich, R. Simha, *J. Chem. Phys.*, **7** (1939) 116.
- [165] W. Kauzmann, H. Eyring, *J. Am. Chem. Soc.*, **62** (1940) 3113.
- [166] J. G. Kirkwood, *J. Polym. Sci.*, **12** (1954) 1.
- [167] S. Glasstone, “*Textbook of Physical Chemistry*”, New York, (1940), 253.
- [168] G. J. Van Amerongen, *J. Appl. Phys.* **17** (1946) 972.
- [169] F. Bueche, *J. Chem. Phys.*, **20** (1952) 1959.

- [170] A. N. Gent, L. Ginger, *J. Polym. Sci, Part B: Polym. Phys.*, **29** (1991).
- [171] T. Ito, K. Aizawa, J. Seta, *Colloid Polym. Sci.*, **262** (1991) 1224.
- [172] R. M. Barrer, *Nature*, Lond., **140** (1937) 106.
- [173] G. J. Van Amerongen, *J. Polym. Sci.*, **5** (1950) 307.
- [174] A. D. Roberts, *Natural Rubber Science and Technology*, Oxford University Press (1988).
- [175] A. Y. Coran, *Rubber Chem. Technol.*, **68** (1995) 351.
- [176] J. L. Koenig, *Rubber Chem. Technol.*, **73** (2000) 385.
- [177] J. B. Class, *Processing at Meeting of the Rubber Division* (1997).
- [178] A. V. Chapman, M. Porter; "Sulphur Vulcanization Chemistry", in: A. D. Roberts, "Natural Rubber Science and Technology", Oxford Science Publications, Oxford, (1988) 511.
- [179] J. M. G. Cowie, "Chemie und Physik der synthetischen Polymeren", Verlag Vieweg – Wiesbaden, (1997).
- [180] W. Gronski, U. Hoffmann, G. Simon, A. Wutzler, E. Straube, *Rubber Chem. Technol.*, **63** (1992) 65.
- [181] F. Grinberg, F. Grinberg, N. Nestle, W. Kuhn, *J. Polym. Sci.*, **39** (2001) 2207.
- [182] G. Simon, H. Schneider, K.-G. Haeusler, *Prog. Colloid Polym. Sci.*, **78** (1988) 30.
- [183] R. M. Barrer, *Trans. Faraday Soc.*, **36** (1940) 644.
- [184] A. Aitken, R. M. Barrer, *Trans. Faraday Soc.*, **51** (1955) 116.
- [185] J. B. Donnet, R. C. Bansal, M. J. Wang, "Carbon Black Science and Technology", Marcel Dekker, New York, (1993) 289.
- [186] G. Kraus, "Reinforcement of elastomers", Wiley-Interscience, New York, (1965).
- [187] R. H. Schuster; "Füllstoffe", in W. Hofmann and H. Gupta "Handbuch der Kautschuktechnologie", Gupta Verlag, (2001) 1.
- [188] H. M. Hess, P. C. Vegvari, R. A. Swor, *Rubber Chem. Technol.*, **58** (1985) 350.
- [189] M. P. Wagner, *Rubber Chem. Technol.*, **49** (1976) 703.
- [190] U. Görl, A. Hunsche, A. Müller, H. G. Koban, *Rubber Chem. Technol.*, **70** (1997) 608.
- [191] J. Fröhlich, H. D. Luginsland, *Rubber World*, **28** (2001) 244.
- [192] A. Einstein, *Ann. Phys.*, **17**, (1905), 549.
- [193] A. Einstein, *Ann. Phys.*, **34**, (1911), 591.
- [194] H. M. Smallwood, *J. Appl. Phys.*, **15**, (1944) 758.
- [195] E. Guth and O. Gold, *Phys. Rev.*, **53** (1938) 322.
- [196] E. Guth, O. Gold, *J. Appl. Phys.*, **16**, (1945) 20.
- [197] S. Wolff and J.-B. Donnet, *Rubber Chem. Technol.*, **63** (1990) 32.
- [198] M. J. Wang, S. Wolff, E. H. Tan, *Rubber Chem. Technol.*, **66**, (1993) 178.
- [199] A. I. Medalia, *J. Colloid Interface Sci.*, **24** (1967) 393.
- [200] W. M. Hess, G. C. McDonald, E. Urban, *Rubber Chem. Technol.*, **46**, (1973) 204.

- [201] A. R. Payne, *J. Polymer Sci.*, **6** (1962) 57.
- [202] A. R. Payne, R. E. Wittaker, *Rubber Chem. Technol.*, **44**, (1971) 440.
- [203] A. R. Payne, *J. Polymer Sci.*, **7** (1963) 873.
- [204] H. Ishida, *Rubber Chem. Technol.*, **60** (1980) 497.
- [205] R. H. Doremus, "Diffusion of reactive molecules in solids and metals", A Wiley-Interscience Publication, (2002).
- [206] A. J. Tinker, *Rubber Chem. Technol.*, **68** (1995) 461.
- [207] J. B. Gardiner, *Rubber Chem. Technol.*, **41** (1968) 1312.
- [208] A. V. Chapman, A. J. Tinker, *Kautschuk Gummi Kunststoffe*, **56** (2003) 533.
- [209] C. A. Gagliardi, L. B. Muire, D. E. Hirt, *Ann. Techn. Conf. – Society of Plastic Engineers*, **2** (1999) 2502.
- [210] J. B. Gardiner, *Rubber Chem. Technol.*, **42** (1968) 1058.
- [211] M. E. Glicksman, "Diffusion in Solids", John Wiley&Sons Inc., (2000).
- [212] D. A. Lederer, K. E. Kear and G. H. Kuhls, *Rubber Chem. Technol.*, **55** (1982) 1482.
- [213] C. B. Skidmore, *J. Polym. Sci., Part B: Polymer Physics*, **42** (2004) 3258.
- [214] K. Saalwächter, F. Kleinschmidt, *Verhandl. Deutsch. Physikal. Gesellsch.*, **40** (2005) 120.
- [215] J. L. Duda, J. S. Vrentas, S. T. Ju, H. T. Liu, *AIChE J.*, **28** (1982) 279.
- [216] J. Stastna, D. D. Kee, "Transport Properties in Polymers", Technomic, Lancaster, USA, (1995).
- [217] D. A. Edwards, D. S. Cohen, *AIChE J.*, **41** (1995) 2345.
- [218] C. F. Fong, Y. Li, D. D. Kee, J. Bovenkamp, *Rubber Chem. Technol.*, **71** (1998) 285.
- [219] M. Doi and S. F. Edwards, *J. Chem. Soc. Faraday Trans. II*, **74** (1978) 1789.
- [220] J. Meier, M. Klüppel, R. H. Schuster and E. Giebel, *Kautsch. Gummi Kunstst.*, **56** (2003) 465.
- [221] J. Guja, M. Bravar and J. Jelencic, *Kautschuk Gummi Kunststoffe*, **38** (1985) 28.
- [222] A. B. Ahmad, D. W. Aubrey, A. J. Tinker, *J. Nat. Rubb. Res.*, **9** (1994) 1.
- [223] R. Schmidt, G. Pampus, R.H. Schuster, H. Abendroth, H. Umland, *Kautschuk Gummi Kunststoffe*, **42** (1989) 582.
- [224] R. Wommelsdorff, *Kautschuk Gummi Kunststoffe*, **41** (1988) 248.
- [225] E. Southern, A. G. Thomas, *Trans. Faraday Soc.*, **63** (1967) 1913.
- [226] A. B. Ahmad, D. W. Aubrey, A. J. Tinker, *J. Nat. Rubb. Res.*, **10** (1995) 1.
- [227] A. Neppel, *Rubber Chem. Technol.*, **59** (1986) 47.
- [228] J. Auerbach, W. Miller, W. Kuryla, S. Gehman, *J. Polym. Sci.*, **28** (1958) 129.
- [229] I. Auerbach, S. D. Gehman, *Rubber Chem. and Technol.*, **27** (1954) 772.
- [230] G. Kraus, R.L. Collins, *Rubber World*, **139** (1958) 219.

- [231] E. Killmann, R. Eckart, *Makrolol. Chem.*, **144** (1971) 45.
- [232] S. George, K. Varughese, S. Thomas, *Polymer*, **41** (2000) 579.
- [233] S. George, K. Ninan, G. Groeninckx, S. Thomas, *J. Appl. Polym. Sci.*, **78** (2000) 280.
- [234] A. E. Mathai, R. P. Singh, S. Thomas, *J. Membr. Sci.*, **202** (2002) 35.
- [235] N. Sombatsompop, K. Christodoulou, *J. Polym. & Polym. Compos.* **5** (1997) 377.
- [236] T. Johnson, S. Thomas, *J. Macromol. Sci.*, **36** (1997) 401.
- [237] S. C. George, S. Thomas, *Prog. Polym. Sci.*, **26** (2001) 985.
- [238] A. Berens, H. Hopfenberg, *J. Membr. Sci.*, **10** (1982) 283.
- [239] H. J. Hübschmann, "Handbuch der GC/MS", VCH publishing, New York, (1996).
- [240] A. Wildberger, DIK Internal report (2006).
- [241] H. Krump, M. Jasso, I. Hudec, M. Bafnec, J. Sustek, L. Jurica, *Kautschuk Gummi Kunststoffe*, **11** (2005) 557.
- [242] ASTM D2000 Standard Classification.
- [243] F. Ohm, "Introduction to the Structure and Properties of Rubber", in Vanderbilt Rubber Handbook, 13<sup>th</sup> Edition, (1990) 2.
- [244] M. Morton, "Rubber Technology", 3rd Edition, Van Nostrand Reinhold Company Inc. (1987).
- [245] B. G. Corman, *Rubber Chem. and Technol.*, **44** (1971) 278.
- [246] W. Steinhilper und St. Britz, *Kautschuk Gummi Kunststoffe* **46** (1993) 978.
- [247] B. N. Dinzborg, R. W. Keller, R. Bond, *Gummi Asbest Kunststoffe*, **8** (1988) 398.
- [248] J. Brandrup, E. H. Immergut, E. A. Grulke, "Polymer Handbook", Willey-Interscience Publication, New York, 1999.
- [249] P. Fernandez und S. Bowers: The Standard Fluoroelastomer for Automotive Fuel Systems., *Kautschuk Gummi Kunststoffe* **52** (1999) 429.
- [250] B. Dinzborg. Influence of Oil Aeration on Dynamic Rotary shaft seals Under Laboratory and Field Conditions. SAE Paper Nr. 930535. SAE, Detroit (1993).
- [251] A. Ismat Abu-Isa und H. E. Trexler: Mechanism of Degradation of Fluorocarbon Elastomers in Engine Oil. *Rubber Chem. Technol.* **58** (1985) 326.
- [252] C. Debler, "Bestimmung und Vorhersage des Verschleißes für die Auslegung von Dichtungen", Ph.D Thesis, Universität Hannover, (2005).
- [253] H. Bender, E. Campomizzi, *Rubber Chem. and Technol.*, **1** (2001) 14.
- [254] S. Bhattacharjee, A. K. Bhowmick, B. N. Avasthi, *Polymer Degradation and Stability*, **31** (1991) 71.
- [255] K. C. Smith, B. S. Tripathy, *Rubber World*, 217 (1998) 28.
- [256] G. Ivan, M. Giurginca, S. Basuc, *Revue Roumanine de Chemie*, 43 (1998) 231.



- [259] T. L. A. C. Rocha, "*Influência da Modificação Química de Polidienos sobre suas Propriedades Finais*", Ph.D. Thesis, University Federal of Rio Grande do Sul.

**Curriculum vitae****Personal data:**

Name: Rosca

First name: Cristina

Date of birthday: 26.04.1976

Place of birthday: Avrig, Romania

Status: Single

Nationality: Romanian

**Educational background:**

09/1990-06/1994	High school in Sibiu, Romania School-leaving examination. Focus area: Chemistry, Biology, English
10/1994-07/1999	Study of Chemical Engineering (Dipl.-Chem. Ing.) at University Politehnica Timisoara, Romania
10/1999-07/2000	Advanced course of Rubber Technology at University Politehnica Timisoara, Romania, with practical work in Deutschen Institut für Kautschuktechnologie e.V., Hannover

**Work experience:**

11/2000-03/2002	Responsible for the environmental protection department at Continental Automotive Products SRL Timisoara, Romania
05/2002-04/2006	Dissertation study at University of Hannover, Institute for inorganic chemistry. The experimental work was done in Deutsches Institut für Kautschuktechnologie e.V. in Hannover, based on research projects financed by the industry.
05/2006-till today	Chemist at Rhein Chemie Rheinau GmbH in Applications Technology/Rubber Division/ Automotive Department.

Hannover, 08.10.2007

Cristina Rosca